MITIGATING WEAR ON SURFACES UTILIZING SELF-ASSEMBLED WEAR PASSIVATING FILMS

A Dissertation

by

RYAN LANE JONES

Submitted to the Office of Graduate Studies of
Texas A&M University
in partial fulfillment of the requirements for the degree of

DOCTOR OF PHILOSOPHY

May 2011

Major Subject: Chemistry

MITIGATING WEAR ON SURFACES UTILIZING SELF-ASSEMBLED WEAR PASSIVATING FILMS

A Dissertation

by

RYAN LANE JONES

Submitted to the Office of Graduate Studies of
Texas A&M University
in partial fulfillment of the requirements for the degree of

DOCTOR OF PHILOSOPHY

Approved by:

Chair of Committee,	James D. Batteas
Committee Members,	David H. Russell
	D. Wayne Goodman
	Hong Liang
Head of Department,	David H. Russell

May 2011

Major Subject: Chemistry

ABSTRACT

Mitigating Wear on Surfaces Utilizing Self-Assembled Wear Passivating Films.

(May 2011)

Ryan Lane Jones, B.S., Texas A&M University Corpus Christi

Chair of Advisory Committee: Dr. James D. Batteas

Controlling tribological interactions, such as friction and adhesion between contacting interfaces is critical for the advancement of technologies such as microelectromechanical systems (MEMS) devices. The challenge in MEMS device lubrication lies in the inherent nature of the material's surface at the nanoscale as well as the nature of the surfaces typically used during experimentation. Device surfaces often display nanoscale roughness with surface asperities dictating the tribological properties between interfaces, yet the vast majority of past research has focused predominately on nanotribological studies of thin films on flat silicon substrates to model the behavior of these self-assembled wear-reducing coatings. New model surfaces have been manufactured and integrated into experiments in which surfaces with controlled asperity sizes act as more realistic models of MEMS surfaces. As friction and adhesion between real surfaces in sliding contact are dominated by the interactions of nanoscaled surface asperities, this research is an extension of previous work, moving beyond smooth surfaces by manufacturing and implementing new experimental platforms possessing controlled asperity sizes. The influence of asperity size on the tribological properties of

these contacts is being studied for both native oxide and organosilane derivatized surfaces. These studies more readily mimic the conditions found at true asperity-asperity contacts.

This research has aimed to develop new lubricant thin films that can effectively protect MEMS device surfaces during use with the long term goal of bringing MEMS devices out of the laboratory and into wide scale commercial use. This work investigates how self-assembled monolayers (SAMs) on curved surfaces can be utilized in manners that their analogs on flat surfaces cannot. SAMs on curved asperities can be used to trap short chain alcohols, which during contact may be released to function as an additional lubricant layer on the surface. Both atomic force microscopy and Fourier transform infrared spectroscopy have been employed to evaluate how chain disorder influences the protective function of these molecular lubricant layers on asperities. It was found that functionalized surfaces resisted wear and were able to operate under continuous scanning for longer time frames than unfunctionalized surfaces and that multicomponent films improved upon the performance of their base, single component analogs.

DEDICATION

I dedicate this work to my family, especially my wife, because without her unwavering support, none of this would have been possible.

ACKNOWLEDGEMENTS

I would first like to thank my research advisor, Dr. James D. Batteas, for enthusiastically mentoring and teaching me over the last five years, as well as for his support both in and outside of the laboratory. I would also like to thank my committee members, Dr. D. Wayne Goodman, Dr. David Russell, and Dr. Hong Liang for the help and advice they have provided during my studies. Other Texas A&M Chemistry faculty I would like to thank are Dr. Paul Cremer, Dr. Danny Yeager, and Dr. Simon North for bringing a passion to the classroom and sharing their knowledge of chemistry during my coursework.

I would also like to extend my appreciation to the Batteas Research Group for all the help and support they have graciously and willingly provided throughout the years. I would also like to individually thank Dr. Amanda Schuckman, Dr. Jixin Chen, Albert Wan, Dr. Gang Liang, Bradley Ewers, Chi-Yuan Chang, Arika Pravitasari, Carrie Carpenter and Ainsley Allen for their unending enthusiasm to render aid, advice, and friendship during my time at Texas A&M University.

I would like to thank my professors at Texas A&M University - Corpus Christi for their mentoring, teaching and advice during the time I spent as a student there. Specifically, I would like to thank Dr. Eugene Billiot and his wife, Dr. Fereshteh Billiot for their willingness to take in a transfer student and make him a part of their research family. I would also like to thank my undergraduate research group members, Melissa Griffith, Dr. Mark Olsen, (soon to be Dr.) Jennifer Bartels, and Dr. Amanda Treviño.

Although we did not succeed in conquering the world, we are all well on our way to finding our paths through it.

I would like to thank my family and friends for all of their love, support and encouragement during my time in graduate school. The trials and tribulations were a little less daunting knowing there were people who believed in me even when I did not. I would like to thank my son, Jackson Lane Jones, whose infectious laughter and unbridled curiosity about the world makes me remember why I am so happy to be a part of it. I would like to thank my mother, Kathy Jones for raising me and helping me find my way. I honestly do not know if I even can fully appreciate how difficult it was for you to support and raise a family by yourself while working the hours you did; all I know is that somehow we survived and thrived. I would like to thank my father, David Jones for supporting me when I was down and encouraging me to be successful in spite of myself. I sincerely hope you have found what you are looking for, wherever you may be. I would like to thank my brothers, Jason Mallia and Adam Jones for being there with me through the hard times. I would also like to thank my grandparents, Fred and Shirley Jones for their love and encouragement over the years. You two are my rock and my inspiration. I do not know what I would have become without your presence in my life. I would be remiss if I did not take a moment to thank my in-laws for bringing me in and making me one of the family. I am truly blessed to have you all in my life. Finally, I would like to thank my grandfather, Bill Brunson. I am sorry that I was not with you when you left us; I will never again forget where my true priorities lie.

At last I would like to thank my wife, Melissa Jones, who has been with me on this journey from the beginning, for better and for worse. You have been there for me in more ways than I think I can appreciate. You have been there to offer encouragement and provide support. You have been my confidant in joy and in anger. You have held me up, motivated me, consoled me, scolded me, cajoled me and otherwise to see me through even when I did not believe it was possible. For all of those things, I thank you and I love you.

NOMENCLATURE

3P1P	3-phenyl-1-propanol
AFM	Atomic Force Microscope
C_x	Alkyl Chain Possessing "x" Carbon Units
DMT	Derjaguin, Muller and Toporov Theory of Continuum Mechanics
DTS	Dodecyltrichlorosilane
FFM	Friction Force Microscopy
FIB	Focused Ion Beam
FTIR	Fourier Transform Infrared Spectroscopy
JKR	Johnson-Kendall-Roberts Theory of Continuum Mechanics
LFM	Lateral Force Microscopy
MEMS	Microelectromechanical Systems
ODS	Octadecyltrichlorosilane
OTE	Octadecyltriethoxysilane
OTS	Octadecyltrichlorosilane
SAM	Self-Assembled Monolayer
STM	Scanning Tunneling Microscope
TGA	Thermal Gravimetric Analysis
THF	Tetrahydrofuran
XPS	X-Ray Photoelectron Spectroscopy

TABLE OF CONTENTS

CHAPTER Page

Page

LIST OF FIGURES

FIGURE Page

FIGURE Page

FIGURE Page

FIGURE Page

FIGURE Page

FIGURE Page

FIGURE Page

LIST OF TABLES

CHAPTER I

INTRODUCTION

1.1 Overview

Controlling friction and adhesion at surfaces is paramount for the development of advanced technologies such as microelectromechanical systems (MEMS) devices. As many MEMS devices are fabricated predominantly from Si, the surface of which is typically covered by an oxide (SiO_2), water has been found to play a key role in catalyzing the formation of defects. To protect such surfaces, self-assembled monolayers (SAMs) have been employed to reduce friction and help control water-surface interactions. Assembly of high quality monolayers on the typically rough surfaces found in such devices however, can be very challenging as surface roughness can dramatically impact the extent of disorder within the surface bound molecular layers. Thus, understanding how SAMs assemble on rough surfaces and how this influences their efficacy in reducing friction and adhesion is key to engineering molecular based surface lubricants. As friction and adhesion between real surfaces in sliding contact are dominated by the interactions of nanoscaled surface asperities, the work presented in this dissertation aims to move beyond smooth surfaces by generating surfaces with controlled asperity sizes. The influence of asperity size on the tribological properties of these contacts was studied for both native oxide and organosilane derivatized surfaces. These studies more readily mimic the conditions found at true asperity-asperity contacts.

This dissertation follows the style of *The Journal of the American Chemical Society*.

Combinations of AFM and IR spectroscopy were employed to evaluate how chain disorder influences the protective function of the reported molecular lubricant layers on asperities. Overall, these studies aim to address one primary question: how does asperity size influence defect nucleation in molecular lubricant layers and how does this alter their nanomechanical properties? Studies described herein are aimed at determining how surface curvature affects thin film molecular ordering, the mechanics of these films on curved surfaces, employing mixed monolayers of 3-phenyl-1-propanol (3P1P) and octadecyltrichlorosilane (OTS) on silica nanoasperities for friction modification and how probing rates affect mechanical responses.

1.2 MEMS, SAMs and the Current State of Nanotribology

Controlling friction, adhesion and wear of surfaces is of key importance to the proper function of micro-electromechanical systems (MEMS) devices (Figure 1.1).

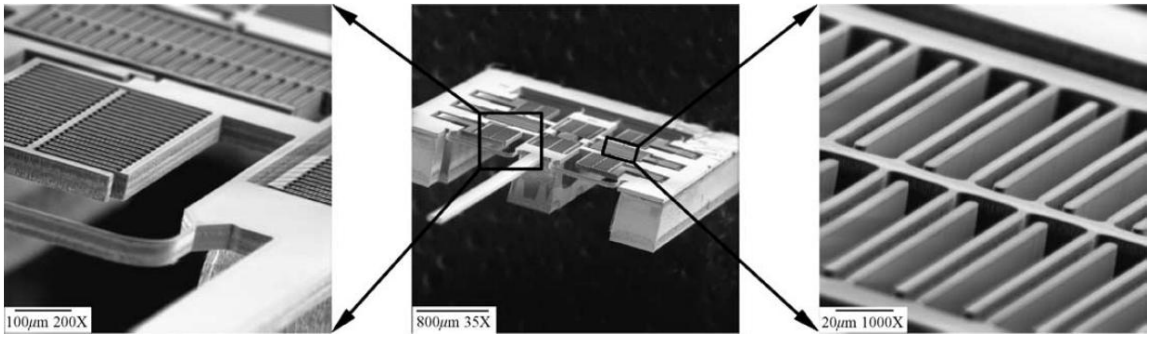

FIGURE 1.1: Scanning electron microscope image of a two-axis electrostatic micromotor microelectromechanical systems device. Reused with permission. Copyright 2002 Elsevier.[1]

Because the surfaces of these devices typically possess asperities on the order of 10 – 20 nm in dimension,[2] most interactions between two surfaces in contact, whether planned or incidental, will be dominated by these nanoscopic asperity-asperity interactions. Over the last decade, much work has been invested in understanding how self-assembled monolayers might be used to control and reduce the effects of friction, adhesion and wear in microdevices (Figure 1.2). [2-4] Most recent studies of these systems have

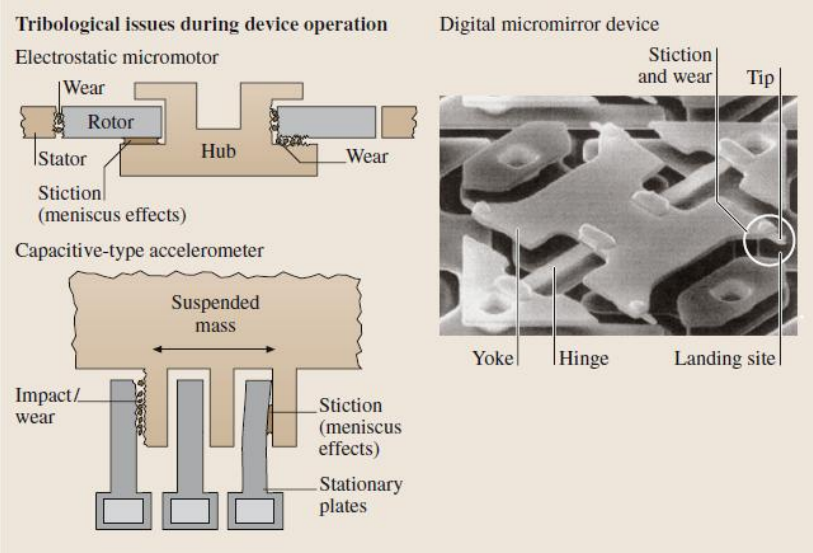

FIGURE 1.2: Two examples of MEMS devices including a micromotor and an accelerometer. Water vapor can condense in these device junctions yielding stiction. This can be reduced by control of surface roughness and chemistry. Intermittent contact between device components nucleates defects ultimately yielding wear debris. The generation of defects at surfaces in sliding contacts is the catalyst for the eventual wear of the materials. Reused with permission. Copyright 2004 Springer Science+Business Media, LLC.[5]

attempted to apply conclusions found during experimentation on model flat systems to real device surfaces. To do this, researchers have employed functionalized atomic force

microscopy tips, whose dimensions closely resemble those of MEMS device surface asperities to act as mobile single asperity research platforms.[4, 6-11] While research into single asperity interactions have benefited the field, controlling wear at asperity-asperity contacts is the ultimate goal. To that end, self-assembled monolayers (SAMs) of alkylsilane and fluorosilane compounds with chain lengths ranging from C_{10}-C_{18} have shown the capacity to reduce friction and adhesion, therefore reducing wear in these devices.[12-14] In order to more accurately probe the molecular level details of tribological interactions between multiple asperities, lubricant film assembly and stability must be more thoroughly understood. The importance of gaining molecular level understanding becomes paramount when one considers that reaction conditions and self-assembled monolayer constituent choices play a critical role in the performance of the film.[15]

Nanotribology is the study of lubrication, friction, adhesion and wear on the nanometer scale. It has become a multidisciplinary field wherein the ultimate goal is to better understand the interactions between two surfaces in contact. Fundamentally, nanotribologist are tasked with ascertaining how forces are produced and energy is dissipated during contact. As devices are miniaturized, surface forces are known to dominate interactions between components, ultimately controlling the functionality of a microdevice. This phenomenon has been observed time and again in MEMS, with surfaces forces acting to create stiction and wear during use, ultimately leading to device failure.[5, 16-18] Due to the ease at which interfacial contact can quickly become endlessly complicated, fundamental studies have focused on experiments at well-defined

interfaces, and because of this, AFM based single-asperity contact experiments have been widely used.[6, 19-65]

Because of the importance of utilizing well understood interfaces in nanotribological research, experiments are typically designed to model single-asperity contacts. Having a single, uninterrupted contact area necessarily avoids complications that arise from interactions due to multiple simultaneous contacts, but in the case of research to be utilized in MEMS systems, ignores the true nature of the contacts found in working devices. While it is in fact easier to understand and correlate information gleaned from single-asperity based nanotribological research, there comes a time when more realistic systems need to be tested and ultimately implemented.

1.3 Nanoscale Contact Mechanics

Contact mechanics are a major theme in tribology and cannot be overlooked as the field is the basis for the mathematical understanding of contact area, indentation, stiffness as well as stress and strain fields associated with asperity contacts. Contact mechanics grew from the work of Hertz while he studied the inference patterns between glass lenses under compressive contact.[66] Hertz postulated that the circular contact area between a spherical lens and a flat plane subjected to a normal load P could be defined by the equation:

$$a = \left(\frac{PR}{K} \right)^{1/3}$$

where R is the sphere radius and

$$K = \frac{4}{3}\left(\frac{1-\nu_1^2}{E_1} + \frac{1-\nu_2^2}{E_2}\right)^{-1}$$

while E_1 and E_2 are the sphere and flat plane Young's moduli, and ν_1, ν_2 are the sphere and flat plane Poisson's ratios. Hertz's work would be the basis for the evolution of contact mechanics as a field, because while his equations described the area of a macroscopic contact between homogeneous, isotropic, and linear elastic materials, it ignored the effects of adhesive interactions between the contacting interfaces.

The effects of adhesion inside a contact were subsequently described by two independent research groups. Johnson, Kendall and Roberts (JKR) proposed a model that included a factor for adhesion between two elastic bodies in contact by focusing on minimizing the contributions of strain energy and surface energy to the total energy in the contact.[67] They described the contact radius between the surfaces as

$$a = \left(\frac{P}{K}\left(P + 3\pi\gamma R + \sqrt{6\pi\gamma RP + (3\pi\gamma R)^2}\right)\right)^{1/3}$$

where γ is described as the work of adhesion or the Dupr´e energy of adhesion, which is defined as $\gamma = \gamma_1 + \gamma_2 - \gamma_{12}$, where γ_1 and γ_2 are the respective surface energies of the two contacting surfaces and γ_{12} the interfacial energy between them. By this definition, γ encompasses all interfacial forces and represents the work per unit area required to separate the surfaces from contact to infinity. JKR assumed that the adhesive interactions between the contacts were of an infinitely short range and the free energy of the system is only reduced by γ units of energy for each unit of area in contact. This description concludes that there is no adhesive interaction from regions of the bodies

outside of a defined separation between the surfaces. JKR's formula therefore predicts that adhesion makes possible a contact area greater than zero under zero applied load and some normal load must be applied to separate the surfaces from contact. This normal load is referred to as the adhesive force or the critical load P_c and is defined as

$$P_c = -\frac{3}{2}\pi\gamma R$$

While JKR were proposing their theory to account for adhesive contacts, Derjaguin, Muller and Toporov (DMT) had developed their own equations to define the effects of adhesion in elastic contacts.[68] DMT proposed that the contact profile in their system was unchanged from the contact profile described by Hertz, but contained and adhesive component which increased the overall load in the system. In essence, the DMT model assumes that attractive interactions act on the two surfaces at all separations, with the expression taking the form of

$$a = \left(\frac{R}{K}(P + 2\pi\gamma R)\right)^{1/3}$$

while the adhesive force was described as

$$P_c = -2\pi\gamma R$$

DMT concluded the contact area was equal to zero when the system was at the point of contact separation, or when the pull-off force was at its maximum. Because of this, the DMT model for contact mechanics is often referred to as the Hertz-plus-offset model as it is equivalent to the Hertz model plus the adhesive force.

While both models presented by JKR and DMT were found to be valid, the validity applies to opposite limits of contact behavior. The JKR model applies when the attractive forces between the contacts are small in comparison to the elastic deformations of the materials in contact, which holds true for compliant materials with large sphere radii and strong, but short range adhesive interactions. Conversely, the DMT model is used when the materials in contact can be described as relatively stiff with small sphere radii and weak long range adhesive forces working between the surfaces. Both of these limits were described by Tabor, who proposed nondimensional physical parameter (μ_T) to quantitatively express both behaviors.[69]

$$\mu_T = \left(\frac{16R\gamma^2}{9K^2 Z_0^3} \right)^{1/3}$$

In the equation, Z_0 describes the equilibrium bond length for the two materials in contact. If the contact is considered to be atomistic interaction such as the Lennard-Jones potential, then Z_0 is the equilibrium separation of the surfaces and the spatial range of the attractive force scales directly with it. As such, Tabor's parameter is essentially the ratio between the normal elastic deformation caused by adhesion and the spatial range of the adhesion forces between the contacts which is denoted by Z_0.

In order to quantitatively describe contacts between the extremes of DMT and JKR, Maugis proposed a square well potential to account for the attractive forces between the two surfaces.[70] His potential worked under the assumption that a constant adhesive stress (σ_0) was present over a defined range of separation (δ_t). Outside of δ_t,

adhesion between the surfaces would be zero. According to Maugis, the work of adhesion could be defined as the adhesive stress times the defined separation range:

$$\gamma = \sigma_0 \cdot \delta_t$$

Maugis then went on to define a transition parameter similar to the one proposed by Tabor,

$$\lambda = 2\sigma_0 \left(\frac{R}{\pi \gamma K^2} \right)^{1/3}$$

where λ is the so called Maugis parameter. Following the equation, if σ_0 is defined as being equal to the minimum adhesive stress allowed by a Lennard-Jones potential then λ and μ_T can be said to be equivalent. As such, it has been determined that the JKR model applies to cases when $\lambda > 5$ while the DMT model is used in systems where $\lambda < 0.1$. Values inside the DMT and JKR limits correspond to the transition between them.

The contact mechanics models described above are defined by a contact consisting of a sphere and a plane or two spheres. It is important to note that in these systems, the contact radius is considered to be much smaller than the sphere radius while all loading is strictly in the normal direction. For each of these systems, the materials must be homogeneous, isotropic, linear and elastic. Obviously, deviations readily occur in practice and as such, many variations on these theories have been developed to account for this. While the field of contact mechanics is still experiencing constant development, the models presented above represent the basis from which the discipline is defined. These models have proven to be excellent tools for understanding the fundamentals of materials in contact. A number of developments are still required as

there remains a very real deficiency of mathematical formulations to describe a number of real contacts, such as those possessing arbitrary geometries, contacts under shear stresses and plastic deformation, as well as a number of other systems which have yet to be explored.

1.4 SAMs on Flat Surfaces

Nanotribology studies of self-assembled monolayers (SAMs) have been performed over the course of several decades due to their potential to act as a lubricating agent in microelectromechanical systems (MEMS) devices. Typically, a SAM is a self ordered arrangement of molecules that aggregate on a surface through chemical or physical adsorption and by doing so; alter the surface chemistry in some desirable way. The actual makeup of the molecules that comprise an individual SAM differs depending on the type of molecule employed on the surface, but most fall within a basic scheme in which a head group binds to the surface; such as thiol binding to the surface of a gold substrate[71] or chlorosilanes assembling on exposed oxide surfaces;[72] however, the focus of this dissertation is on alkylsilane SAMs on silicon oxide surfaces.

Attached to the head group is typically some sort of hydro or fluorocarbon backbone, which provides stability to the film through van der Waals interactions between the molecules contained within the SAM, with the number of carbons contained within the backbone controlling many of the material properties of the SAM by altering the local crystalline environment. As such, the overall degree of ordering in the SAM is closely tied to the chain length of the molecules within the film, with longer chains typically allowing for more crystalline, well ordered films due to the increase in the

number of stabilizing lateral interactions. A large number of alkylsilane nanotribology studies have been performed with a focus on the effect that chain length plays in the tribological properties of these films. While most nanotribological studies are performed on SAMs possessing hydrocarbon backbones of the same length, some studies have been performed utilizing mixed SAMs with both hydro and fluorocarbon substituents in the same film as well as SAMs comprised of molecules possessing different chain lengths.[49, 73] At the terminus of the molecule is the end group, which serves as the new surface boundary. Careful selection of the chemical entity which comprises the end group and even later chemical modification of this group allows for tailoring the chemical properties of the exposed surface in a variety of ways.

Owing to the potential applications for MEMS, SAM formation on silica surfaces has been widely researched over the last few decades.[74-84] For film formation on the oxide layer of crystalline silicon samples, which are nominally flat at the nanoscale, researchers have concluded that SAMs on these surfaces most likely assemble by means of two possible strategies. The first proposed method is that of an "island aggregation" pathway in which small collections of molecules aggregate and subsequently bind to the surface and grow, eventually forming a complete molecular film on the surface.[80, 84] The other likely assembly scheme involves a continuous formation where the monolayer constituents are uniformly distributed over the surface, slowly building as more molecules are inserted into the growing film until a well order monolayer is formed.[85] While the process by which these SAMs are formed is thought to be mostly understood, the actual way in which the films are bound to the surface over large domains is not.

The silicon atom in an alkylsilane molecule has the potential to form as many as three covalent siloxane linkages with the surface or nearest neighbor molecules. Steric hindrances make it impossible for one silane molecule to form three covalent bonds with the silica surface due to the distribution of available hydroxyl groups on the surface and the distances between them. Likewise, sterics dictate that silanes cannot be simultaneously bound to both the surface and nearest neighbor molecules over large areas.[86] The most likely explanation for how these monolayers are arranged on the surface is a hybrid form, with a mixture of surface binding and cross polymerization occurring with molecules that comprise the film.

Hydrosilation chemistry, either via solution based methods or aerosol deposition is currently the most widely used method for passivating silicon and silicon oxide surfaces. Multiple variations of these methods have been devised which create well ordered SAMs with a myriad of potential head group, chain substituent and end group functionalities. The number of methods by which well ordered films can be produced are numerous; techniques can employ equipment such as a Langmuir trough,[87] but are more often simpler, solvent based preparations. Alkylsilane thin films can be made from a variety of solvent systems including, but not limited to hexadecane,[15, 78] THF, hexanes,[88] toluene,[89] or mixtures of solvents.[72, 76, 90] Data collected while characterizing these SAMs show that well ordered self-assembled films on the oxide layer of Si(100) can be constructed via all of these methods, however, several of the methods which produce well ordered films on nominally flat interfaces have proven unable to do so on surfaces possessing nanoscopic curvature,[88] indicating that care must be taken during the

assembly process, as a number of reaction conditions have to be optimized to produce a film with the desired results.[76] While spectroscopic data for these various functionalization methods can be compared, very little to no work has been performed evaluating the relative mechanical performance of the films produced by the various methods.

The potential shown by SAMs to act as lubricants in MEMS devices has seen considerable interest applied toward research of these systems on silicon surfaces with researchers focusing on a wide range of properties in an effort to find a SAM system with the ability to protect MEMS contacts over reasonably useful device lifetimes.[4, 7, 11, 14, 91-94] Early examples studied the effects of varying molecular interactions between SAMs on opposing surfaces by changing end-group functionalities,[95-99] with the interactions between tips and substrates functionalized with SAMs possessing varied functional groups was highly dependent of nature of the end groups used. In one study, both AFM tips and substrates were functionalized with either methyl or carboxylic acid terminated SAMs and their interactions were probed using force-distance spectroscopy. When tips and substrates were coated with different functionalities (CH_3/COOH), the observed adhesion values were lowest, owing to the relatively low amount of non-bonding interactions expected between polar and nonpolar end groups interacting during contact. The amount of adhesion was observed to almost double when both tip and substrate were coated with methyl terminations; when tips and substrates were both coated with SAMs possessing polar carboxylic acid terminations the interactions were the greatest, with adhesion values three times greater than the next highest interaction.[100]

Perhaps of more critical importance to developing films for MEMS device operation is the understanding of what role interfilm interactions play in the stability of the film and by extension, its ability to inhibit wear on the surface. Most likely the most important aspect of film ordering is the packaging density of the SAM's constituent molecules. The overall ordering and structure of a self-assembled film is directly related to the number and spacing of the molecules comprising it. The interactions between neighboring molecules dictate the stiffness of the film, as is seen in films with long chain constituents which produce stiffer and more well ordered films than their shorter chained analogs. This is mostly due to the greater number of interchain van der Waals interactions available to the longer chains. Packing density is controlled by a number of factors mostly revolving around the chemical makeup of the molecules which comprise the film and the number of available surface sites to which these molecules can bind. Molecular factors that influence packing density and the overall ordering of the film can include the creation of inter-chain lateral interactions, molecular orientation and variations in chain length,[33, 101, 102] the accidental or intentional inclusion of chain entanglements or defects within the film,[103-107] as well as head group functionalities.[108] As such, all of these factors influence the tribological properties of these SAMs.[100, 109-113]

Increasing the packing density of the chains improves the overall order within a monolayer, explaining why longer chain SAMs, which are stabilized by a greater number of van der Waals interactions are better able to maintain order during shearing and possess better performance than films composed of shorter chains. Figure 1.3 readily demonstrates this trend as dodecanethiol monolayers on gold (C_{12}-SH) are

compared to an analogous dodecycltrichlorosilane film formed on the native oxide layer of Si(100) (C_{12}-$SiCl_3$).[114]

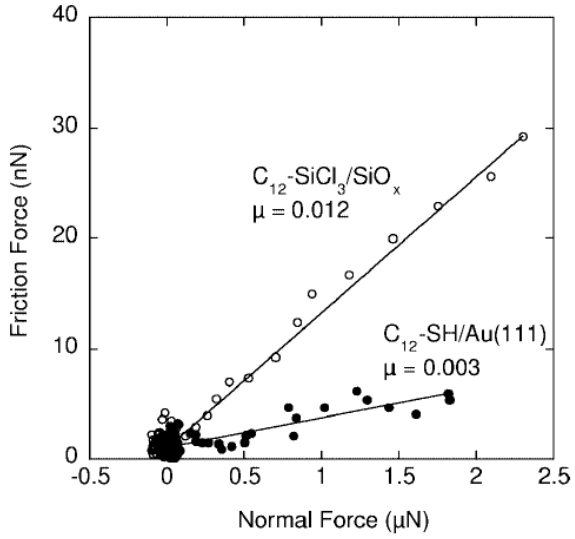

FIGURE 1.3: Friction versus load map for a dodecanethiol (C_{12}–SH) SAM on Au(111) (•) and dodecyltrichlorosilane (C_{12}–$SiCl_3$) SAM on silica (◦). The friction coefficient (μ) of the C_{12}–$SiCl_3$ film is seen to be approximately four times greater than the friction coefficient of the C_{12}–SH film. Reused with permission. Copyright 2001 Plenum Publishing Corporation.[114]

When both films were probed for their adhesive properties, the authors discovered that packing density had little to no effect on the observed adhesion values, as both films produced similar results. However, when the films were probed for their relative friction response under load, their relative performance was found to be quite different. The C_{12}-SH films revealed a relatively low friction coefficient of 0.003, typical of alkanethiols on gold. Conversely, the C_{12}-$SiCl_3$ films displayed a friction coefficient three times higher than their more densely packed analogs, clearly

demonstrating the importance of self-assembled monolayer packing density to tribological performance. These conclusions are supported by studies of the frictional response for two phases of an OTS coated Si(100) substrate. It was reported that higher density portions of OTS SAMs display much lower relative friction over a range of loads than more liquid crystalline, lower density portions of the same SAM.[91]

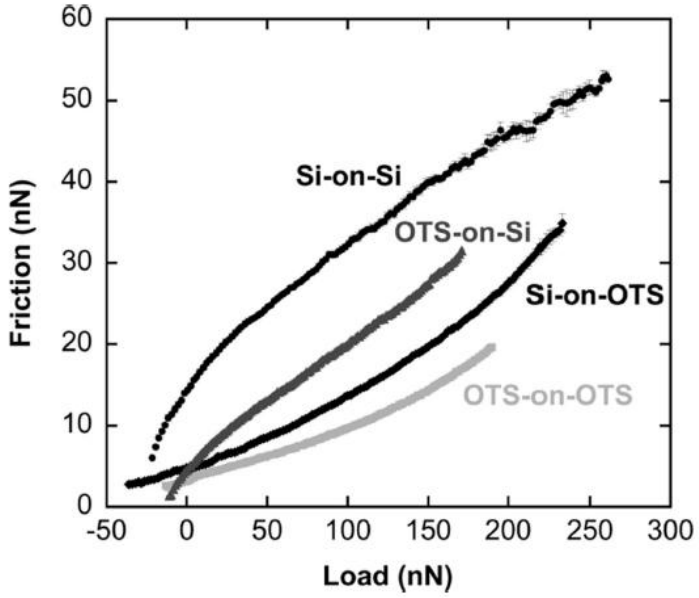

Figure 1.4: Plots of friction versus load studies of bare silicon AFM probes on bare silica surfaces (Si-on-Si), bare silicon probes on OTS SAM coated surfaces (Si-on-OTS), OTS coated probes on bare silicon surfaces (OTS-on-Si), and OTS coated tips on OTS coated surfaces (OTS-on-OTS). Reused with permission from. Copyright 2007 American Chemical Society.[91]

Flater and Carpick studied the frictional properties of OTS monolayers in great detail, precisely monitoring and accounting for experimental parameters inherent with AFM based tribology measurements while making comparisons of the interfacial

properties of OTS functionalized and unfunctionalized AFM probes on both OTS functionalized and unfunctionalized Si(100) substrates.[91] Reported work of adhesion values for systems where one or more surfaces were functionalized with an OTS film were five times lower than the interactions between unfunctionalized tips and substrates. The large increase in adhesion for the two unfunctionalized surfaces can most likely be attributed to the interactions between surface silanols on both the tip and substrate; while the large distribution in adhesion values observed is most likely owed to the random distribution and density of the surface silanols and their charge interactions with the silanols on the AFM tip.[115] Figure 1.4 shows the results of friction versus loading ramps for each variation of functionalized/unfunctionalized tip and substrate interactions. The authors found the curve for the interaction between unfunctionalized tips and substrates displayed the sublinear behavior typical for single asperity contacts. When the same tip was used to probe an OTS coated substrate, the friction versus load response manifested itself in a superlinear manner, as did OTS coated tips when interacting with OTS coated substrates. The superlinear behavior was attributed to kinematic contribution to the friction signal which arose from the additional force needed for the tip to plow through the film assembled on the substrate. Interestingly, when an OTS coated AFM tip was used to probe a Si(100) surface, the friction versus load curve demonstrated a similar, sublinear behavior as was seen in the Si tip on Si(100) substrate system, indicating that the surface chemistry of the asperity is much less influential to the friction versus load response was the surface chemistry of the substrate in single asperity experiments.

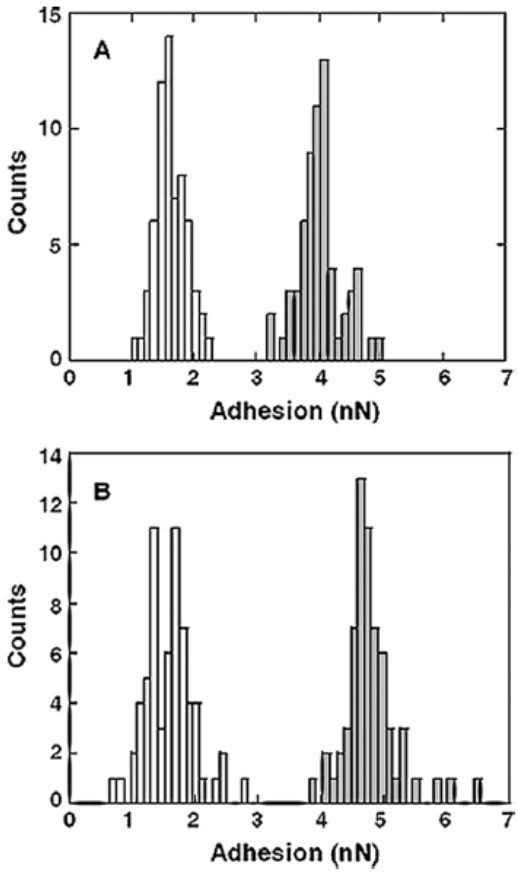

FIGURE 1.5: Adhesion plots for a ■: bare silicon tip and OTE covered surface; ■: OTE covered tip and bare silicon surface measured before A) and after B) performing a separate friction measurement. Each data set contains a histogram of adhesion distributions for 64 adhesion measurements at different locations on the substrate. The shift in the distribution for the bare silicon tip indicates that the unmodified tip was worn during the friction studies. Reused with permission. Copyright 2008 Wiley Periodicals, Inc.[116]

Figure 1.5 shows adhesions distributions between an octadecyltriethoxysilane (OTE) functionalized AFM tip with an unfunctionalized Si(100) substrate (white) as well as an unfunctionalized AFM tip and an OTE SAM on a Si(100) substrate (gray) before (A) and after (B) friction measurements were collected.[116] Adhesion forces

between the OTE functionalized silicon surface and the unfunctionalized AFM tip were higher than those between the functionalized tip and unfunctionalized substrate before and after the friction measurements. Interestingly, the adhesion was clearly seen to increase after the friction experiments for the unfunctionalized tip, indicating that the unfunctionalized tip wore during the friction studies, increasing the contact area between the tip and the substrate, while the surface functionalization on the OTE coated tip was able to limit or inhibit wear during use.

Other work has moved away from single molecule systems to more closely observe the behavior of systems comprised of two or more different types of molecules, in hopes that multicomponent systems can provide additional lubricant properties over films comprised of a single component. Examples include SAMs with different molecules integrated into the actual SAM matrix,[73] or systems where a separate, mobile lubricant is applied on top of the self assembled film to create a second, liquid phase on the surface of the original film.[59] In the case of mobile lubricant systems, it was observed that the addiction of planar cyclopentane which had been functionalized with alkyl chains to the surface of an OTS SAM improved the performance of the friction response of the film compared to the SAM alone. This multicomponent film also displayed more longevity under wear than the OTS film. The authors attribute the improved performance to the ability of the planar molecules to act as mobile lubricants between the contacts, dissipating load and decreasing friction through minimizing interactions between the tip and the monolayer. It was also suggested that the presence of the mobile component endowed the film with some amount of self-healing ability as

the mobile lubricant could settle into areas where the lower lying SAM had been damaged, protecting the exposed surface and in essence, repairing the film in situ.[59]

In the case of mixed SAMs containing straight chain components of different lengths, performance was reliant on the relative number of methylene units comprising the different chains, with films containing relatively long chains combined with shorter chains outperforming both single phase OTS SAMs as well as mixed films of two longer chained constituents. Figure 1.6 demonstrates the nature of the friction versus load response for an OTS SAM and three different mixed SAMs in air, with two component SAMs displaying a linear friction response with respect to load while the pure OTS film and film comprised of OTS and hexadecyltrichlorosilane clearly display nonlinearity at lower loads as well as higher friction response at larger loading values than the other two mixed films. The differences can be attributed to the physical makeup of the films. For example, SAMs comprised of short chained molecules are more disordered and loosely packed, inhibiting their ability to protect the surface from asperities it comes in contact with; contrastingly, films of long chained molecules can form denser, more crystalline films that reduce friction and better protect the surface during contact. Mixed SAMs containing both long and short chained molecules behave as a low density, liquid film bound to a crystalline support. The combination of these two phases produces a film that is both dense enough to protect the surface but also exhibits low shearing due to the presence of the surface liquid phase to which the authors attributed the lower friction response at higher loads.

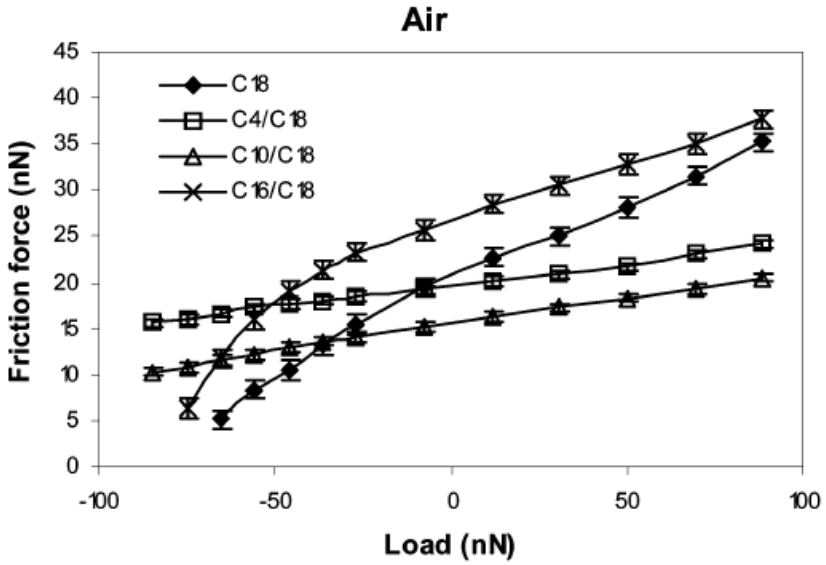

FIGURE 1.6: Friction versus load maps for bare AFM tips and mixed monolayer SAMs. The sliding speed for each measurement was 4 μm/s and the same AFM tip was used in all measurements. Reused with permission. Copyright 2005 American Chemical Society.[73]

1.5 Probing Asperity-Asperity Contacts

While a great number of AFM tribological studies have been performed on flat surfaces, far fewer studies have probed actual asperity-asperity contacts in order to more closely mimic those contacts seen in real interfaces, as surfaces that appear smooth on the macroscopic scale often posses nanoscale roughness. As MEMS devices are typically constructed from machined polysilicon, the surfaces of MEMS typically exhibit nanoscale roughness with asperities typically being on the order of 10-20 nm.[17] The presence of these asperities dictates that even long range interactions between surfaces will be focused at the site of asperity-asperity contacts such that designed and even incidental interactions between these surface asperities will control adhesion, friction

and wear between them.[12, 117] With the majority of any applied load being directed through these asperity contact sites, extremely high pressures are localized at the contact points, causing the materials to fail when the local field stresses exceed the failure strengths of the materials.[12] AFM has become the nanoscale tribology tool of choice due to the fact that the probe contact radius exhibits nanoscopic curvature on the order of a typical polysilicon surface asperity, thus creating a reliable single asperity study platform.

Much like self-assembled films on flat surfaces, the packing density and ordering inherent within the film is dependent on the chemical composition of the molecules of which it is comprised. However, unlike SAMs assembled on nominally flat surfaces, the structure of a molecular film is correlates to the curvature of the available surface asperities on which it is assembled, as these nanoscopic asperities as well as their applied films must be able to resist wear during device operation. Understanding how these films assemble and the nature of their surface structure is of the upmost importance. Both alkylsilane and fluorosilane based SAMs have been shown to reduce friction and adhesion in MEMS,[12] yet much is still unknown about the nature of the film when assembled on a real surface, whether it be a surface that is the result of a micromachining process or a surface where roughness has been purposefully introduced as a means to reduce stiction.[8] Studies aimed at understanding the nature of these films when assembled on surfaces with nanoscale curvature often utilize self-assembled films on AFM tips and it is often assumed that these films possess a similar make-up as their analogs on flat surfaces,[118-126] yet FTIR studies of alkylsilane SAMs assembled on

surfaces possessing radii of curvature on the order of a typical asperity seen in a MEMS device have shown this assumption to be incorrect.[88] Studies of alkylsilane SAMs utilizing IR spectroscopy have determined that in the absence of lateral interactions within the SAM matrix, the film cannot exist in a crystalline state and the long range order of the monolayer is reduced.[127] Similarly, molecular dynamics simulations of SAMs under compression reveal the formation of gauche defects within a SAM occur during the initial stages of compression and begin to propagate,[128] with these gauche defects altering the typically trans conformations of the molecules in the film, reducing the number of stabilizing chain-chain interactions, weakening the film and reducing its ability to protect against wear,[129] and in doing so, must be accounted for in some way.

Figure 1.7 displays the relationship between asperity size, the number of lateral chain-chain interactions and the overall ordering of a self-assembled film when assembled on silica surfaces possessing nanoscale curvature.[88] In this study, silica nanoparticles ranging in size from 7 to 40 nm in diameter were functionalized with straight chain alkylsilane SAMs comprised of molecules possessing between 8 and 18 carbon atoms, respectively. The relative ordering within each SAM was observed using FTIR spectroscopy to track the location of the CH_2 asymmetric stretching band. This particular peak has been shown to provide a qualitative indication of the relative order within self-assembled films and lipid bilayers.[130-138] The results clearly indicate that both surface curvature and the number of available methylene-methylene interactions available to the molecules within the film dictate the amount of stability within the SAM, with shorter chains substituents producing films with less internal order than those

with longer chains. Also, the radius of curvature of the surface plays an important role in monolayer ordering, with films able to better order themselves on surfaces exhibiting lower degrees of curvature until the curvature becomes so large that the surface essentially becomes flat and the ordering mimics that of SAMs assembled on flat, crystalline substrates.[89] This research provides a simple method to directly probe the ordering of SAMs on asperities and AFM tips.

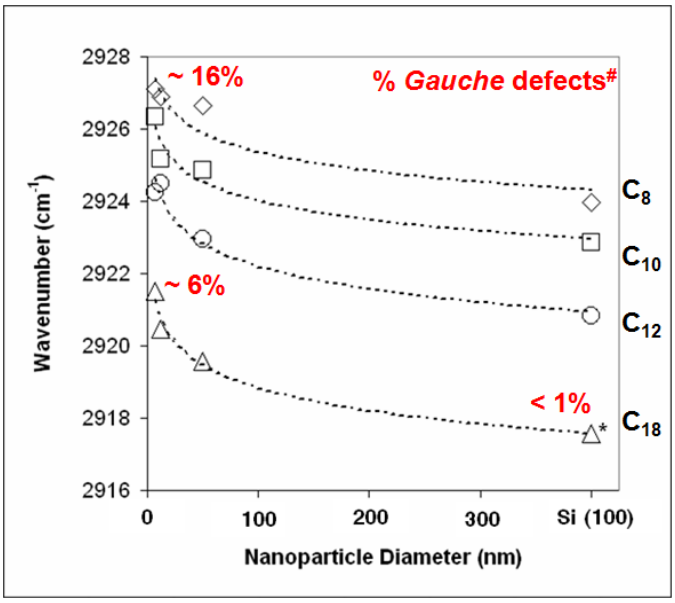

FIGURE 1.7: Plot of the influence of molecular film chain length and asperity size on monolayer ordering. Plots represent data for nanoparticles functionalized with straight chain alkylsilane SAMs with chain lengths of: a) 18 - □; b) 12 - ○; c) 10 - □; and d) 8 - ◊ carbon atoms. *The values used for 400 nm particles are the actual values found for these SAMs on Si(100), as previous studies have shown that films assembled on 400 nm particles exhibit the same type of ordering as films assembled on flat substrates.[89] #The gauche defect percentage is estimated based on temperature dependant IR data collected by molecular dynamics simulations.[132] Reused with permission. Copyright 2009 American Chemical Society.[88]

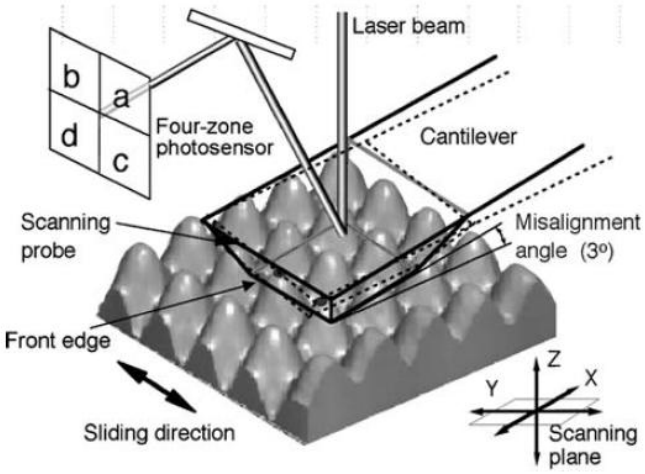

FIGURE 1.8: Schematic of an asperity-asperity probe utilizing an AFM based probe and a Focused Ion Beam manufactured multi-asperity array. The maximum number of contact points is reported to be two, but only when the edge of the flat probe aligns with the direction of the array. Reused with permission. Copyright 2007 Springer Science+Business Media, LLC.[139]

Ando and coworkers utilized a focused ion beam (FIB) manufactured two-dimensional silicon asperity array to test the effects of a SAM film on the friction and pull-off forces (Figure 1.8).[139] The arrays were comprised of a number of milled 25 μm^2 areas with equally spaced asperity peaks ranging from 200 to 2500 nm in radius of curvature. The arrays were functionalized with a variety of alkylsilanes and it was determined via AFM that the friction coefficient for each was equivalent to the inverse of the alkyl-chain length of the SAM. However, the adhesion between the testing probe and the surfaces was discovered to correspond to the radius of curvature of the asperity peaks, with larger curvature radii corresponding to lower friction response. The observed magnitude of the pull-off force was found to approximate the capillary force

between the probe and substrate while taking into account the contact angle of water on the surface of the particular SAM.

While Ando's systems produced a number of interesting results, the amount of time and cost used in creating the FIB based arrays make it difficult to produce a high number of substrates in a manner that could be considered inexpensive in terms of time and total cost. In comparison, spin coated nanoparticle films have been shown to be a simple, stable and inexpensive substrate by which to directly probe asperity-asperity interactions with AFM.[116, 140]

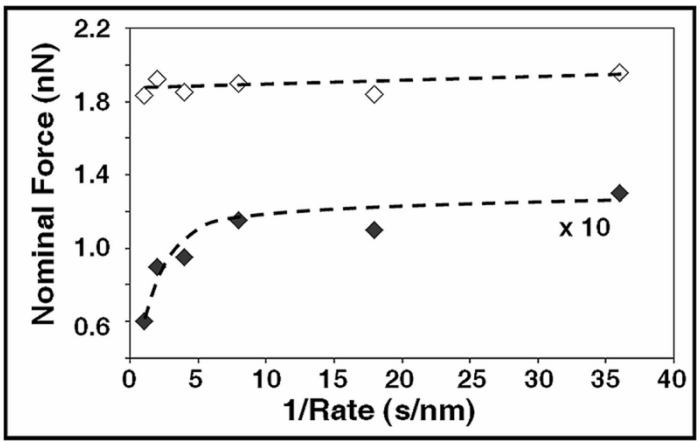

FIGURE 1.9: Adhesion forces between OTE modified AFM tips and OTE modified silicon substrates (◊) exhibited on a small dependence on attract and approach rate, while adhesion forces for OTE modified AFM tips and OTE modified 40 nm spin coated films (♦) where not only ~ 15 times lower, but demonstrated a clear dependence on approach and retract rates where adhesion values were much higher for slower approach/retract rates. The data for the OTE modified AFM tips and nanoparticle surfaces (♦) have been scaled by a factor of 10 for comparison. The lines connecting the data points are intended only to be guides to the eye and do not denote any trend. Copyright 2008 Wiley Periodicals, Inc.[116]

By utilizing AFM tips in conjunction with spin coated nanoparticle films; the authors were able to directly observe real asperity-asperity contacts utilizing AFM, in particular, they were able to directly investigate the tribological behavior of self-assembled films on surfaces possessing nanoscopic curvature.[116, 140]

While SAM coatings reduced friction and adhesion in both flat and nanoparticle surfaces compared to their unfunctionalized analogs, it was reported that SAM modified surfaces with nanoscopic curvature were less adhesive than SAMs on flat surfaces, and that the measured adhesion of the nanoparticle films was dependent on approach and retract rate.[116] Adhesion measured between the OTE modified tip and the OTE modified spin coated nanoparticle surface was also found to be approximately 15 times smaller than the same type of self-assembled film on flat silica substrates. Measurements of adhesion between OTE functionalized AFM tips and both OTE modified silicon surfaces and OTE modified silica nanoparticle spin coated films were found. Figure 1.9 shows the measured adhesion forces for each experiment. The measured adhesion between the OTSE functionalized AFM tip and a likewise functionalized flat Si substrate was found to be approximately 15 times greater than the measured adhesion between OTE functionalized AFM tips and OTE functionalized spin coated nanoparticle substrates. Perhaps more interestingly, the adhesion forces acting on the OTE coated AFM tips and the OTE modified silica nanoparticle surfaces demonstrated a clear dependence on the probe's approach and retract rates during adhesion testing. Intriguingly, higher adhesion forces were always observed at slower approach and retract rates. This phenomenon was attributed to the reduced radius of contact between the AFM tip and the nanoparticle

substrate compared to an AFM tip and the flat silicon substrate. According to JKR theory, the adhesion between the contacts is directly proportional to the reduced radius of the contact itself, where the adhesion force (F_{adh}) is determined by the equation:

$$F_{adh} = -\frac{4}{3}\pi W_{adh} R$$

where W_{adh} is the work of adhesion between the tip and the sample, $R = R_1R_2/(R_1 + R_2)$ and R_1 and R_2 are the respective radii of the two surfaces in contact.[141] Taking into consideration that the reduced radius of the contact between the tip and the nanoparticle surface was only approximately 30 percent less than that of the tip/flat surface interaction, the relative contact area between the two experiments does not explain the difference in the observed F_{adh} values. It was concluded that the discrepancy was based in the molecular organization of the SAMs on the various surfaces and that the results indicated the presence of some sort of equilibrium process at work during the force-distance measurements.

Similar to research of mixed monolayers in single asperity studies,[73] mixed monolayers have also recently been demonstrated to show some promise in mitigating wear in asperity-asperity contacts. Uptake of a mobile lubricant molecule into the self-assembled film matrix has been shown not only to reduce friction but also to improve the overall function of a self-assembled OTS film on spin coated nanoparticle substrates.[140] The inherent disorder found within a film assembled on an asperity surface provided the avenue to act as both a source and a sink of a short chained alcohol, 3-phenyl-1-propanol, which acted as the mobile lubricant in the multicomponent film. These mixed films also appear to have some capacity to self regenerate as they uptake and release the

mobile lubricant similar to systems which use a continually regenerated alcohol vapor to lubricate MEMS devices.[142] These films suggest a simple to use, self-assembly based method for lubricating MEMS may yet be achieved.

1.6 Summary and Outlook

Nanotribology has grown from simple studies examining the friction response between two interacting surfaces to a field which encompasses an array of materials, techniques and environments while examining the processes of wear down to the most fundamental of levels. Atomic scale wear studies seek to discover and alleviate the most basic causes of wear. Self-assembled monolayers have now been studied for decades as both a method to readily change the surface chemistry of materials and perhaps more importantly, as a means by which to lubricate the contacts within microscale devices. While much work has focused on the nature of single asperity contacts, a shift towards research on surfaces that more closely mimic those seen in materials, especially those used in microscale devices is just beginning. A number of questions remain unanswered when considering how materials behave in true asperity-asperity junctions. Spin coated nanoparticle substrates provide a simple and inexpensive means by which to create substrates that allow for asperity-asperity research to be readily conducted. In addition to conducting research on more complicated substrates, a virtually inexhaustible number of molecule combinations for multicomponent films exist; simple films possessing chains of differing lengths, or more complicated systems possessing various interchain and end group interactions or films with mobile character can be conceived. There also exists a major need within the scan probed tribology community to create experimental

standards that ensure the information collected by a myriad of researchers can be more easily correlated with information gathered by others. While the AFM has proven to be the workhorse of nanoscale tribology research, improvements in experimental methods, especially the development of rigid, standardized characterization requirements for the probes used during experimentation is paramount to ensure results are comparable from study to study.

1.7 Introduction to Subsequent Chapters

The information which follows in this dissertation will cover the areas of self-assembled film formation on curved surfaces and explore the tribological properties of the resultant films. Chapter II will briefly outline the experimental methods most commonly called upon during the research described throughout the rest of the material; what effects curvature radius and film constituent chain length have on self-assembled film ordering are examined in Chapter III. The fourth chapter is dedicated to introducing a new self-assembled film based MEMS lubricant which uses the lubrication power of an additional, physisorbed material to protect contacting interfaces during operation. Chapter V expands on the previous chapter and reports on the affects that environmental conditions have on these multicomponent self assembled films. How these self-assembled films behave in regards to probing rates is discussed in Chapter VI. Finally, Chapter VII provides a summary of the material presented herein.

CHAPTER II

EXPERIMENTAL METHODS

2.1 Silane Self-Assembled Monolayer Formation

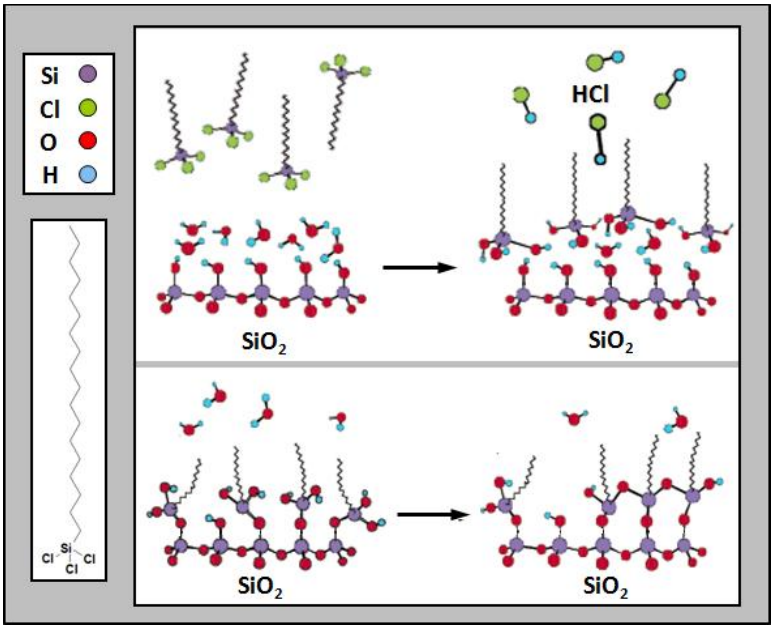

FIGURE 2.1: Schematic diagram of silane SAM formation on SiO_2 modified from reference.[76] Reused with permission. Copyright 2003 American Chemical Society.[76]

Due to the abundant amount of research focused on self-assembled films, and specifically self-assembled films on silica surfaces specifically, the formation of SAMs on silica surfaces has been highly researched.[74-84] It is known from SAM assembly on flat surfaces, such as the native oxide layer on Si single crystals that film formation proceeds via one of two proposed pathways. The first is an island aggregation process by which molecules aggregate in solution forming floating islands which eventually bind

with the surface and grow together to form complete films.[80, 84] A second proposed pathway is a more continual process whereby a slow accumulation of OTS molecules evenly distributed across the substrate slowly build up over time and as more and more molecules bind with the surface, growth is eventually halted once a single layer is formed.[85] The means by which the film constituents bind to the surface is through a surface hydrolysis reaction where water molecules physisorbed on the surface work to facilitate the reaction (Figure 2.1). As such, hydrosilation chemistry is typically employed when functionalizing silicon surfaces with silane SAMs as the various methods utilizing the process have been shown to form well ordered films on flat substrates, yet it has been shown that because a variety of reactions can occur during film formation, care must be taken to ensure the resulting films possess the required properties of a well ordered silane SAM.[76]

2.2 Fourier Transform Infrared Spectroscopy

Fourier Transform Infrared (FTIR) Spectroscopy was utilized throughout this research as means to determine if surface functionalization had occurred, to measure the amount of order within a self-assembled film after surface functionalization as well as to determine the relative amount of solvent intercalated into the SAM matrix. It is known that the location of the CH_2 asymmetric can be used to qualitatively estimate the relative amount of ordering within the self-assembled film. The total degree of film disorder can be observed experimentally as a shift in the location of the CH_2 asymmetric and symmetric stretch frequencies in the FTIR spectrum, which is known to occur as the

number of *gauche* defect sites in the film increase and the film becomes more disordered.

2.3 Atomic Force Microscopy

Atomic force microscopy is a high resolution form of scanned probe microscopy with reported resolutions in the realm of fractions of a nanometer, well below the optical diffraction limit. The AFM was the natural evolution of the Scanning Tunneling Microscope (STM), developed by Binnig and Rohrer at IBM in the early 1980's and earning the pair a Nobel Prize in Physics in 1986. Binnig, Quate and Gerber developed the AFM due to a desire to analyze nonconductive samples, which was impossible with the STM.[143] Since its development, the AFM has become one of, if not the principle instrument for conducting research at the nanoscale. AFM data is acquired by interacting with the surface using a mechanical probe that is either 1) in contact with the surface, 2) in a state of intermittent, oscillating contact with the surface, or in some rare cases 3) by simply interacting with long range forces between the probe and sample with no contact at all. The interaction between the probe and sample is controlled by piezoelectric translators that enable precisely defined movement based on data interpreted by the feedback loop during scanning.

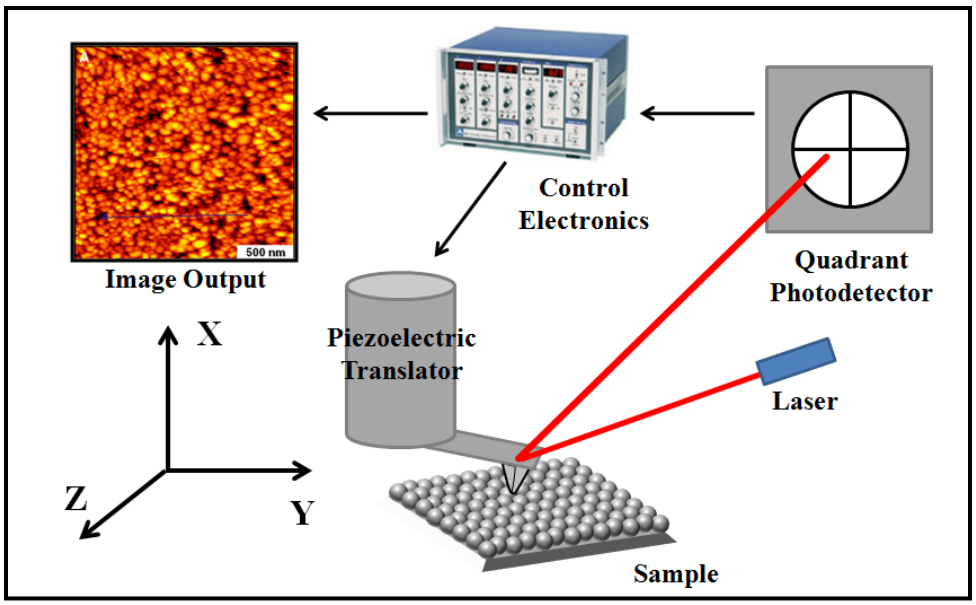

FIGURE 2.2: Schematic Diagram of an Atomic Force Microscope (AFM).

Due to this precise control, the AFM is the most commonly utilized tool in nanotribological research. The AFM has moved to the forefront in nanotribology research because of its ability to easily provide a relatively simple platform to create a controllable single-asperity contact with a sample surface. Because of its sensitivity, which allows the AFM to be easily capable of obtaining atomic level precision, force data can be acquired on the nano and piconewton level. In addition, the experimental environment can be readily controlled, giving the user the ability to precisely manage most aspects surrounding the contact.

The AFM consists of a cantilever terminated with a sharp probe that is used to image the sample surface (Figure 2.2). When the tip (Figure 2.3) comes into the range of the sample's surface, the forces interacting between the tip and the sample eventually overcome the deflection strength of the cantilever and cause a sudden move into contact.

Contact between the tip and the surface is defined by many parameters. Experimentally, the chemical makeup of the tip and the sample can affect the probe-substrate interactions, while the mechanical strength of the cantilever assembly can be used to control the amount of force being applied to the surface according to Hooke's Law. Chemical forces between the tip and sample can include, but are not limited to, van der Waals forces, electrostatic forces, capillary forces, chemical bonding and bond breaking, magnetic forces, Casimir forces, and solvation forces, among others.

In most AFM systems, the deflection of the cantilever as it interacts with the surface is monitored by utilizing a laser beam reflected off of the top of the cantilever onto the face of a quadrant photodiode. As the tip travels across the sample, the control

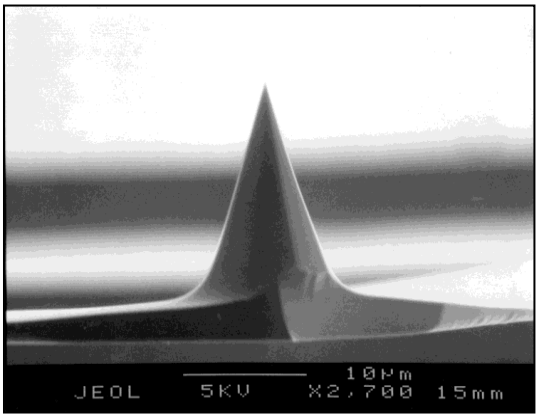

FIGURE 2.3: Close up Scanning Electron Microscope image of an Atomic Force Microscope Tip.

electronics monitor the movement of the laser spot on the detector and a feedback loop changes the height position of the tip in response to the inputs. The constant cycle of the feedback loop is necessitated by the desire to minimize damage to the probe as well as

the sample and to maintain a constant load on the surface throughout an experiment. Depending on the layout of the AFM used, either the sample or the probe is mounted to the piezoelectric translator. A typical piezoelectric translator is shaped as a tube with thin electrodes on the outside of the tube controlling translation in the x and y directions with another set of electrodes inside the tube controlling movement in the z direction.

2.4 Force-Distance Spectroscopy

One major application of AFM which gives the user the ability to measure the adhesive force interactions between the AFM probe and the sample is Force-Distance Spectroscopy. During the collection of a Force-Distance Spectrum, the AFM probe is slowly extended towards the surface until the long range interactions between the tip and the sample causes the tip to "snap" into contact with the surface (Figure 2.4). After contact, the piezo continues to press the tip into the surface until a predetermined loading force is achieved. Once the downward motion of the tip is suspended, the probe is drawn away from the surface until the tip is fully out of contact. The measured adhesion between the tip and substrate can be calculated from the resulting spectrum with the measured adhesion being the "pull-off" force measured between the tip's initial, out of contact position and its position *just before* coming out of contact with the surface during retraction. Force-Distance Spectroscopy has been used to measure a number of interactions found within nanoscale contacts; including atomic bonding, Van der Waals forces, Casimir forces, dissolution forces in liquids and single molecule stretching and rupture forces. Due to advances in modern instrumentation, state-of-the-art AFMs can readily measure forces on the order of a few piconewtons.

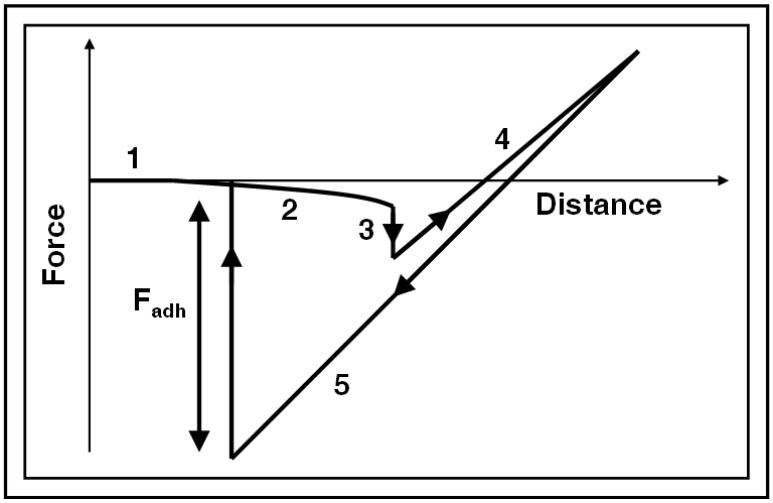

FIGURE 2.4: Schematic of an AFM Force-Distance Spectrum, which is a plot of cantilever deflection as a function of sample position along the z-axis. A typical force-distance curve consists of a non-contact region where no tip-sample interaction is observed (1), an attractive region (2) just before the tip jumps into contact with the surface (3), a contact region (4), and an adhesive contact region (5). The measured adhesion is the "pull-off" (F_{adh}) force measured between regions 5 and 1. Copyright 2008 Wiley Periodicals, Inc.[116]

2.5 Lateral Force Microscopy

Lateral force microscopy (LFM) is an AFM mode that measures and plots the lateral deflection of the cantilever that arises from forces acting on the cantilever during scanning. The lateral deflection of the cantilever can be calibrated to quantitatively determine the amount of friction acting between the tip and the surface while imaging. Lateral twisting of the cantilever can occur for a variety of reasons, but the two primary causes of these deflections are changes in the surface friction and changes in the local slope of the sample plane. As the tip travels across the surface during image collection, changes in localized surface forces cause the tip to twist in response. This is common

when the tip interacts with a portion of the sample that exhibits a higher friction response than another area, causing a greater amount of deflection in the cantilever assembly. A similar effect can be caused by a local change in the slope of the surface as the tip scans. By collecting topography and friction images simultaneously, slope artifacts can be identified and compensated for experimentally.

2.6 Thermal Gravimetric Analysis

Thermal gravimetric analysis (TGA) is an experimental analysis method used to determine the precise degree of weight change in a sample in relation to temperature. The TGA is comprised of a sampling compartment containing a sample holder attached to a highly accurate balance. The sampling compartment itself acts as an electronically heated oven as a thermocouple serves as the input for the computer-controlled temperature feedback loop. Additionally, the environment inside of the sample compartment can be purged with a variety of different gasses, typically inert species that prevent sample oxidation during the heating cycles.

As the sample is heated, a computer tracks the output from the sample balance until all temperature modulations are complete. The output tracks the changes in weight versus time and temperature. TGA was used in this research to determine the surface coverage of silane molecules on functionalized silica nanoparticles as well as to verify the relative degree of uptake of foreign molecules by the self-assembled films.

CHAPTER III

DISORDER IN ALKYLSILANE MONOLAYERS ASSEMBLED ON SURFACES WITH NANOSCOPIC CURVATURE*

3.1 Overview

Assembly of molecular layers on surfaces with nanoscopic curvature play an important role in nanoparticle functionalization, friction modification of surfaces with nanoscale roughness and derivatization of atomic force microscopy (AFM) tips. Here we have investigated the assembly of alkylsilane monolayers on silica surfaces with nanoscopic curvature using FTIR spectroscopy. It was observed that the degree of order of alkylsilane self-assembled monolayers (SAMs) on curved surfaces such as silica nanoparticles with sub-40 nm radius of curvature varies, depending on surface curvature (particle diameter), chain length, and the self-assembly reaction conditions. FTIR data show that as the radius of curvature decreases, the predominately *trans* conformations of molecules typically found for silanes assembled on smooth surfaces, such as the oxide of Si(100) begin to disappear with more radically curved surfaces exhibiting a greater numbers of *gauche* defects. The extent of disorder can be readily observed experimentally as a shift towards higher wavenumber in the CH_2 asymmetric and symmetric stretch frequencies in the FTIR spectrum, which is known to occur as the

---

*Reproduced with permission from the *Journal of Physical Chemistry - C*; Ryan L. Jones, Nicole Pearsall and James D. Batteas, "Disorder in Alkylsilane Monolayers Assembled on Surfaces with Nanoscopic Curvature" *JPCC.*; **2009**; 113(11); 4507-4514.

number of *gauche* defect sites in the film increase. Such studies of SAM assembly on silica nanoparticles also provide a convenient platform for the spectroscopic characterization of surfaces with controlled nanoscopic roughness as well as a means of evaluating the assembly of related molecules on AFM tips that possess a similar radius of curvature.

3.2 Introduction

Controlling friction, adhesion and wear of surfaces is of key importance to the proper function of micro-electromechanical systems (MEMS) devices. As the surfaces of these devices often exhibit nanoasperities on the order of 10 – 20 nm in dimension,[2] the interactions between these nanoscopic asperities during intentional or intermittent contact will dominate the tribological properties of the surfaces. In recent years, many studies have been dedicated to understanding how self-assembled monolayers may be used to modulate friction, adhesion, and wear in such microdevices.[2-4] To mimic the interactions of single asperities with surfaces, many of these studies employ functionalized atomic force microscopy (AFM) tips whose dimensions closely match those of typical nanoscopic asperties.[4, 6-11] Controlling wear at asperity-asperity contacts is vastly important in the design and construction of MEMS devices, and self-assembled monolayers (SAMs) of alkylsilane and fluorosilane compounds with chain lengths ranging from C_{10}-C_{18} have shown the capacity to reduce friction and adhesion, reducing wear in these devices.[12-14]

Much of the growing research in nanotribology involves AFM studies on model atomically smooth surfaces,[144] which leaves a need to broaden investigations to include

controlled studies of true nanoscale asperity-asperity contacts. In order to probe the molecular level tribological details of the adhesive interactions, lubricant film assembly and stability must be thoroughly understood. This becomes especially important when one considers that assembly conditions and film composition play a critical role in the performance of the film.[15]

Due to the ubiquitous nature of silica, the formation of self assembled monolayers on silica surfaces has been heavily studied.[74-84] For surfaces such as the native oxide of Si single crystals, which are nominally flat (i.e. roughness *ca*. 0.1 nm RMS over 1 μm^2) researchers have found that film formation occurs via one of two pathways. Maoz and Sagiv proposed an "island aggregation" mechanism for the formation of octadecyltrichlorosilane (OTS) SAMs, which proceeds via the aggregation of molecular islands in solution which bind with the surface and grow to form a complete monolayer.[80, 84] Wasserman and coworkers reported a "continuous" mechanism of assembly whereby OTS molecules are uniformly distributed over the surface slowly building up as more molecules were added until a well ordered SAM had formed.[85] The use of hydrosilation chemistry has become the standard method of surface passivation for silicon and silicon oxide surfaces, as it allows for assembly of well ordered organic thin films with the added ability to include desirable terminal functional moieties. However, due to the various types of reactions that can occur during deposition of SAMs it has been shown that reaction conditions can have dramatic affects on the formation and properties of the resulting films.[76]

While preparation techniques vary and include methods such as film deposition on Si(100) with a Langmuir trough as well as aerosol based functionalization of Si nanoparticles,[87, 145, 146] most assembly conditions consist of solution based methods utilizing a variety of solvent systems. Alkylsilanes have been formed on Si(100) substrates in a wide variety of solvents such as THF,[55, 147] hexadecane,[15, 78] toluene,[89] trichloromethane, carbon tetrachloride, Isopar-G,[76] and mixtures of multiple solvents such as hexadecane, THF and carbon tetrachloride.[72] Infrared and other data reported from these experiments often demonstrate that well ordered films are constructed on Si(100) oxide surfaces however, we have found that several published techniques that have been shown to produce high quality films on flat surfaces are inadequate for producing satisfactory SAMs on silica nanoparticles.

The behavior of SAMs as well as their ability to create well ordered assemblies on surfaces have been an area of interest for some time. Early theoretical studies of lipid monolayers demonstrated that phase transitions seen within monolayer films approximated the melting transitions observed in bilayer systems. These transitions were reported to resemble a first-order transition from liquid to solid surface phases mediated by a continual increase in monolayer film order.[148] Lipid bilayer phase transitions from gel to liquid crystal states can be observed by IR as a small shift in the CH_2 symmetric (d^+) stretching modes from 2850 cm^{-1} to 2853 cm^{-1}.[149] For monolayer systems such as alkanethiols on Au, the film order is found to vary depending on surface coverage, in which the films can be described as a lattice gas at low coverage, which finally condense into a final ordered solid phase at high coverages.[150] Even for high coverages however,

disorder can be imparted into a system thermally, increasing the percentage of *gauche* defects seen within the film by upwards of 10%.[151]

Despite the significant body of work on the assembly of silanes on surfaces, few studies of comparable detail for the assembly of alkylsilanes on surfaces with nanoscopic curvature such nanoasperities or nanoparticles have been conducted.[87, 90] While less work has surrounded the functionalization of silica nanoparticles,[152, 153] numerous studies have centered around monolayers on metallic nanoparticles.[154-169] Previous studies of alkanethiols on metal nanoparticles have examined thermally induced disorder in SAMs using FTIR,[159, 170] and have found that monolayer disorder increased slightly with decreasing particle size, however no correlation between changes in particle size and chain length were investigated. Other studies of thiols on gold[171] and copper[138] nanoclusters used FTIR to probe thiols of varied chain length, but the particle systems lacked monodispersity, showing a relatively broad distribution of sizes. Recent work from Bendarskii and co-workers employed IR-sum frequency generation spectroscopy to explore monolayer disorder verses particles size for dodecanethiol on gold nanoparticles ranging from *ca*. 2 nm – 25 nm in diameter, showing increased disorder with decreasing particle size.[172, 173] Similarly, it was discovered that the packing density of alkanethiols increases with chain length when assembly takes place on copper nanoclusters.[138]

Self-assembled films on larger particles, such as those used in chromatographic column packings have been found to be very disordered at room temperature due to a smaller degree of surface coverage compared to nonporous silica.[174, 175] Order in these

systems could be induced by lowering the ambient temperature below the phase transition temperature which exists at approximately 20 °C.[176] These systems were also observed to be quite sensitive to salvation effects when the films were exposed to a wide range of solvents, with these interactions typically lowering the conformation ordering within the SAMs.[177, 178]

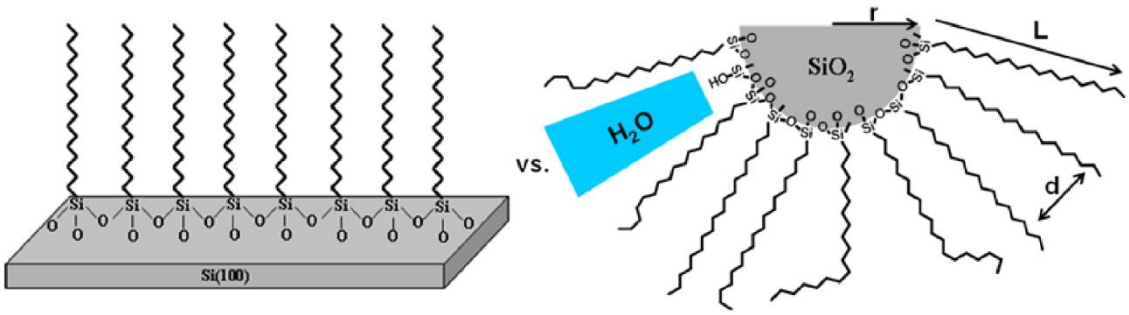

FIGURE 3.1: Schematic comparing organosilane SAM structure on a smooth oxidized Si(100) surface vs. a silica nanoparticle. For nanoparticles, as the radius (r) is reduced, the nearest neighbor chain end distance (d), must increase with increasing chain length (L), providing greater opportunity for *gauche* defect formation. Voids of unreacted surface groups may also exist which may also lead to greater film disorder and reorganization in the presence of water or other solvent molecules. Reused with permission. Copyright 2009 American Chemical Society.[88]

In this paper we compare assembly of alkylsilanes with chain lengths ranging from C_8 to C_{18} on the oxidized surface of Si(100) and their assembly on 7 nm, 12 nm and 40 nm silica nanoparticles. Molecular dynamics simulations of SAMs under compression[179] have shown that during the initial stages of compression by an asperity, *gauche* defects within the typically all *trans* conformations of the molecules in the SAM appear and begin to propagate. Thus, understanding the relationship between monolayer

order on imperfect surfaces and their ability to act as lubricant films is critical. These defects further catalyze weakening of chain-chain lateral interactions, resulting in a reduction in film integrity.[180] IR spectroscopic studies of alkylsilane SAMs confirm that without the presence of strong lateral chain-chain interactions, *gauche* defects readily appear within the molecular structure, reducing overall order within the film (Figure 3.1).[181] Spectroscopic studies of SAMs on these nanoparticle surfaces provide insight to the important question of how molecules assemble on nanoscopic asperities such as AFM tips, an issue that is rarely addressed in any AFM studies using functionalized tips.

3.3 Experimental Methods

Three sizes of silica nanoparticles (7 nm, 12 nm, and 40 nm in diameter, Degussa) and flat Si(100) substrates were functionalized with four different straight chain alkylsilanes: n-octyltrichlorosilane (C_8), n-decyltrichlorosilane (C_{10}), n-dodecyltrichlorosilane (C_{12}), and n-octadecyltrichlorosilane (C_{18}) using three separate functionalization methods. The effects that variations in chain length, nanoparticle size, as well as functionalization method have on the degree of disorder within alkylsilane monolayers were compared to the same systems on flat Si(100) substrates, using transmission FTIR to follow shifts in the methylene symmetric (d^+) ca. 2850 cm^{-1} and methylene asymmetric (d^-) ca. 2920 cm^{-1} stretch frequencies as a function of chain length and surface curvature.

While a variety of methods for functionalizing silica nanoparticles have been reported,[90, 145] our experimental techniques differ slightly from those currently in the literature. Monolayer films of the desired alkylsilanes were first prepared on cleaned and

oxidized Si(100) and silica nanoparticles through self assembly using a THF based stock solution (THF Method).[116] Before assembly, Si(100) substrates were cleaned and hydroxylated in a 4:1:1 (v:v:v) mixture of high purity H_2O, 30% H_2O_2 and NH_4OH at 80 ºC for 30 minutes. The substrates were then thoroughly rinsed with high purity H_2O and dried under streaming nitrogen. The monolayers were synthesized using a stock hydrolysis solution composed of 0.25 g of the desired SAM molecule, 0.75 mL of 6 M HCl and 20 mL of THF. The solution was then stirred for a minimum of four hours prior to use. Film formation on Si(100) was carried out in a Wheaton staining jar, using 1 mL of the stock solution and 20 mL of cyclohexane. After three hours, the substrates were removed, sonicated in THF, rinsed with high purity H_2O, and were either used immediately or stored in a vacuum until later use. For the formation of alkylsilane SAMs on fused silica nanoparticles, colloidal silica nanoparticles of 7 nm, 12 nm, and 40 nm in diameter were utilized. Self assembly on nanoparticle samples was accomplished by adding 0.2 grams of the as supplied silica nanoparticles to 30 mL of cyclohexane and 2 mL of the alkylsilane stock solution. The solution was sonicated for a period of three hours and then left to sit overnight to allow time for complete film formation. The particles were collected via centrifugation, followed by subsequent rinsing and further centrifugation in THF, high purity H_2O, and ethanol. The samples were then dried over a period of five days under streaming nitrogen and were used immediately or stored under vacuum at ambient temperatures.

Alkylsilane SAMs were then assembled on cleaned and oxidized Si(100) substrates through self assembly using a hexane based reaction solution (Hexanes

Method or HM). Each monolayer was prepared using a solution composed of 30 mL of hexane isomers and 15 μL of the desired alkylsilane and was carried out in a Wheaton staining jar. The substrates were next sonicated for 90 minutes and allowed to sit overnight. The substrates were removed, sonicated for 30 minutes in THF, rinsed with high purity H_2O, dried with nitrogen, and immediately put into the spectrometer or placed under vacuum at ambient temperature until used. For the formation of alkylsilane SAMs on silica nanoparticles using the Hexanes Method, self assembly of the desired alkylsilane on each particle was accomplished by adding 0.2 grams of as supplied silica nanoparticles to 30 mL of hexane isomers and 15 μL of the desired alkylsilane (Hexanes Method – Uncleaned or HMU). The solution was sonicated for a period of three hours and then left to sit overnight to allow time for complete film formation. The particles were collected via centrifugation, followed by subsequent rinsing and further centrifugation in hexanes and twice in ethanol. The samples were dried for a period of five days under streaming nitrogen and were again used immediately or stored under vacuum at ambient temperatures. A second functionalization of nanoparticles based on the Hexanes Method was also employed (Hexanes Method – Cleaned or HMC). The experimental procedure for the functionalization and collection process was identical, however in this scheme the particles were cleaned and hydroxylated utilizing a 4:1:1(v:v:v) mixture of high purity H_2O, 30% H_2O_2 and NH_4OH, similar to the process used on the Si(100) substrates. Typically, 0.2 g of the silica nanoparticles were soaked in 30 mL of the hydroxylation solution at room temperature for a period of 90 minutes. The

nanoparticles were collected via centrifugation, followed by rinsing twice in high purity H_2O, ethanol, and hexane isomers before subsequent functionalization.

Finally, thin films of 40 nm colloidal silica were formed by spin-coating onto cleaned and oxidized Si(100) wafers. To ensure a stable nanoparticle film during later evaluations, the nanoparticles were sintered to each other as well as the substrate by heating to a temperature of 80ºC for one minute.[37] The nanoparticle films and supports were cleaned, hydroxylated, and functionalized using the Hexanes Method. In order to ensure that functionalization could proceed in the same manner as the Si(100) substrates, nanoparticle films were adhered to both sides of the wafer and the entire sample was submerged in a Wheaton staining jar.

All FTIR measurements were carried out on a Thermo Nicolet 6700 FTIR using a liquid nitrogen cooled MCT A (HgCdTe) detector. Spectra for the monolayers on the Si(100) substrates and nanoparticle films that were functionalized after spin coating onto Si(100) supports were taken by transmission measurements at the Brewster's angle for silicon (~74º). Each spectrum was collected with 256 scans at a resolution of 1 cm^{-1}. Spectra for the functionalized silica nanoparticles were collected by transmission measurements of the silica particles suspended in a 9% functionalized nanoparticles by weight KBr matrix. Backgrounds of unfunctionalized silica nanoparticles that had undergone the same preparations steps as the functionalized particles in the 9% by mass preparation were used. These were also subsequently compared to functionalized nanoparticles spin coated on Si supports. These spectra were found to be identical to those of the functionalized particles in KBr. Each spectrum was collected with 256 scans

at a resolution of 1 cm^{-1}. All peak locations and spectral shift data reported is from raw, unaltered spectra.

3.4 Results and Discussion

All of the sample preparation methods used here were found to produce well ordered films when assembly took place on the oxidized surface of Si(100). However, when films are assembled on curved surfaces, the CH_2 symmetric (d^+) and asymmetric (d^-) stretches are seen to broaden and shift to higher wavenumber. This occurs in agreement with an increase in disorder as the location of the asymmetrical stretching band of methylene is indicative of the degree of crystallinity of the molecules in the SAM.[108, 151, 182-185] Similarly, the location of the methylene symmetrical stretching band also shifts to higher wavenumber as film ordering decreases, closely paralleling the shifts of the CH_2 asymmetric stretch.[186] Another trend apparent in subsequent figures is the intensity losses as well as the broadening of the peaks in the CH_2 symmetric stretching bands as the number of methylene units decreases, which are also indicative of increasing liquidity of the films.[77] As all of these factors are indicators of the same phenomena, and because the location of the CH_2 asymmetric stretch has become the de facto gauge of self-assembled film crystallinity, the location of the CH_2 asymmetric stretching peak will be used as the gauge for film order throughout this paper. Also worthy of note, the CH_3 asymmetric stretch appears to increase in size as the chain length decreases, which can be attributed to two factors, the first is a function of the relative number of methyl to methylene groups in the constituent film molecules, with films comprised of smaller chains exhibition a larger relative CH_3 asymmetric stretching

intensity than the longer chained species. The second is an artifact of the normalization process, due to the CH_2 asymmetric stretching frequency for shorter chain SAM constituent molecules being given the same arbitrary intensity value of one as their longer counterparts. Because of these, the relative intensity of the CH_3 asymmetric stretch peak on C_8 appears higher than those of the other species.

It has been reported that crystalline microenvironments exist when SAMs with alkyl chain lengths greater than 6 carbons are assembled on oxidized Si(100). Disordered, liquid like systems have a CH_2 asymmetric stretching band near 2924 cm^{-1}, while for more ordered monolayers, this band appears in the proximity of 2917 cm^{-1}, indicating a more crystalline state.[15] The CH_2 asymmetric stretch frequencies based on surface curvature and assembly method measured are outlined in Table 3.1.

TABLE 3.1: CH_2 asymmetric (d-) stretching frequency (cm^{-1}) for both curvature and assembly method; first standard deviation of the data is given in parenthesis.

	7 nm particles $\nu_{as}CH_2$ Location - Average		
	THF	HMU	HMC
C_8	2929 (0.3)	2929 (.3)	2927 (0.1)
C_{10}	2929 (0.8)	2927 (0.2)	2926 (0.2)
C_{12}	2928 (1.3)	2927 (0.4)	2924 (0.2)
C_{18}	2927 (0.4)	2925 (0.3)	2921 (0.3)

	12 nm particles $\nu_{as}CH_2$ Location - Average		
	THF	HMU	HMC
C_8	2929 (0.2)	2928 (0.2)	2927 (0.2)
C_{10}	2929 (0.3)	2927 (0.7)	2925 (0.1)
C_{12}	2928 (0.7)	2926 (0.2)	2925 (0.2)
C_{18}	2926 (0.3)	2925 (0.2)	2921 (0.2)

	40 nm particles $\nu_{as}CH_2$ Location - Average		
	THF	HMU	HMC / NP Films
C_8	2929 (0.8)	2927 (0.3)	2927 (0.2) / 2927 (0.4)
C_{10}	2929 (0.6)	2927 (0.2)	2925 (0.2) / 2925 (0.1)
C_{12}	2928 (0.7)	2926 (0.1)	2923 (0.2) / 2925 (0.1)
C_{18}	2927 (0.9)	2923 (0.1)	2920 (0.2) / 2919 (0.1)

	Si(100) $\nu_{as}CH_2$ Location - Average		
	THF	HMU	HMC
C_8	2924 (0.1)		2924 (0.1)
C_{10}	2922 (0.1)		2923 (0.1)
C_{12}	2921 (0.1)		2921 (0.1)
C_{18}	2918 (0.3)		2918 (0.1)

Figure 3.2 illustrates FTIR spectra in the C-H stretching region of different chain length alkylsilanes ranging from octylsilane to octadecylsilane. The location, relative

size, peak width, and shape of both the CH_2 symmetric (d^+) and asymmetric (d^-) stretching bands are consistent with an increase in the degree of disorder as the number of methylene units is reduced from 17 to 7. The location of the CH_2 asymmetric stretch peak for C_{18} was found to be centered at 2918 cm^{-1}, characteristic of a well ordered, self assembled OTS film. While the same peak frequency for C_8 was located at 2924 cm^{-1}, indicating more liquid-like behavior.

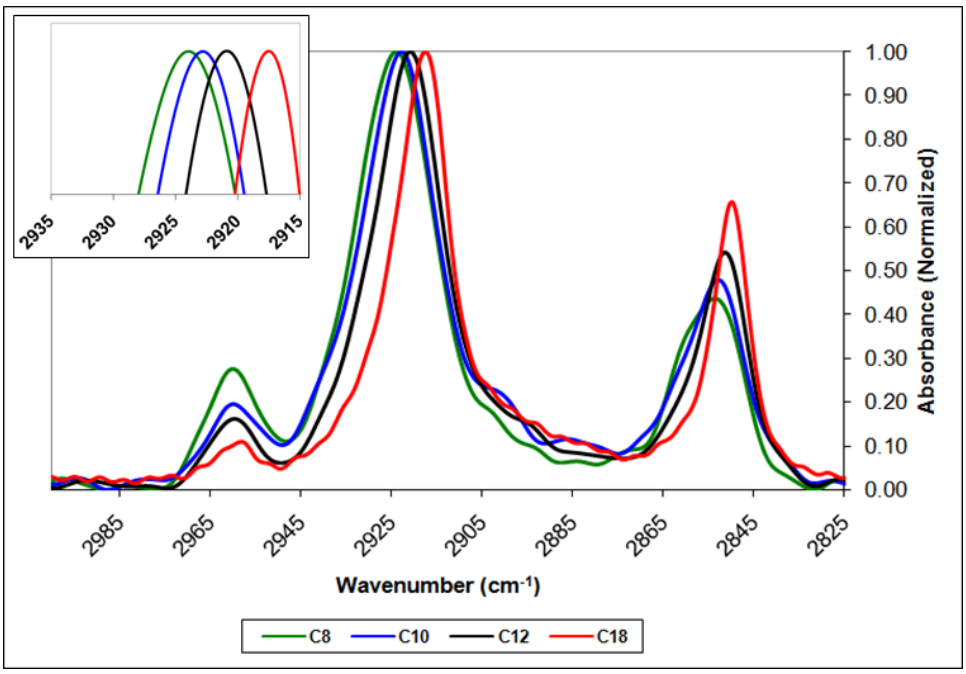

FIGURE 3.2: Transmission FTIR spectra of C_8, C_{10}, C_{12}, and C_{18} assembled on oxidized Si(100) using the HMC method, showing the variations in the methylene asymmetric (d^-), symmetric (d^+) and methyl symmetric (r^+) stretches. All spectra have been normalized to one. Reused with permission. Copyright 2009 American Chemical Society.[88]

The locations of the CH_2 asymmetric stretch for C_{12} and C_{10} (2921 cm^{-1} and 2923 cm^{-1}, respectively) points toward SAMs with both crystalline and liquid qualities. It is

noteworthy that assembly on Si(100) produces similar film quality regardless of assembly method, unlike the disparity in film order observed when assembly takes place on nanoparticles, as will be discussed below. For comparison, a spectrum of C_{18} assembled on the oxidized surface of Si(100) is included in each set of nanoparticle spectra shown.

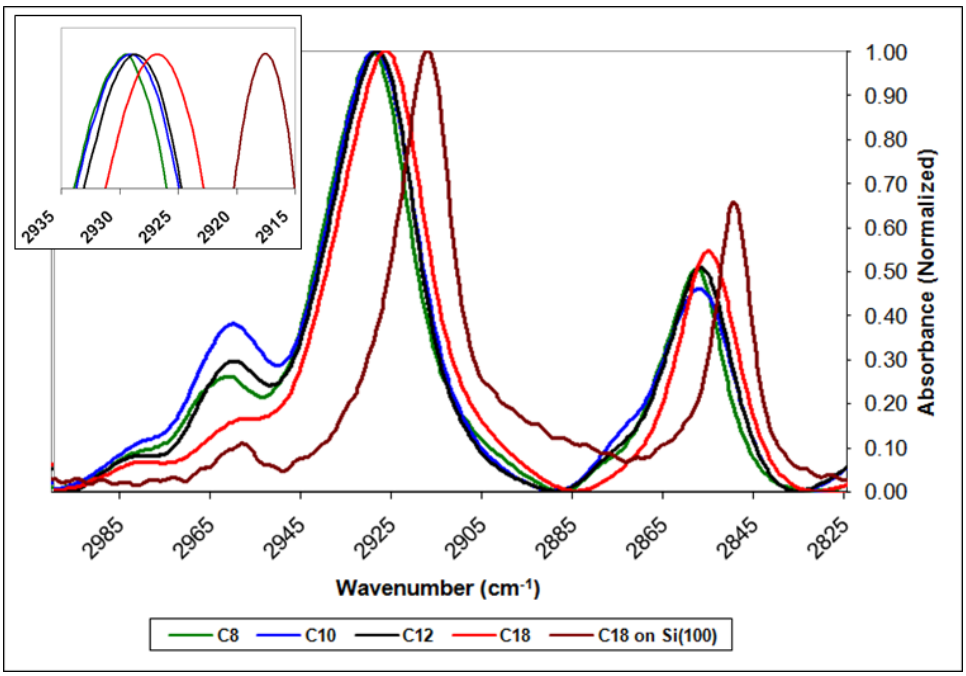

FIGURE 3.3: Transmission FTIR spectra of C_8, C_{10}, C_{12}, and C_{18} assembled on 7 nm silica nanoparticles using the THF method and C_{18} assembled on oxidized Si(100) using the HMC method. All spectra have been normalized to one. The spectra in this figure have also undergone baseline subtraction in order to more easily compare the data from nanoparticles functionalized using the THF method to those functionalized via the HMU and HMC methods. The peak at ca. 2982 cm^{-1} is due to presence of THF within the SAM matrix. Reused with permission. Copyright 2009 American Chemical Society.[88]

When assembly occurs on nanoparticles, the functionalization method was found to play a critical role in the overall quality of the SAM, unlike what has been reported

for alkylsilane based chromatographic stationary phases.[185, 187] The spectra obtained from assembly of the alkylsilanes on nanoparticle surfaces by the three different methods are shown in Figures 3.3 and subsequent figures. While relatively well ordered C_{18} films have been found to form on 7 nm and 40 nm silica nanoparticles, Raman spectroscopic studies showed a similar packing density for the two particle sizes. The actual ordering of the films however was found to be significantly different, with the authors reporting better ordering on 7 nm versus 40 nm particles,[153] in contrast to our FTIR results presented herein. Assembly on particles via the THF method (Figure 3.5) results in films with relatively low variations in order between both particle size and chain length. Assembly of C_{18} on any particle size using the THF method results in films possessing CH_2 asymmetric stretching frequencies around 2926 cm^{-1}, signifying that the films not only possess minimal structural order, but that even the additional methylene-methylene interactions that would typically increase the stability in such monolayers are unable to aid in providing order on nanoparticle surfaces under these reaction conditions. Results from variations in chain length do indicate that ordering is still dependent on the number of methylene units available to the molecules during assembly; however the overall shift in the CH_2 asymmetric stretch frequencies is considerably smaller for the THF method compared to the HMU or HMC methods. The overall shift from C_{18} assembled on 40 nm particles to C_8 assembled on 7 nm particles is approximately 3 cm^{-1} for the THF method, while these same shifts are on the order of 5 cm^{-1} and 7 cm^{-1} for the HMU and HMC methods, respectively. The high degree of disorder seen in the films produced via the THF method is likely due to the presence of THF that becomes

incorporated within the SAM matrix, which is most apparent in the spectra for these films as a distinct peak centered around 2985 cm^{-1}. Whether the THF is physically or chemically bound to the surface is unknown, however the intercalation of the relatively planar molecule is likely due to the presence of water in the reaction solution, as previous studies which have observed similar molecules (including water itself) also diffuse into an alkyl monolayer in the presence of water.[188-191]

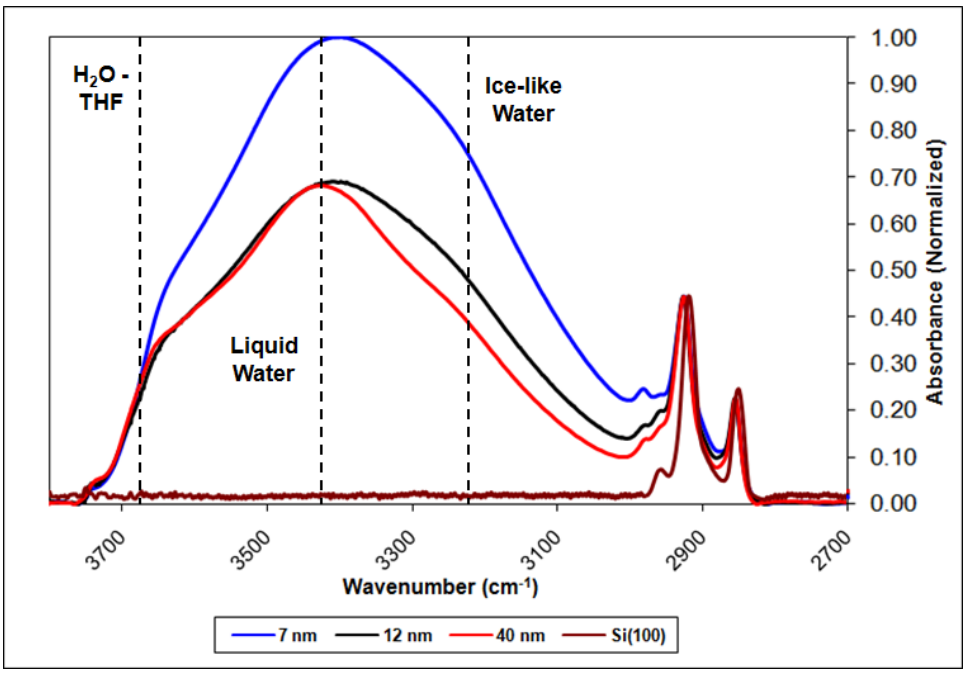

FIGURE 3.4: Transmission FTIR spectra of C_{18} assembled on 7 nm, 12 nm, and 40 nm silica nanoparticles as well as oxidized Si(100) using the THF method. All spectra have been normalized with respect to the CH_2 asymmetric stretch. The large peak centered at approximately 3400 cm^{-1} is due to the inclusion of water into the film. Evidence of both liquid-like and ice-like water are seen within the spectra; also apparent are two shoulders which correspond to water which is bound to THF via hydrogen bonds (3650 cm^{-1}),[192] shoulder around and the presence of unreacted surface silanols (3745 cm^{-1}). Reused with permission. Copyright 2009 American Chemical Society.[88]

The role THF plays inside the monolayer can be considered to be analogous to the role of cholesterol in phospholipid membranes, inhibiting crystallization of the hydrocarbons which make up the film. THF is known to have a negative effect on conformational order in chromatographic stationary phases with low film surface coverage, enhancing film mobility due to solvation effects.[185, 193]

It should also be noted that water was also observed to be intercalated into the SAM layer, as evidenced by the presence of the -OH bands around 3410 cm^{-1} for the samples prepared using the THF method (Figure 3.4). These data suggest that poor film formation will have significant deleterious effects on the ability of the SAM layer to passivate the surface and protect the underlying oxide from reaction with water in the local environment, as theoretical studies have shown for films that have been mechanically damaged.[191, 192] Unlike THF, there was no evidence signifying an intercalation of either cyclohexane from the THF method or hexanes from the hexanes methods in the SAMs. Analysis of the relative peak areas for each of the films reveals that the relative ratio of peak area for the CH_2 asymmetric and CH_3 asymmetric stretching regions correlated to the relative number of methylene and methyl groups in the given film's constituent molecule. Inclusion of either hexanes or cyclohexane into the SAMs would be further evidenced by a morphing of the peak shapes and intensities in the FTIR spectra as the relative ratios of CH_2 to CH_3 groups would become distorted.

The spectra acquired for the films assembled using the HMU and HMC methods are shown in Figures 3.5 and 3.6. Similar to the films assembled utilizing the THF method; the relative degree of molecular order within the films is dependent on both

molecular chain length and nanoparticle size. Films created via the HMU method exhibit a greater degree of order compared to those same films assembled using the THF method; while SAMs assembled using the HMC method possessed the greatest degree of crystallinity for all chain lengths.

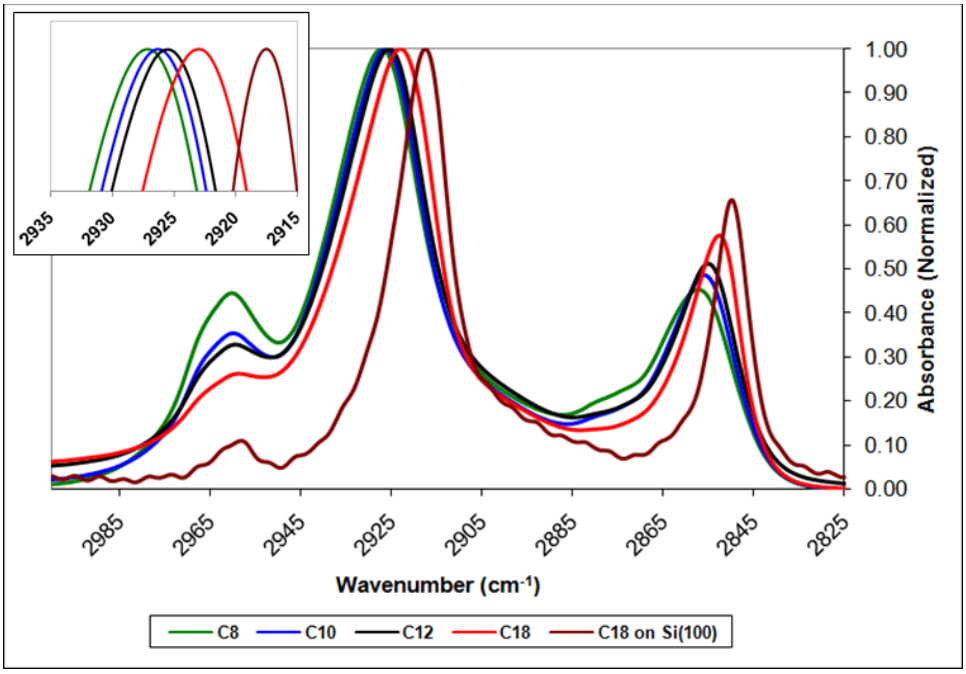

FIGURE 3.5: Transmission FTIR spectra of C_8, C_{10}, C_{12}, and C_{18} assembled on 40 nm silica using the HMU method and C_{18} assembled on Si(100) using the HMC method. All spectra have been normalized to one. Reused with permission. Copyright 2009 American Chemical Society.[88]

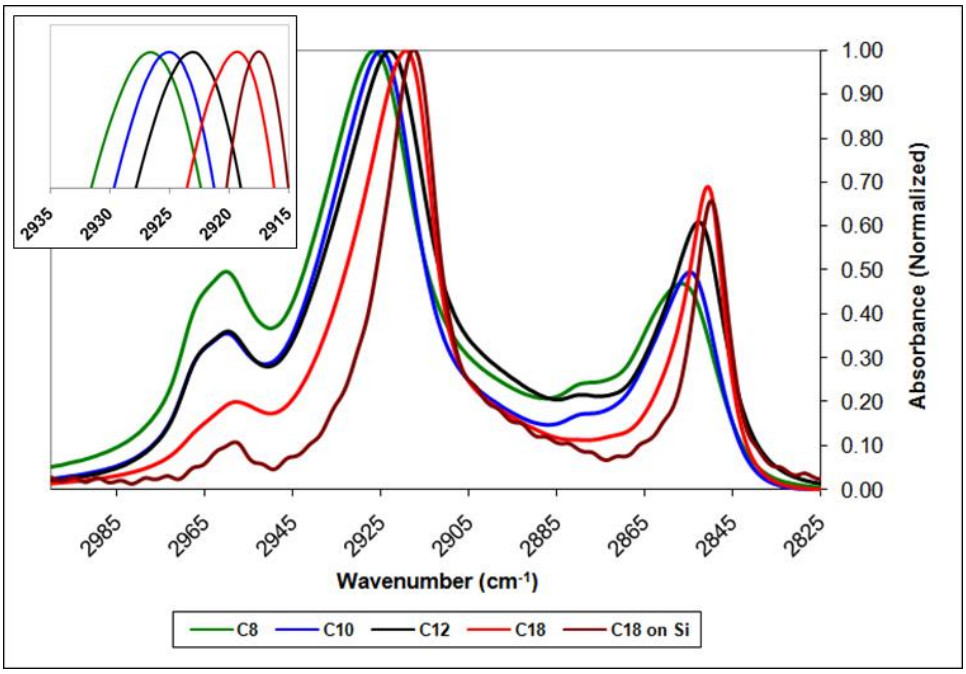

FIGURE 3.6: Transmission FTIR spectra of C_8, C_{10}, C_{12}, and C_{18} assembled on 40 nm silica nanoparticles and C_{18} assembled on Si(100) using the HMC method. All spectra have been normalized to one. Reused with permission. Copyright 2009 American Chemical Society.[88]

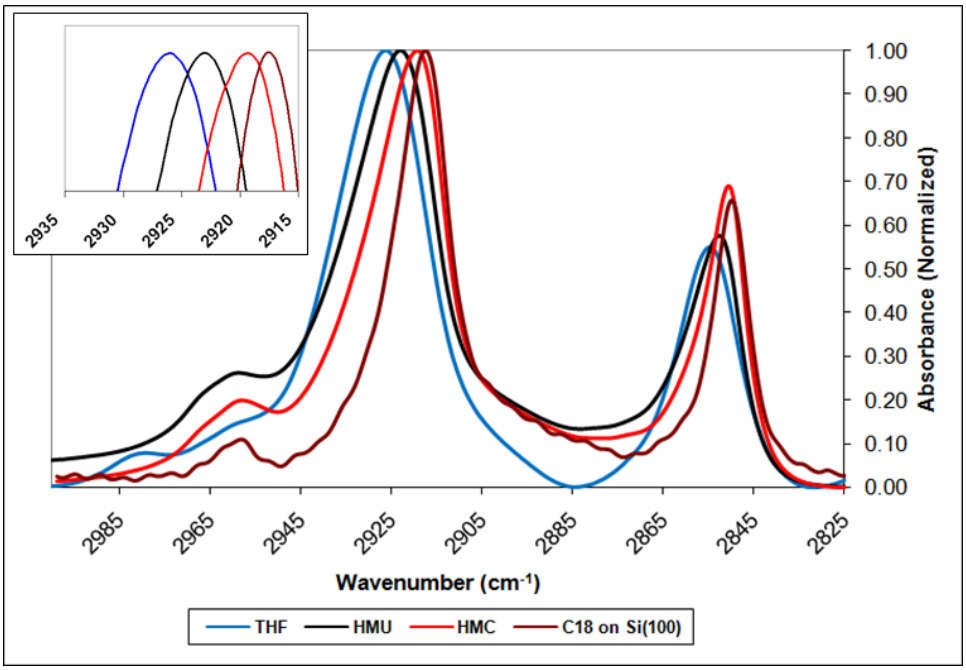

FIGURE 3.7: Transmission FTIR spectra of C_{18} assembled on 40 nm silica nanoparticles using the THF method, HMU method, HMC method, and C_{18} assembled on Si(100) using the HMC method. All spectra have been normalized to one. Reused with permission. Copyright 2009 American Chemical Society.[88]

A comparison of C_{18} films assembled via each of the methods (Figure 3.7) demonstrates this trend as OTS SAMs assembled via the HMC method are better ordered than films generated by the other methods. The formation of higher quality films via the HMC method is likely due to the increased availability of surface silanols for binding events on the cleaned particles versus the as received particles as previous research has shown OTS to assemble with a higher packing density and greater degree of ordering on silica particles possessing a higher number of surface silanols.[152, 153] Due to the higher degree of order seen for the SAMs produced via the HMC method, all further discussion will center on assembly by this method, unless noted otherwise.

As the size of the nanoparticles decrease, the shift of the peak frequencies continues to higher wavenumber indicating that higher surface curvature imparts greater disorder within the SAMs (Figure 3.8). When comparing monolayer order on flat vs. curved surfaces, a small shift in the CH_2 asymmetric stretch on the order of 2 cm^{-1} for C_{18} assembled on a 40 nm nanoparticle can be seen. For shorter chains assembled on smaller particles an even greater shift was observed.

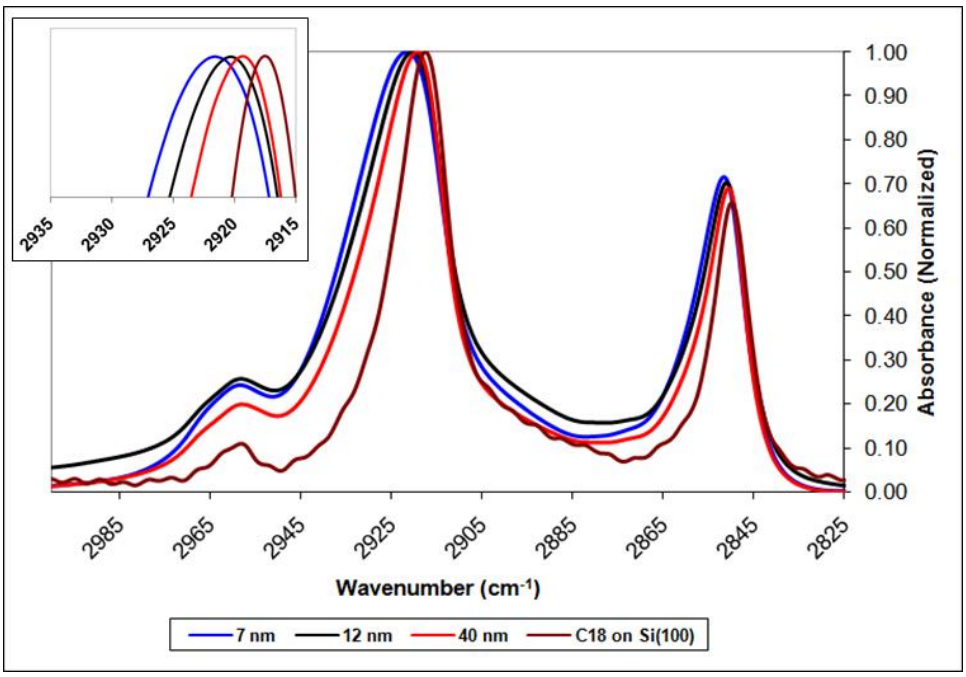

FIGURE 3.8: Transmission FTIR spectra of C_{18} assembled on 7 nm, 12 nm, and 40 nm silica nanoparticles as well as oxidized Si(100) using the HMC method. All spectra have been normalized to one. Reused with permission. Copyright 2009 American Chemical Society.[88]

The trend was less evident for films assembled via the HMU and THF methods, due to the inability of the longer chained species to assemble with the same degree of

order seen in the HMC samples. Disorder in these systems occur as increases in surface curvature allow for the ready formation of *gauche* defects manifested by a reduction in chain-chain interactions as the molecules spread apart the further they extend from the surface. Recent studies of C_{18} monolayers assembled on larger (ca. 400-500 nm) silica particles found no difference in the CH_2 symmetric and asymmetric stretching regions when compared to C_{18} assembled on flat Si substrates.[89] Additionally, assembly of OTS on 400 nm silica asperities fabricated by micromachining show the same peak positions as those on oxidized Si(100).[139] These results indicate that there exists some size limit at which curvature no longer has any bearing on assembly and the surface appears essentially flat to an individual molecule. These results for all chain lengths and particle sizes are summarized in Figure 3.9.

Another discernable trend reveals that as the number of methylene units in the carbon chain decreases, a shift toward higher wavenumber is observed as defects form in each of these systems when *gauche* conformations proliferate at the terminal functional groups.[194] The CH_2 asymmetric stretch for C_{18} on flat Si was located at 2918 cm^{-1}, but as the chain length decreased, the CH_2 asymmetric stretch progressively shifts to higher wavenumber ending with the CH_2 asymmetric stretch for C_8 being observed at 2925 cm^{-1}. When looking at the same transitions on 40 nm silica nanoparticles, the transition from C_8 to C_{18} was on the order of 7 cm^{-1}. The shifts from C_8 to C_{18} on 7 and 12 nm particles were found to be approximately 6 cm^{-1}. Since the high radius of curvature of the smaller nanoparticles do not allow for formation of well ordered structures regardless of the alkyl chain length, the subsequent lack of crystallinity is likely due to the inability of the

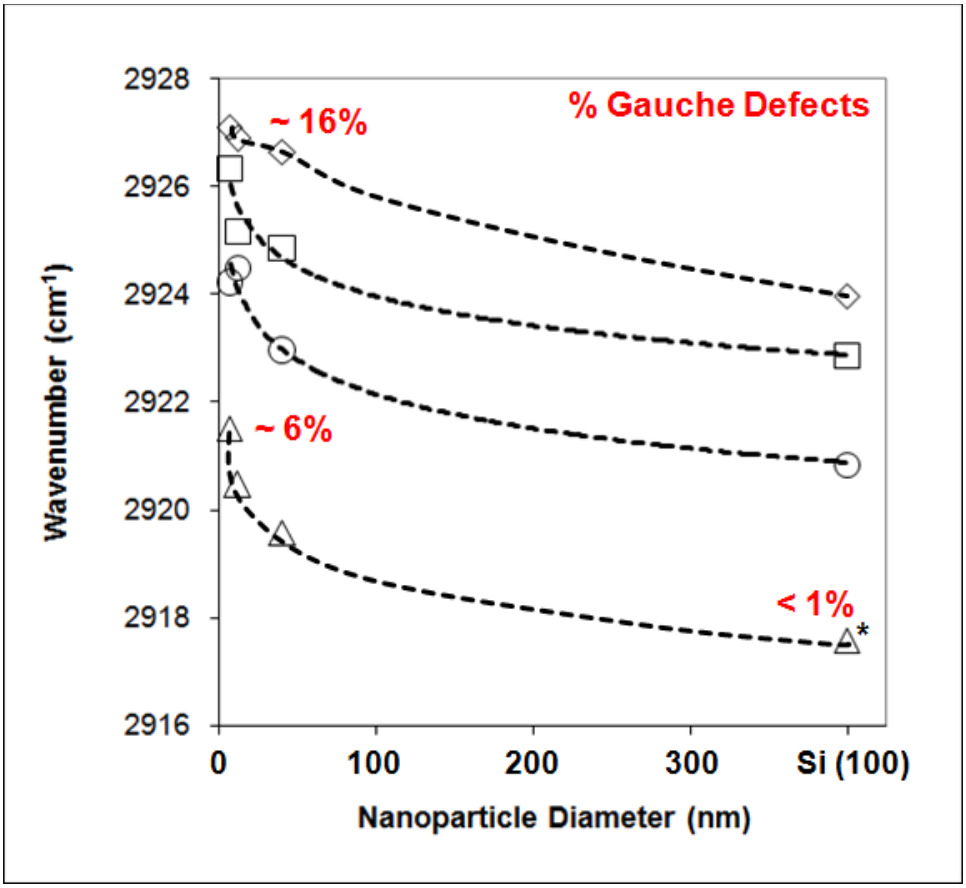

FIGURE 3.9: Plots of the CH_2 asymmetric stretch frequency vs. nanoparticle diameter for films synthesized via Hexanes Method with previously cleaned and hydroxylated nanoparticles (HMC) and Si (100). Plots represent data for nanoparticles functionalized with: a) C_{18} - □; b) C_{12} - ○; c) C_{10} - □; and d) C_8 - ◊. All error bars are within the size of the data point. * Films assembled on Si(100) are shown as being assembled on 400 nm particles as assembly on particles of this size has been previously reported to mimic assembly on flat surfaces for C_{18}.[89] #The percentage of gauche defects has been estimated based on temperature dependent IR studies with molecular dynamic simulations.[132] The guidelines are intended to only be guides to the eyes. Reused with permission. Copyright 2009 American Chemical Society.[88]

molecules to experience the number of chain stabilizing lateral interactions with neighboring molecules as would be found on surfaces with lesser degrees of curvature. Creating disorder by imparting curvature to the surface on which a monolayer is

assembled on is comparable to other systems in which disorder has been induced into a self-assembled organic film. The introduction of gauche defects into the film by increasing the energy of the system is analogous to reducing the ability of a SAM to form stabilizing interactions by the introduction of surface curvature. This information can be correlated by the FTIR data due to the frequency of the CH_2 asymmetric stretching band being conformation sensitive, shifting as a function of the ratio of trans/gauche conformers in the acyl chains, independent of what method is responsible for the shift. For example, the relative shifts in the location of the CH_2 asymmetric stretch frequency has also been used as a qualitative indicator of film order for SAMs as a function of temperature and pressure.[130-138] Temperature dependent studies performed by Prathima and coworkers examined the shifts in the CH_2 asymmetric stretch peak frequency vs. temperature for alkanethiols on Au.[130] Molecular dynamics simulations were also employed to track the percentage of *gauche* defects present as the system temperature was increased. The temperature and computational data was then correlated in order to quantify film disorder based on the CH_2 asymmetric stretch peak frequency. At room temperature, a well ordered, full coverage SAM assembled on a flat surface exhibits a defect profile with approximately 1% of the chains exhibiting *gauche* defects.[132] Consistent with the FTIR picture of a well ordered C_{18} SAM which shows the location of the CH_2 asymmetric stretch in the range of 2917-2919 cm^{-1}.[186] Correlating the shifts detected during high temperature studies to those observed on the nanoparticle surfaces reveals that C_{18} assembled utilizing the Hexanes Method with cleaned and hydroxylated 40 nm particle produces a film with a relatively low number of *gauche*

defects, on the order of 1%. A C_8 film assembled with the same method on a 40 nm particle possesses *gauche* defects in roughly 14% of the film's alkyl chains. Interestingly, C_8 and C_{18} films assembled on 7 nm particles using the same method display ca. 16% and 6% *gauche* defects respectively. The C_8 films experience little change in relative order regardless of the curvature of the surface. This behavior can be

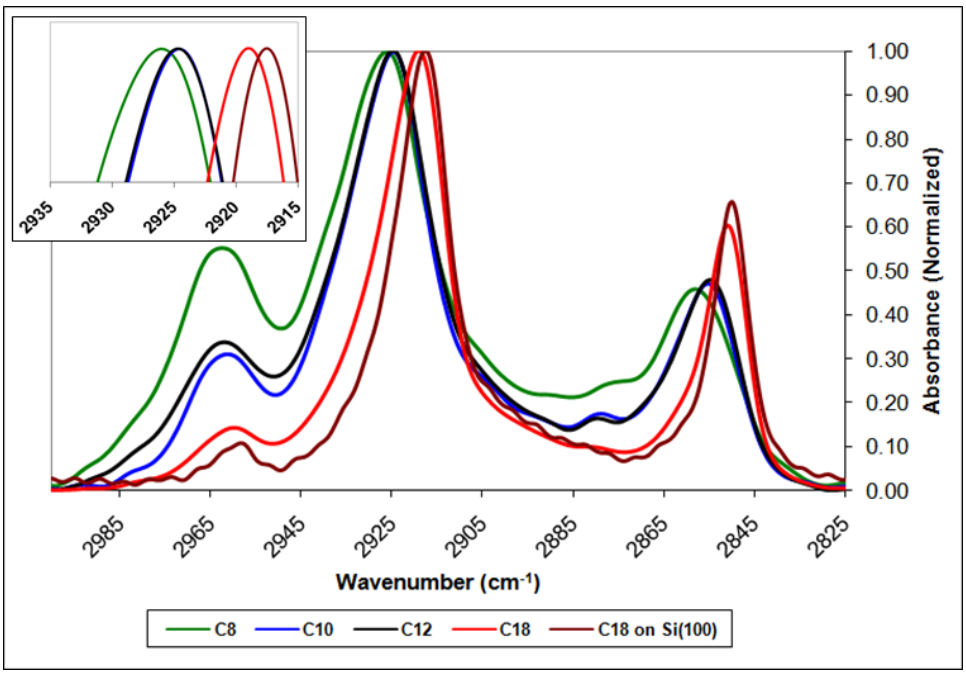

FIGURE 3.10: Transmission FTIR spectra of C_8, C_{10}, C_{12}, and C_{18} assembled on spin coated 40 nm silica nanoparticle films and C_{18} assembled on Si(100) using the HMC method. The small peak at 2880 cm^{-1} is due to the CH_3 symmetric stretching band. All spectra have been normalized to one. Reused with permission. Copyright 2009 American Chemical Society.[88]

attributed to a saturation of the number of *gauche* defects that can be experienced by a film composed of C_8 molecules at these curvatures and the overall reduction of lateral stabilization for packing through methylene-methylene interactions.

Lastly, to compare assembly on free nanoparticles to that of surface films with nanoscale roughness, we examined assembly of C_{18} on 40 nm particles deposited on and fused to a Si(100) surface (Figure 3.10). Spin coating of nanoparticles onto a Si(100) support creates a surface which exhibits small scale spheroids but intentionally eliminates portions of the spheroid from functionalization.[116] Figure 3.10 shows that functionalization of spin coated nanoparticle films leads to ordering which falls between that of SAMs on flat silicon and SAMs on nanoparticles (CH_2 asymmetric stretch for C_{18} on spin coated nanoparticles was found at 2919 cm^{-1} versus flat Si which was located at 2918 cm^{-1} and 2920 cm^{-1} for the free 40 nm particles). This suggests that the arrangement of the nanoparticles on the surface provides a means for the SAM molecules to organize themselves in a manner which allows a greater amount of interaction between neighboring molecules. This is likely as the boundaries between particles provide sites for the molecules to pack more densely as compared to a purely spheroidal surface such as a free nanoparticle. While the close packed arrangement of the nanoparticles allows for an increase in film order, the curved nature of the small domains which comprise the surface are insufficient at providing a support for a film as well ordered as a SAM on a flat Si surface.

3.5 Conclusions

These results demonstrate the relationship between not only nanoscale geometry such as the surface curvature, but also the role that alkyl chain length plays in the molecular order and conformation of alkylsilane self assembled monolayers on silica surfaces. It was observed that layer disorder can be readily tracked via simple linear

spectroscopies, such as FTIR spectroscopy for alkylsilane monolayers on both flat surfaces and other surfaces with varying degrees of curvature. Under controlled assembly conditions, reasonably well ordered films of long chain C_{18} SAMs can be formed on surfaces with high degrees of curvature. Common procedures that produce nominally high quality films on the oxidized surface of Si(100), such as the procedure using THF however, show defective film quality on nanoparticles as THF is found to intercalate into the film. The more disordered surfaces also show a greater propensity for uptake of water likely due to interactions with residual free silanols on the surface which aid in water penetration. Further work currently in progress is devoted to understanding the effects of modifying the chain end functionalities and chain branching on monolayer formation and film stability on nanoasperities. Armed with a simple direct probe for the extent of film disorder on such surface bound nanoasperities, the influence of film order on their mechanical stability and efficacy as monolayer lubricants in high pressure contacts, such as those found in microdevices, can be further explored. Moreover, this approach of following SAM assembly on nanoparticles which exhibit similar curvature to that of AFM probes provides a simple spectroscopic diagnostic approach to gain insight into SAM assembly on AFM tips.

CHAPTER IV

INTERCALATION OF 3-PHENYL-1-PROPONOL INTO OTS SAMS ON SILICA NANOASPERITIES TO CREATE SELF-REPAIRING INTERFACES FOR MEMS LUBRICATION*

4.1 Overview

Self-assembled monolayers (SAMs) have been widely studied as potential lubricants for microelectromechanical system (MEMS) devices. However, these single layer films have nominally been found to be insufficient for mitigating wear in sliding contacts due to their rapid breakdown under the high pressures found within the nanoasperity junctions at such interfaces. As such, there is a critical need to explore approaches beyond simple, single component SAMs, towards films which introduce additional lubricant molecules into the system. As alcohol vapors have previously been shown to reduce wear in MEMS devices, here we have investigated a mixed monolayer consisting of an octadecyltrichlorosilane (OTS) SAM infused with 3-phenyl-1-propanol (3P1P), assembled on silica nanoparticle films. A combination of Atomic Force Microscopy (AFM) and FTIR spectroscopy was employed to investigate the structural and frictional properties of the mixed monolayers and to evaluate surface wear as a function of time. The nanoparticle film/AFM tip junction provides a ready mimic for

---

*Reproduced with permission from *Langmuir*; Ryan L. Jones, Bronwyn L. Harrod and James D. Batteas, "Intercalation of 3-phenyl-1-proponol into OTS SAMs on Silica Nanoasperities to Create Self-Repairing Interfaces for MEMS Lubrication" *Langmuir.*; **2010**; 26(21); 16355–16361.

the asperity-asperity contacts found in MEMS devices. Here it was found that for a mixed monolayer of OTS with *ca.* 15% 3P1P, that the surfaces showed dramatically reduced friction and no wear under the same load conditions as surfaces with an OTS SAM alone. Moreover, the multi-component film also displayed no increase in friction, or exhibited any wear, ever after 14 hours of shearing contact in an AFM at loads that would breakdown the OTS layer. The ability of the OTS SAM to trap short chain alcohols, such as 3P1P, and to release them under load, suggests a simple MEMS lubrication scheme which could be readily integrated into MEMS device architectures.

4.2 Introduction

Microelectromechanical system (MEMS) devices have the potential to be utilized across a broad spectrum of applications. However, even with over a decade of research and development in MEMS, most devices being utilized outside of the laboratory are those that do not employ components in motion, as sliding contacts have proven to be disastrous in terms of device lifetime.[195-198] As such, minimizing surface friction, adhesion and wear is of paramount importance for the development and large scale implementation of dynamic MEMS devices. Due to the manner in which these devices are constructed, their surfaces typically exhibit nanoasperities on the order of 10-20 nm in dimension.[2] This inherent surface roughness dictates the interactions between any two surfaces in contact, and shear and damage to the device surfaces initiate at these sharp asperity-asperity contacts, which ultimately govern the tribological properties of the surfaces during both directed and random contact.[12, 17, 117] As such, it is at that these points where defect nucleation and wear of the asperities occurs, leading to breakdown

of the surface, and ultimately leading the material to yield and fail during sliding contact.[12]

To aid in mitigating friction, adhesion and wear in MEMS devices, significant effort has been aimed at understanding how self-assembled monolayers (SAMs) could be used to minimize these effects[2-4, 7-11, 91, 199] In particular, various silane based SAMs have been shown to passivate hydrophilic silicon surfaces and to reduce both friction and adhesion in MEMS devices.[9, 11, 92-94] To investigate their potential for surface passivation and lubrication in MEMS, a number of model systems based on SAMs have been examined and a number of parameters have been found to affect a film's performance. These include variations in terminal-group functionality (*e.g.* hydrophobic *vs.* hydrophilic),[95-99, 200] lateral chain-chain interactions,[102] the presence of defects within the film (*e.g. gauche* defects in alkyl based SAMs),[103-107, 201] molecular orientation,[202] and chain length.[203]

While SAMs have been nominally observed to mitigate friction and wear on surfaces under low loads with minimal contact; studies under high loads and continuous shear have shown that they are incapable of passivating the silicon oxide surfaces that comprise most devices for any meaningful operational time.[204-210] Attempts at solving the contact lubrication issue have lead to the investigation of other strategies for device lubrication. Notably, studies utilizing acid or alcohol vapors have shown that with constant surface passivation,[142, 211-213] via a continual regeneration of the surface protecting coating, wear can be dramatically impeded.[59] In fact, one of the most readily identifiable MEMS devices in large scale use that actually involves a sliding contact, the

digital micromirror assembly used in Texas Instrument's Digital Light Processing (DLP) technology, utilizes perfluorodecanoic acid vapor to lubricate the devices. The perfluorodecanoic acid, which is a solid at room temperature, produces a significant vapor pressure at operating temperatures (~ 70 ^{o}C), which acts to continually passivate the surfaces in contact.[211] This temperature dependence however is a key drawback for using perfluorodecanoic acid in other MEMS devices where operation at room temperature or below is desirable.

Other vapor phase systems have also been recently explored by Kim and co-workers which can avoid this temperature dependent operating window. In their work, alcohol based lubricants possessing high vapor pressures at room temperature and below have been explored.[142, 212, 214, 215] In these seminal studies, a diagnostic MEMS based tribometer operating inside a controlled environmental chamber was utilized to test the influence of alcohol vapor (*e.g.* pentanol) on the frictional properties of the sliding contacts, whereby the desired lubricant molecule was introduced to the test device via a nitrogen flow. These studies showed that the tribometer was able to operate continuously without failure even after millions of cycles, demonstrating that short chain alcohols could readily function as active lubricants in MEMs devices.[142] A key challenge that remains in making vapor phase lubrication a viable commercial approach however, is the need for an integrated delivery system that can be incorporated directly into the MEMS device, such that an external replenishment source or delivery system would not be required.

Recently we have investigated the assembly of alkylsilane based monolayers on silica nanoasperities (*ca.* 3 – 20 nm radius of curvature) to understand how these molecular layers assembly on the sharply curved surfaces typically found in MEMS devices.[88] Here we found that even for long chain silanes, such as octadecyltrichlorosilane (OTS) assembled on silica nanoasperities, that these monolayers exhibited between *ca.* 6% - 16% *gauche* defects, depending on chain length and surface curvature. Additionally, monolayer formation on these rough surfaces was found to be generally incomplete due to the poor packing of the silanes. Previous studies have found the packing density of OTS films on 20 nm radius of curvature silica particles to be on the order of 1.5 molecules per square nanometer,[88] as opposed to the 2.5 molecules per square nanometer generally observed on the flat, oxidized surface of Si(100).[186, 216] Interestingly, as compared to their counterparts assembled on atomically smooth surfaces such as Si(100), the SAMs on the nanoasperities also showed an increased propensity for the uptake and intercalation of other molecules such as water, THF and short chain alkanes. While it has seemly become apparent that SAMs are a poor choice for use in MEMS devices, likely due to many of these factors (low surface coverage and disorder), some promising results have recently emerged in which multi-component based SAMs comprised of self-assembled films paired with weakly bound molecules, which could act as mobile lubricants, were found to exhibit enhanced performance for surface lubrication.[59]

In the work described in this paper, we have explored the ability of SAMs on nanoasperities to uptake short chain alcohols as a means to both protect the surfaces in

sliding contact from water uptake, and to weakly trap and store alcohols within the SAM, which during shear can be dislodged, and act as a mobile lubricant during sliding contact. In particular, we have examined the tribological properties of a mixed monolayer consisting of a stationary octadecyltrichlorosilane (OTS) self-assembled monolayer combined with 3-phenyl-1-propanol (3P1P) incorporated into the SAM matrix. This combination acts as an enhanced multi-component based lubricant and serves to create a self-healing film with the ability act simultaneously as a protective layer, mitigating H_2O uptake and reducing friction, and a means of storage for weakly bound mobile lubricant molecules. Here we have found that for OTS SAMs with *ca.* 15% 3P1P, the frictional properties of the surfaces are dramatically improved and show dramatically reduced friction and wear.

4.3 Experimental Methods

In order to have surfaces that mimic those of MEMS devices, in these studies we used a silica nanoparticle film to mimic the asperities found in such systems. The fabrication of these surfaces has been detailed previously.[37] Briefly, nanoparticle films were formed by first suspending 40 nm colloidal silica nanoparticles (OX-50) obtained from Degussa in a pH 13 sol. Before spin coating, Si(100) substrates (Virginia Semiconductor) were cleaned and hydroxylated in a 4:1:1 (v:v:v) mixture of high purity H_2O (18.2 M□•cm, Barnstead), H_2O_2 (30 %) and concentrated NH_4OH, at 80° C for 30 minutes. Immediately following cleaning, the substrates were rinsed under high purity water for 60 seconds and dried under streaming nitrogen. Colloidal silica thin films were created by spin coating the nanoparticle sol onto the cleaned Si(100) substrates.

After spin coating, the nanoparticle films where annealed by heating to a temperature of 500° C for a period of 5 hrs. This annealing step ensures the formation of a stable nanoparticle film by creating additional siloxane linkages between the particles and substrate, stabilizing the films during functionalization and later when performing AFM measurements on them.[37] After annealing, the substrates were again submersed into the (4:1:1) cleaning solution for a period of 30 minutes at 80° C and then were rinsed once more for a period of 60 seconds under high purity H_2O. To ensure that both sides of the substrate would be functionalized in the same manner, each substrate was then coated with a nanoparticle film on the backside using the same procedure. This step was taken to ensure that transmission FTIR analysis wouldn't be altered by the presence of an OTS functionalized flat oxide surface on the reverse face. A number of these unfunctionalized spin coated films were reserved and stored in an environmentally controlled dry box with an oxygen and water free Ar atmosphere until use. Functionalized spin coated nanoparticle films were created utilizing a hexane based functionalization procedure. Octadecyltrichlorosilane (Gelest) monolayers were prepared using a solution composed of 30 mL of hexane isomers and 15 μL of OTS in a Wheaton staining jar. [88]

The substrates and functionalization solution were then sonicated for a period of 2 hours. After sonication, the substrates were removed from the functionalization solution, sonicated for 30 min in THF, rinsed with high purity H_2O for 60 seconds, dried under streaming nitrogen, immediately put into a nitrogen purged FTIR spectrometer for analysis and then placed under an Ar atmosphere for later use.

To create mixed SAM layers, OTS functionalized nanoparticle surfaces were infused with 3-phenyl-1-propanol (3P1P, Sigma-Aldrich) by submerging the substrates in a neat solution of 3P1P, sonicating for a period of 3 hours and then allowing them to sit overnight in the neat solute. The substrates were then removed from the 3P1P, rinsed with copious amounts of ethanol, dried with streaming nitrogen, analyzed with FTIR and then stored under an Ar atmosphere for later measurement.

A Thermo Nicolet 6700 FTIR equipped with a liquid-nitrogen-cooled MCT A (HgCdTe) detector was used for all IR measurements. Spectra for the monolayers on the flat Si(100) substrates as well as on the nanoparticle films on the Si(100) supports were taken by transmission measurements at Brewster's angle for silicon (~74°). Each spectrum was collected with 1024 scans at a resolution of 1 cm^{-1}.

AFM images and friction measurements were collected with an Agilent/Molecular Imaging PicoSPM coupled with an RHK Technology SPM 1000 Electronics Revision 8. The experiments were performed with commercially available, rectangular Si cantilevers (MikroMasch), with force constants ranging from 0.15 N/m to 0.5 N/m and experimentally determined average tip radii of ~20 nm. To quantify the forces, exact force constants for each cantilever were determined using the Sader method, and all reported forces are based on calibrated levers.[217] The lateral force constant for each cantilever was then calibrated utilizing the direct force balance method.[218] Prior to use, the AFM tips were cleaned and hydroxylated by submerging the tips into a (4:1:1) hydroxylation solution for a period 60 seconds. In order to provide a consistent measurement environment and to avoid contributions from capillary forces,

all data was gathered in high purity water at pH 2–3 at ambient temperature. This pH is the isoelectric point for the native oxide on Si, ensuring that that any charge interactions between the tip and the substrate will be mitigated during scanning..[219, 220]

AFM friction measurements were performed by scanning five 1 μm^2 regions under the same load and then averaging the total lateral force value for each image with the final value calculated by averaging the total lateral force number for all five images collected at each load. The load was increased until the AFM tip was either destroyed in use or a load value of 300 nN was reached. The performance of the films under wear was determined by collecting frictional force data using an AFM tip at a load of 125 nN. The AFM was programmed to repeatedly scan a single 0.5 μm long line at a rate of 0.1 μm/s while collecting the lateral force signal in the forward and reverse directions. The output for every tenth scan was then analyzed for the lateral force and plotted versus the number of cycles. The scans were continued under load until 5000 cycles (13.9 hrs) were performed or failure was achieved. Immediately following each the experiments, each substrate was analyzed with FTIR to determine if any film damage could be spectroscopically observed due to immersion in water (*i.e.* uptake of water or loss of surface bound silanes, or 3P1P) and none was found.

4.5 Results and Discussion

The OTS SAMs on the spin coated silica nanoparticle films were first analyzed with FTIR spectroscopy to determine the degree of ordering within the monolayer. It is known that the location of the CH_2 asymmetric stretch band (d-) can be used to qualitatively estimate the extent of ordering within an alkylsilane or alkylthiol SAM.[108,

[151, 182-184, 186, 187] Disordered, liquid like films exhibit a CH_2 asymmetric stretching frequency in the region of 2924 cm^{-1}, while in more ordered systems the peak tends to appear near 2917 cm^{-1}, signifying a film which exists in a more crystalline state with the chains in an all *trans* conformation.[15]

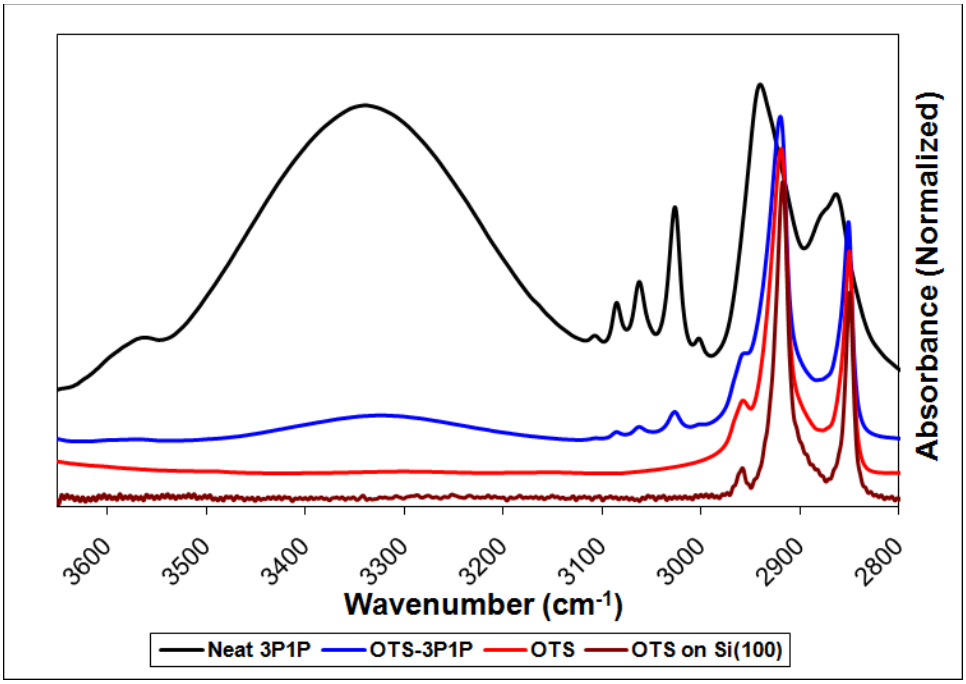

FIGURE 4.1: Transmission FTIR spectra of OTS on Si(100), OTS on a nanoparticle film, OTS-3P1P on a nanoparticle film, and neat 3P1P. The inset highlights the variation in the location of the methylene asymmetric (d-) stretching band for the four spectra. All spectra have been normalized to one for the methylene asymmetric peak of each spectrum and the baselines have been offset to reduce spectral overlap. Reused with permission. Copyright 2009 American Chemical Society.[140]

Properly prepared alkylsilane SAMs with chain lengths greater than 6 carbons typically exist in a crystalline phase when assembled on the oxidized surface of Si(100). However, when surface curvature is introduced, the degree of crystallinity is seen to

drop relative to the SAM's molecular chain length and the degree of surface curvature, with the greatest extent of disorder being exhibited by films possessing the shortest carbon chains assembled on surfaces with the highest degree of curvature.[88] The FTIR spectra shown in Figure 4.1 illustrate the C-H stretching region for the two experimental systems, OTS on the silica nanoparticle film and OTS with 3P1P intercalated, as compared to OTS assembled on the oxidized surface of a Si(100) substrate, and neat 3P1P. For the self assembled films, the location of the CH_2 asymmetric (d-) stretch indicates that both films assembled on the nanoparticle substrates (the OTS and OTS with 3P1P) possess a very similar degree of order, with the average location for the CH_2 asymmetric stretch for both films being located at 2919.2 cm^{-1} compared to the CH_2 asymmetric stretch appearing at 2917.6 cm^{-1} for the OTS SAM alone on Si(100). The location of the CH_2 asymmetric stretch for OTS on the nanoparticle film indicates that the self-assembled films on the nanoparticle substrates are slightly more disordered than their counterparts on Si(100), with the nanoparticle coatings exhibiting a *gauche* defect percentage up to 6% compared to less than 1% for a OTS film assembled on Si(100), respectively.[88, 132] Similarly, the CH_2 asymmetric stretch location of 2940.1 cm^{-1} for the neat 3P1P sample is reasonable for a short alkyl chain attached to a relatively bulky substituent in the liquid phase.

It has previously been observed that such alkyl based SAMs have an ability to uptake foreign molecules into the self-assembled film matrix via diffusion[188-190, 192] and solvation effects.[185, 193] Moreover, we have previously noted that solvent intercalation could be readily observed to occur during silane functionalization on curved surfaces

with solvent molecules inserting themselves into spaces within the film matrix.[88] This is more pronounced for OTS on silica nanoparticle surfaces which show reduced coverage as compared to surfaces such as Si(100), with *ca.* 1.5 vs. 2.5 molecules per square nanometer, respectively. As such, by immersing the OTS covered silica nanoparticle film in neat 3P1P, this molecule was also observed be taken up by the OTS SAM layer. The insertion of the 3P1P into the OTS monolayer is likely driven by two main factors. First there are hydrogen bonding interactions between the alcohol group on the propane chain and unreacted surface silanols on the nanoparticle surface. Second, van der Waals interactions between the alkyl chains in the OTS film and 3P1P's propyl chain and phenyl headgroup also provide hydrophobic forces that can aid in stabilizing the interaction between the 3P1P and the OTS SAM. While we cannot unambiguously assign the location of the 3P1P in the film (*i.e.* are all of the molecules intercalated within the SAM or are some weakly bound to the surface?), one indication that 3P1P is inserted into the film is the location of the -OH stretching band for the inserted versus the neat 3P1P. This large, broad band located at 3330.3 cm^{-1} for the neat 3P1P sample is found to be downshifted to 3319.7 cm^{-1} for the multi-component film. The softening of this mode suggests some degree of hydrogen bonding between surface hydroxyl groups and the 3P1P.[221] Additionally, as the methylene asymmetric stretch is not observed to be broadened or shifted for the monolayer once the 3P1P is added to the surface, this also suggests that little weakly bound 3P1P is residing on top of the surface layer.

To determine the degree of 3P1P uptake by the OTS SAM, the intensity of the largest C-H stretching band associated with the phenyl ring (located at 3026.8 cm^{-1}) was

compared to standard solutions of known concentration of 3P1P in ethanol. A Beer's law plot was then assembled with these values and used to calculate the total amount of 3P1P within the multicomponent film based on the height of the same peak in the FTIR spectra. Every value was determined based on the size of the IR beam spot for each measurement and normalized by the amount of transmission intensity seen at the photodetector. The amount of OTS present was determined by first calculating the average surface area from ten 1 μm x 1 μm AFM scans of a nanoparticle film. The average surface area was then extended by the spot size of the FTIR beam used in the IR measurements. The final OTS count was then established by multiplying the total surface area by a surface coverage of 1.5 OTS molecules per square nanometer (see supporting information).[88] Based on this analysis, the relative amount of 3P1P incorporated into the OTS SAMs was found to be ~ 15% ± 1%. This extent of uptake is very consistent with the uptake of other molecules into these disordered SAMs as we have described in our previous studies of alkylsilane SAMs on silica nanoasperties,[88] where we also observed *ca.* 10 – 15% uptake of molecules such as hexane or THF. Notably, no water uptake was observed by IR even for films immersed in H_2O for nearly 14 hours.

AFM studies showed no topological differences between the films of unfunctionalized nanoparticles, with those with an OTS film and those with and OTS film with 3P1P intercalated into the film (Figure 4.2). The films appear to be uniform in coverage as no domain structures or multilayer features observed as determined by lateral force images. Friction versus load studies were performed with the AFM on the

three separate surfaces: unfunctionalized nanoparticle films, OTS functionalized nanoparticle films and OTS/3P1P mixed monolayer films. All three surfaces displayed an average RMS roughness between 20 nm to 25 nm, and as such, are a reasonable model for the surfaces of MEMS devices, which typically exhibit surface roughness on the order of 10-20 nm RMS.[17]

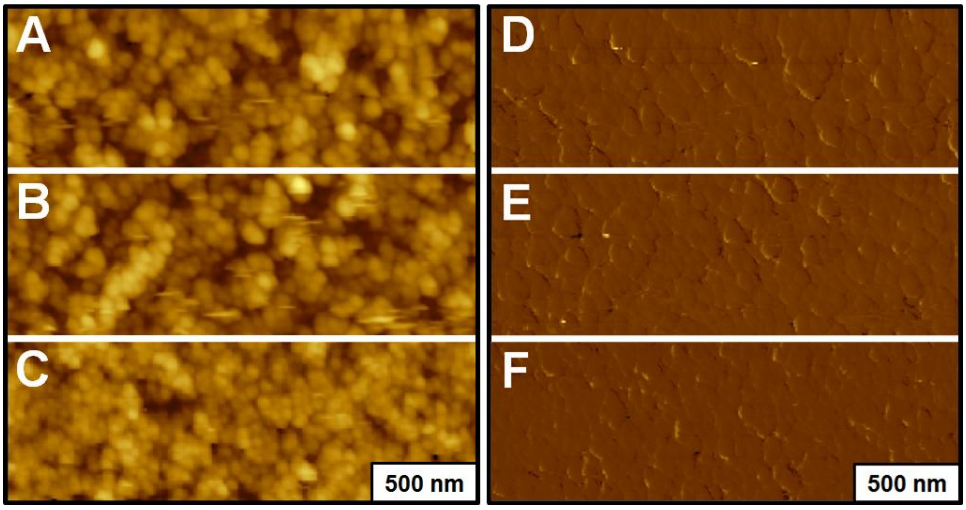

FIGURE 4.2: Topographic (A, B, and C) and the corresponding Friction Force (D, E, and F) AFM images of the three nanoparticle film surfaces. (A and D) an unfunctionalized silica nanoparticle film; (B and E) an OTS coated nanoparticle film; (C and F) a multicomponent OTS-3P1P film. Total image size is 2.25 μm × 2.25 μm and an average roughness of ~24 nm RMS. Reused with permission. Copyright 2009 American Chemical Society.[140]

The results for the friction versus load studies on the three different surfaces are shown in Figure 4.3. For the unfunctionalized silica surface, the friction values were observed to be higher at every load when compared to the two functionalized surfaces. The observed friction force values appear to increase monotonically until a threshold

load of ~ 75 nN at which point the lateral force was observed to increase dramatically for loads up to 150 nN. Under these conditions, the AFM tip reached a failure point and the images were seen to distort, and then all of topographic resolution disappeared, indicating that the tip had worn significantly during use (data not shown).

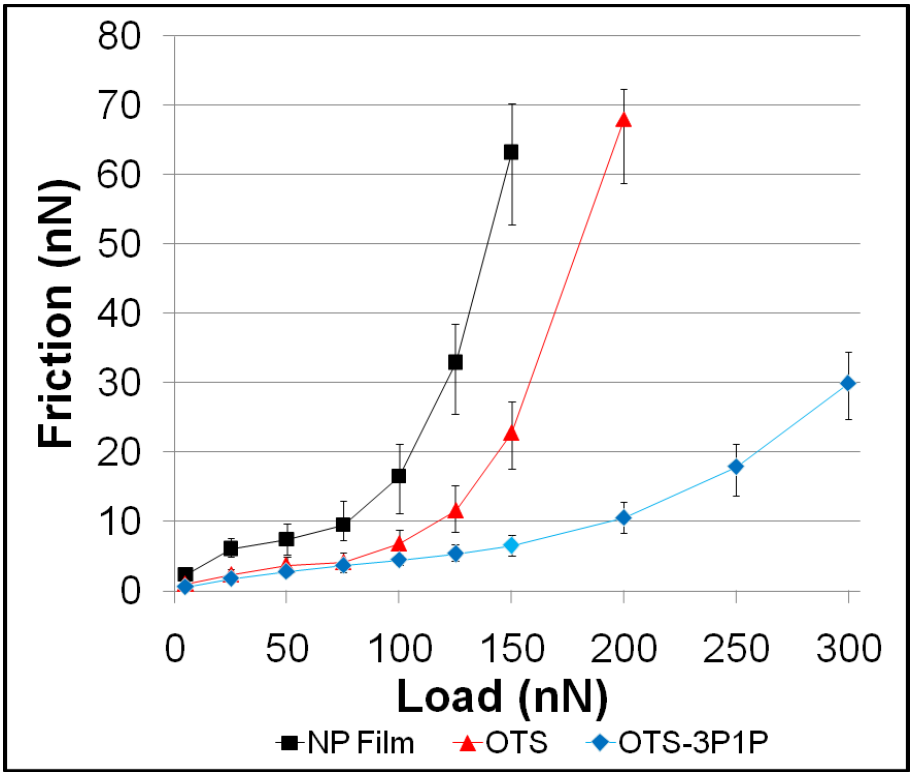

FIGURE 4.3: Friction vs. load results for unfunctionalized nanoparticle films (■), OTS functionalized nanoparticle films (▲), and OTS-3P1P multicomponent films (♦) at a sliding velocity of 0.1 μm/s. Some error bars fall within the size of the marker. The lines connecting the data points are intended only to be guides to the eye and do not denote any trend. Reused with permission. Copyright 2009 American Chemical Society.[140]

OTS SAMs are known to act as wear passivating surface lubricant films, insulating the contacts and reducing friction under low loading forces.[205, 206, 210] Under

load, the SAM acts as a viscoelastic film on the surface, possessing enough mechanical strength to bear a load, but unable to protect the surface once the threshold pressure for breaking the molecule-surface bond is exceeded, compromising the SAM matrix. Similar to previous studies, here the OTS films were seen to break down and fail at higher loads than that of the bare silica surface. While the OTS modified surfaces showed reduced friction under higher loads than an unpassivated nanoparticle film, they proved unable to protect the contact surfaces at loads only 50 nN higher than that which led to damage on the unfunctionalized surface, further illustrating that SAMs alone are incapable of protecting asperity-asperity contacts from friction related failure. The breakdown of these films at loads of *ca.* 150 nN is very consistent with previous studies of OTS SAMs on silica.[91]

Friction versus load studies for the OTS SAM with *ca.* 15% 3P1P showed significantly improved performance, with the ability to lower the friction by as much as 50 percent as compared to the OTS SAMs alone under high load conditions (125 nN). Below this, the performance of the mixed monolayer was seen to be nearly identical to that of the OTS SAM, suggesting that under low stress regimes the tribological properties of the film are dominated by the presence of the OTS SAM. Interestingly, the slopes of the friction versus load curves are all very similar in the low load range (< 75 nN). This may potentially be an effect of water acting as a lubricant under these conditions as well, as has been previously described.[3, 191, 222, 223] This was seen to deviate at higher loads, where the mixed film showed reduced friction, and no signs of gross wear, even up to loads of 300 nN. Even at these high loads, the observed lateral force

was still less than half that which lead to failure in the unfunctionalized and OTS passivated surfaces. This seems even more impressive given that all the measurements all were conducted under water, the presence of which normally aids in the breakdown of silane layers on silica through catalytic Si-O bond breaking.[37, 199, 212, 215]

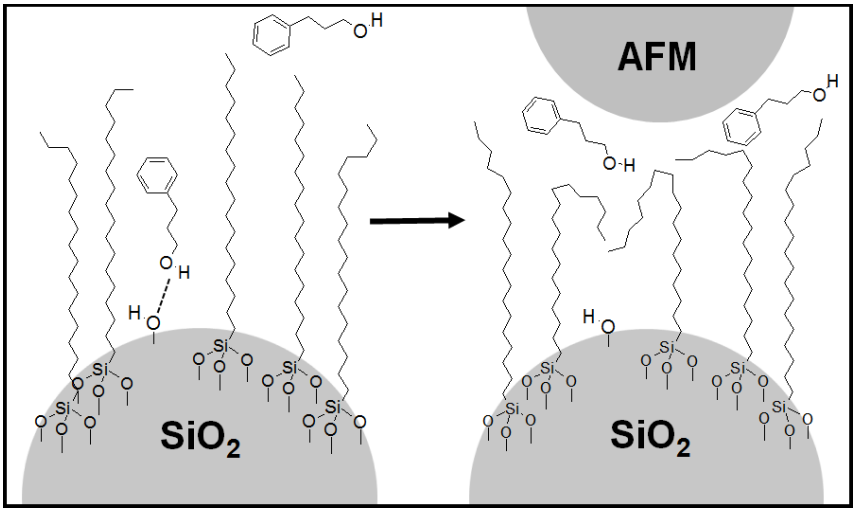

FIGURE 4.4: Schematic representation of 3P1P molecules embedded in an OTS SAM before and during perturbation within an asperity-asperity contact. Reused with permission. Copyright 2009 American Chemical Society.[140]

The disparity between the frictional properties of the OTS and the mixed film can only be attributed to the presence of 3P1P within the OTS SAM. While the specific mechanism is unclear at this time, we speculate that at high loads the pressure exerted in the tip-sample contact likely perturbs the SAM matrix, compressing the film and forcing the physically adsorbed 3P1P to the surface where it act as additional mobile lubricant on top of the OTS SAM (Figure 4.4). FTIR data collected on the substrates before and after the wear studies show that no 3P1P was lost to the water environment by

displacement during the experiment. Moreover, no loss of the OTS SAM was observed either, suggesting that the 3P1P is tightly bound enough within the SAM matrix to also impeded water uptake by the monolayer as was seen in previous studies for silane SAMs alone.[88] This would have many advantages for MEMS devices, where water uptake is known to have deleterious effects on device lifetime.

Upon reducing the load following contact and shearing, the 3P1P is likely re-adsorbed into the monolayer. As such, these mixed films may possess a degree of self-healing ability, as the mobile molecules are capable of replacing themselves within the matrix or moving to new sites to replenish exhausted nearby regions. This mechanism would be consist with the recent report on multiply-alkylated-cyclopentane-octadecyltrichlorosilane double layer films, which were found to repair themselves, suggesting that the presence of a mobile lubricant is a necessary component to form a self-repairing film.[59]

To evaluate the overall ability of the OTS and mixed OTS-3P1P monolayers to mitigate wear, the wear of the surfaces was probed by following friction vs. time during scanning by AFM. Figure 4.5 shows the friction response versus the number of scans at a load of 125 nN. This load was chosen based on the results of the friction versus load studies for the two experimental films, since this load was great enough to show a significant difference in friction between the OTS and the OTS-3P1P layers, yet was still below the failure load of the OTS film. For the OTS SAM, the lateral force was seen to increase with the number of scans until failure, indicating that the portion of the film being subjected to load was slowly wearing under contact until a point was reached that

the remaining SAM was no longer able to protect the surface from wear. The plot also indicates that once the OTS SAM was removed from the surface, its ability to passivate the surface was degraded, leaving the surface essentially unprotected. The resulting

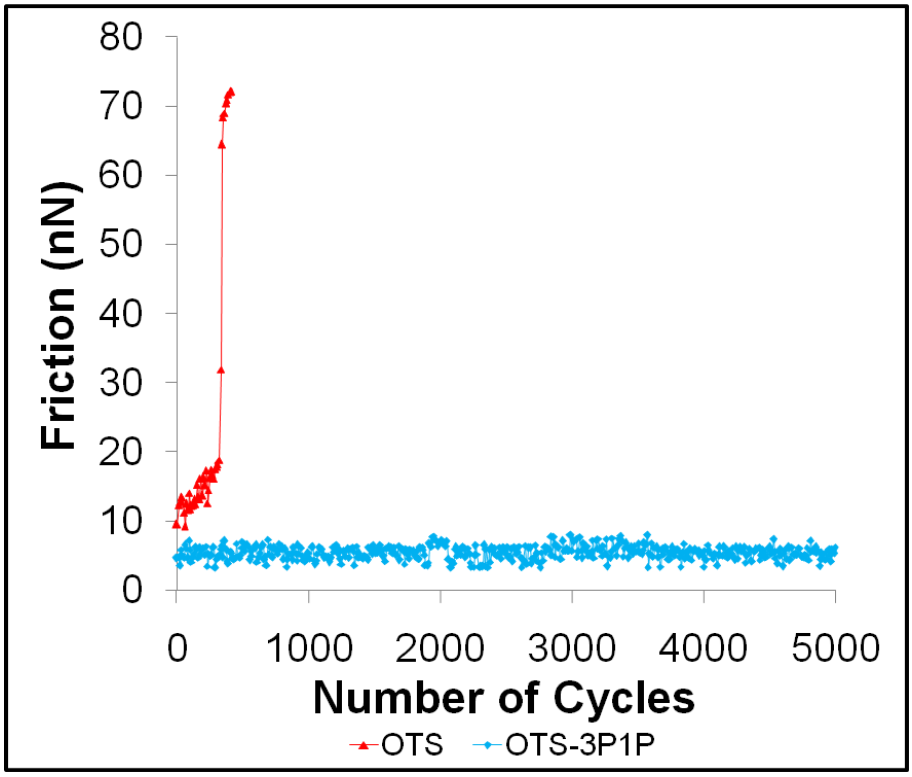

FIGURE 4.5: Friction vs. time test results for OTS functionalized nanoparticle films (▲) and OTS-3P1P multicomponent films (♦) at a load of 125 nN and a sliding velocity of 0.1 μm/s. The lines connecting the data points are intended only to be guides to the eye and do not denote any trend. Reused with permission. Copyright 2009 American Chemical Society.[140]

lateral force response between the AFM probe and the unprotected surface appeared in a range similar to that which was seen by the unfunctionalized nanoparticle film under the same load, although the overall net resulting frictional force was observed to be higher

than that of just the unfunctionalized surface alone, and in this case, we attribute this to the fact that the tip became severely blunted once the film failed during scanning (data not shown).

The mixed monolayer, however appeared to be impervious to wear at the same load conditions, with the friction response remaining relatively constant throughout the experiment. Even after 5000 cycles under load (~14 hours of continuous scanning), the multicomponent film exhibited similar friction to that at the beginning of the trial. This performance is analogous with the results of the friction vs. load studies which showed that the multicomponent film displayed the ability to reduce friction well beyond what was seen for the OTS SAM alone. The comparative longevity of the multicomponent film indicates that any wear that occurred was either insignificant or was mitigated by the film's ability to heal itself *in situ.*

4.5 Conclusions

Here we have shown that the uptake of a short chain alcohol into an alkylsilane SAM layer to form a multicomponent film on surfaces with nanoscale asperities acts to significantly reduce friction and improve the function of the monolayer as a lubricious film. Octadecyltrichlorosilane SAMs assembled on spin coated silica nanoparticle films and then infused with 3-phenyl-1-propanol show reduced friction at all loads and an enhanced lifetime against wear over OTS films alone. These multicomponent systems act as self-maintaining and regenerating films as they demonstrate an ability to uptake and release molecules such as 3P1P which then likely function as mobile lubricants during contact induced stress. These studies demonstrate the means of using a

disordered/reduced coverage SAM as an avenue of storing weakly bound molecules, which can then subsequently be released to lubricate the interface. Such multicomponent films have the potential to proffer a simple, yet readily useful system by which to lubricant dynamic MEMS devices. Further studies will explore how shear rate dependence influences the function of these multicomponent films.

CHAPTER V

ENVIRONMENTAL DEPENDENCE OF MULTICOMPONENT 3-PHENYL-1-PROPANOL/OCTADECYLTRICHLOROSILANE SELF-ASSEMBLED MONOLAYERS ON NANOASPERITIES

5.1 Overview

Previously reported multicomponent self-assembled monolayers (SAMs) deposited on spin coated silica nanoparticle films have been observed for their tribological properties under varying environmental conditions. Multicomponent 3-phenyl-1-propanol (3P1P)/octadecyltrichlorosilane (OTS) SAMs were tested with an Atomic Force Microscope (AFM) to ascertain their performance characteristics under various loads in three different environments: pH 3 water, 12% relative humidity in N_2 and dry N_2. Additionally, the films were then tested for longevity under continuous contact in each of the three environments. It was discovered that the mixed SAMs displayed different friction versus load characteristics depending on the environment, also, the multicomponent films were found to outperform single component OTS SAMs in all of the tested environments. Because of the built in roughness of the spin coated nanoparticle film, the substrate surface more closely mimics those found in actual microelectromechanical systems (MEMS) devices, providing a more accurate picture of the true asperity-asperity contacts found in real device interfaces. It was found that the multicomponent films were additionally able to protect the surfaces of the tip and substrate during continuous scanning in all environmental conditions even over the

course of 5000 scans across the same region of the substrate. This behavior is credited to the ability of the OTS film to uptake and release the 3P1P during scanning as needed to regenerate film damage occurring during continual contact.

5.2 Introduction

Microelectromechanical systems (MEMS) devices stand on the brink of becoming one of the forefronts in modern technology, as they possess the potential to be implemented across a vast span of potential technologies from consumer electronics to biomedical applications. MEMS have yet to realize this potential fully due to the fact that sliding contacts within the devices have proven to limit their lifetimes to currently unacceptable time scales.[195-198] The only examples currently available outside of the laboratory are devices which minimize or eliminate motion within the device architecture. Because of this, developing methods that can reduce or eliminate surface tribological interactions such as friction, adhesion and wear is of the upmost importance to the feasibility of large scale production and implementation of MEMS devices in the marketplace. Because MEMS devices are often built from polycrystalline Si utilizing many of the same processes used in the semiconductor manufacturing industry, their machined surfaces are known to typically possess surface asperities on the order of 10-20 nm in dimension.[2] When taken into account simultaneously, the size scale of a typical MEMS component coupled with the known dimensions of the surfaces asperities preclude that the tribological properties of the materials comprising the device are controlled predominately through surface asperity-asperity interactions.[12, 17, 117] The extremely high pressures found in the contacts dictate that wear originates at these

asperity contacts and it is at that these points where the initial stages of device failure occur.[12]

In order to reduce the effects of friction and adhesion on the surfaces of MEMS, much research has been dedicated to researching self-assembled friction reducing coatings.[2-4, 7-11, 91, 199] The most studied systems to date are silane based SAMs, which are known to passivate silicon surfaces and act to reduce friction and adhesion.[9, 11, 92-94] Because of the potential for wear reduction shown by SAMs, a number of different properties have been studied in hopes of determining what combinations would act to best ensure the mitigation of surface damage. Variations that have been studied to this point include, but aren't limited to: the effects of terminal-group functionality,[95-99, 200] various interfilm stabilizing interactions,[102] the presence of voids and defects within the film,[103-107, 201] as well as the effects of molecular orientation[202] and n-alkane chain length.[202, 203]

Over the course of time, it has been concluded by many that SAMs are capable of reducing the effects of friction, adhesion and wear on silicon surfaces subjected to limited loading forces but are incapable of protecting surfaces from damage when exposed to high loads under continuous contact; limiting the useful lifetime of the materials they are intended to protect.[204-210] However, research utilizing systems which constantly regenerate themselves during device operation have shown huge promise in finally solving the MEMS operation dilemma. The most impressive of these studies employ acid or alcohol vapors to continually regenerate a lubricious surface coating during device operation, significantly reducing the signs and effects of in use wear.[59, 142,

[211-213] Technology utilizing acid vapors is currently commercially available inside of televisions and projectors using Texas Instrument's Digital Light Processing (DLP) technology.[211] Inside of a typically DLP based device, digital micromirror assemblies direct light by controlling the movement of an array of mirrors which project the image onto the screen. The surfaces of the micromotors that control the translation of the mirrors are coated with perfluorodecanoic acid vapor that is sealed inside of the device. Similarly, research into the use of alcohol vapors as replenishable lubricants for MEMS devices has revealed another promising alternative to self-assembled film based MEMS lubricants.[142, 212, 214, 215] It was reported that a steady flow of pentanol vapor into test chamber containing a MEMS based tribometer could sustain the device indefinitely.[142] The only foreseeable drawback to this sort of vapor phased lubrication scheme is implementing it into an easily manufacturable device due to the need to incorporate some sort of integral delivery system to regenerate lost vapor.

While many researchers have concluded that SAMs are unlikely to be a viable solution to the MEMS lubrication problem due to a number of factors, including relatively low surface coverages and a lack of long rang film order, some new results reported in regards to multicomponent SAMs and their performance as potential wear reducing coatings for MEMS have shown promising results. When an OTS SAM was combined with a second, weakly bound molecule with the ability to act as a mobile lubricant on top of the self-assembled monolayer, the resulting film possessed enhanced performance for lubricating the interface compared to OTS alone.[59] In a similar vein, we recently reported on a multicomponent film comprised of OTS coupled with an

intercalated 3P1P mobile layer that was found to also possess significant performance improvements under load than a single component OTS film alone.[140]

The performance enhancement seen in the multicomponent film is attributed to the addition of 3P1P into the SAM matrix. Under load, the high pressure exerted between the tip and substrate perturb the SAM while compression of the monolayer forces the physisorbed 3P1P out onto the surface of the film where it then acts as a mobile lubricant in addition to the more crystalline and immobile OTS SAM. Spectroscopic data collected before and after experimentation concluded that no significant amount of 3P1P was lost to the environment nor was there any significant uptake of water observed, suggesting that the presence of 3P1P obstructs water from reaching the silica surface.[140]

Results also indicate that the 3P1P within the film has the ability to reinsert itself after being perturbed from the SAM matrix. This ability to be re-adsorbed into the film suggests the existence of a self-healing mechanism, as the mobile 3P1P molecules are able to actually replace themselves after use or even move to depleted sites on the surface. Similar results have been seen with multicomponent films of OTS and multiply-alkylated-cyclopentane double layers, which were reported to possess a self healing capability due to the presence of a mobile lubricant component.[59]

Described in the chapter is the continuation of the studies on multicomponent OTS-3P1P self-assembled lubricant monolayers. These studies focus on the performance of the SAMs in comparison to OTS alone in multiple environments: pH 3 water, 12% relative humidity in N_2 and dry N_2.

5.3 Experimental Methods

Spin coated silica nanoparticle films were utilized in order to have substrates possessing surface asperities with sizes that mimic the asperities found in MEMS devices.[37] The colloidal silica nanoparticle thin films were formed by spin coating Si(100) substrates with a pH 13 sol containing suspended 40 nm colloidal silica nanoparticles (OX-50) provided by Degussa. Prior to spin coating, the Si(100) substrates (Virginia Semiconductor) were cleaned and hydroxylated in a 4:1:1 (v:v:v) mixture of high purity H_2O, H_2O_2 (30 %) and concentrated NH_4OH at 80° C for 30 minutes. The cleaned and hydroxylated substrates were rinsed upon removal from the cleaning solution with high purity water for 60 seconds and dried completely under streaming nitrogen. Following spin coating, the nanoparticle films where annealed by heating to a temperature of 500° C for a period of 5 hrs in order to create a stable nanoparticle film possessing additional siloxane linkages between the particles and substrate, ensuring the films remain intact during functionalization and experimentation.[37] Annealed substrates were then submersed into the (4:1:1) cleaning solution for a period of 30 minutes at 80° C and afterwards were rinsed for a period of 60 seconds under high purity H_2O. Unused substrates were stored under an oxygen and water free Ar atmosphere in an environmentally controlled dry box until needed. Functionalization of the spin coated nanoparticle films was carried out using a hexane based functionalization procedure. Octadecyltrichlorosilane (Gelest) monolayers were prepared using a solution composed of 30 mL of hexane isomers and 15 μL of OTS in a Wheaton staining jar.[88] The substrates and functionalization solution were then

sonicated for a period of 2 hours and left to sit overnight inside of a drawer. After a thirty minutes of sonication, the substrates were removed from the functionalization solution, sonicated for 30 min in THF, rinsed with high purity H_2O for a period of 60 seconds, dried thoroughly under streaming nitrogen, immediately put into a nitrogen purged FTIR spectrometer for analysis and then placed under an Ar atmosphere for later use.

Mixed OTS-3P1P SAMs were created by infusing an OTS functionalized spin coated film with 3P1P (Sigma-Aldrich). The substrates were submerged into a neat solution of 3P1P, sonicated for a period of 3 hours and then allowed to sit overnight in the neat solute. In the morning, the substrates were removed from the 3P1P solution, rinsed with ethanol and thoroughly dried with streaming nitrogen. The substrates were then analyzed with FTIR to ensure 3P1P uptake and stored submerged in 3P1P until later use.

Substrates were analyzed for OTS film integrity and 3P1P uptake using a Thermo Nicolet 6700 FTIR equipped with a liquid-nitrogen-cooled MCT A (HgCdTe) detector. Samples were collected by FTIR transmission measurements at Brewster's angle for silicon (~74°). Each spectrum was collected with 1024 scans at a resolution of 1 cm^{-1}. FTIR analysis specifics are detailed more thoroughly in Chapter IV and Appendix B.

AFM friction measurements were collected with an Agilent 5500 and the experiments were performed with commercially available, rectangular Si cantilevers (MikroMasch) with force constants ranging from 0.3 N/m to 0.7 N/m and experimentally

determined average tip radii of ~20 nm. In order to quantify the force values, exact force constants for each cantilever were experimentally determined using the Sader method, and all reported values are from calibrated levers.[217] Cantilever lateral forces were calibrated using the direct force balance method.[218] To protect against any foreign materials being introduced by the AFM probes and to control the chemistry at the tip-substrate interface, the AFM tips were also cleaned using a (4:1:1) hydroxylation solution prior to use. The tips were submerged into the solution for a period 60 seconds, rinsed by submerging twice into high purity water for 60 seconds and once into ethanol for 60 seconds. The tips were then allowed to "air" dry inside of a dry nitrogen environment. Experiments were performed under three different environments to ascertain the performance of the films in a variety of surroundings; pH 3 water, nitrogen with a controlled relative humidity of 12% and dry nitrogen. Twelve percent relative humidity is approximately the amount of humidity found within a commercial MEMS device once it has been sealed.

AFM friction measurements were performed by scanning a 1 μm^2 region under each load and plotting the average total lateral force value for each image. The final reported value was calculated by averaging the total lateral force value for five images collected at each load. The load was increased until the AFM tip was observed to fail in use or a load value of 250 nN was reached. Film performance during repetitive contact was analyzed by collecting frictional force data using an AFM tip at a load of 125 nN. The AFM was set to repeatedly scan a single 0.5 μm long line at a rate of 0.1 μm/s while monitoring the lateral force signal in the forward and reverse directions. Each scan was

collected and analyzed for the lateral force and plotted versus the number of cycles with 5000 cycles being collected for each sample.

5.4 Results and Discussion

Both the OTS SAMs and multicomponent OTS-3P1P films on the spin coated silica nanoparticle supports were analyzed with FTIR spectroscopy to ascertain the degree of order within the SAM matrix. For the OTS-3P1P film, FTIR was also used to determine the relative amount of 3P1P integrated into the OTS SAM. The location of the CH_2 asymmetric stretching band (d-) can be used to approximately determine the overall order of a self-assembled alkylsilane or alkylthiol film.[108, 151, 182-184, 186, 187] Well ordered, crystalline SAMs typically possess a CH_2 asymmetric stretching band with a peak maximum located around 2917 cm^{-1}. If a self-assembled film is disordered, the location of the peak will shift to higher wavenumber, with more liquid like films exhibiting the CH_2 asymmetric stretching peak around 2924 cm^{-1}. Well ordered films exist in a liquid crystalline form with the majority of the film's molecules in an all trans conformation,[15] thus being well ordered, densely packed and in the most desirable state for use as a surface protecting film. While well ordered films can easily be assembled on flat surfaces even when the number of carbon atoms making up the molecules in the film reaches as low as eight, the introduction of surface curvature reduces the ability of a film to achieve long range order on the surface. Much like SAMs on flat surfaces, as the length of the chains for the molecules comprising of the SAM are increased, the local ordering within the film is improved with the greatest amount of order existing for longer chains on surfaces with the lowest degrees of curvature.[88]

We and others have previously reported on the uptake of foreign molecules by alkyl based SAMs by pathways such as diffusion[188-190, 192] and solvation effects,[185, 193] with the intercalated molecules readily seen by spectroscopic techniques such as FTIR.[88, 140] For the functionalized spin coated nanoparticle films, solvent intercalation is observed to occur during silane functionalization with the solvent molecules integrating themselves into spaces in the self-assembled film matrix.[88] The fact that this intercalation is more readily observed for the films assembled on the nanoparticle surfaces compared to their analogs on flat Si(100) is likely due to the lesser degree of surface coverage for OTS on the curved verses flat surfaces, with the curved surfaces averaging one fewer molecule per square nanometer (*ca.* 1.5 vs. 2.5 molecules per square nanometer, respectively).[88, 134] This ability of the OTS SAM to uptake solvent was recently exploited to integrate a more useful molecule into the self-assembled film,[140] by immersing the SAM into a container of 3P1P, the solvent is eventually displaced by the new molecule and a new, two component SAM is formed. FTIR analysis places the relative amount of 3P1P in the film at approximately 15% ± 1%,[140] which is consistent with previous work with alkylsilane SAMs on silica nanoasperities.[88] FTIR analysis also indicates that the majority of the 3P1P within the SAM matrix exists buried within the film with a small percentage stabilized on the surface.[140]

AFM topographic analysis of the spin coated films; both functionalized and unfunctionalized showed no discernable topological differences between the surfaces. All nanoparticle films used in these studies displayed an average RMS roughness between 20 nm to 25 nm, and as such, were a reasonable model for the surfaces of

MEMS devices, which typically exhibit surface roughness on the order of 10-20 nm RMS.[17] The functionalized films were observed to possess uniform coverage with no domain structures or multilayer features observed by topographic or lateral force imaging. Friction versus load studies were performed with the AFM on the three different surfaces under three different environmental conditions: unfunctionalized nanoparticle films, OTS functionalized nanoparticle films and OTS/3P1P multicomponent SAMs where all analyzed under pH 3 water, 12% relative humidity in nitrogen and dry nitrogen. Additionally, friction versus load studies were performed on a spin coated nanoparticle film possessing approximately one monolayer of 3P1P in a dry nitrogen environment.

Figure 5.1 shows the results of a friction versus load study for a nanoparticle film coated with a physisorbed monolayer of 3P1P and a different nanoparticle film coated with a self-assembled OTS monolayer. The 3P1P appears to exhibit two different friction response regimes; an initial region where the friction response appears to rapidly increase under load before settling into a second regime whereby the friction response seen to increase less dramatically under increasingly higher loads. This performance is reminiscent of the friction response transition seen in aromatic self-assembled films where two distinct regimes exist depending on the amount of load present in the system.[224] Under low loads the fiction response was observed to be reproducible over a number of scans with a relatively low error and a higher friction coefficient than the high load regime.[224]

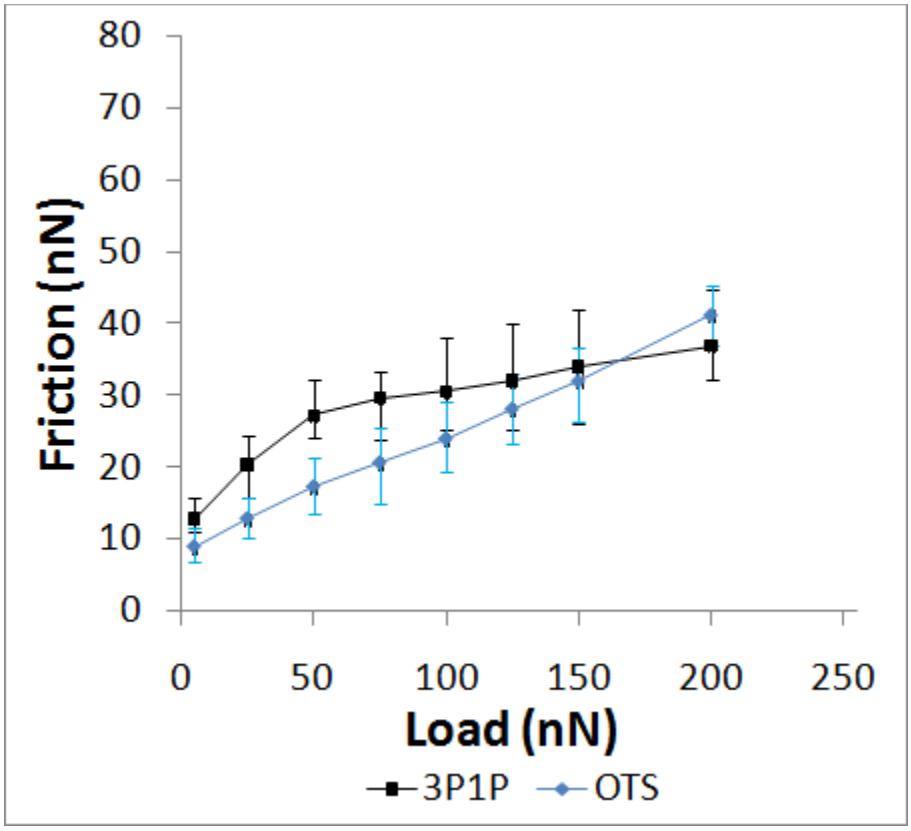

FIGURE 5.1: Friction vs. load results for a monolayer of 3P1P (■) in a nitrogen atmosphere at a sliding velocity of 0.1 μm/s. The lines connecting the data points are intended only to be guides to the eye and do not denote any trend. For comparison, the Friction vs. load results for a self-assembled monolayer of OTS (♦) are also displayed

At higher loads, a transition in the film was observed whereby the amount of error between measurements is seen to escalate while the friction coefficient decreases compared to the low load regime.[224] The film transition was reported to be mostly likely due to the effects of shear within the film and possibly owing to some reversible displacement of the molecules comprising the SAM.[224] The relatively shallow slope of the 3P1P friction versus load response under higher loads may explain the lower friction versus load response for the mixed films under similar conditions. Conversely, self-

assembled OTS SAMs have been widely studied as wear passivating surface films that reduce the observed friction force between two contacting surfaces under load.[205, 206, 210] Alkylsilane SAMs to are known to act as wear passivating surface lubricant films, protecting surface contacts and reducing friction under low loading forces. However, at higher loads the SAM becomes unable to overcome the high pressures produced in the contact and begin to fail as the molecule-surface bond strength is exceeded by the forces present in the tip-substrate contact.

Friction versus load studies on the three types of nanoparticle films (unfunctionalized, OTS functionalized and OTS-3P1P functionalized films) in pH 3 water are shown in Figure 5.2. The unfunctionalized silica surface was observed to have a higher friction response at every load in comparison to the two functionalized surfaces. The friction force is observed to increase gradually under low loads until a threshold load is reached where the friction response is seen to increase dramatically until tip failure. Interestingly, the low load response in pH 3 water for all three surfaces is observed to be lower than the same surfaces in the two other environments. The justification for this observation is twofold. First, water is known to act as a lubricant under similar conditions and is likely lubricating the tip-surface interface, reducing the friction response at low loads where the tip is unable to completely penetrate the ice-like water present at the surface.[3, 191, 222, 223] A second consideration is the loss of the adhesion due to the lack of a capillary meniscus between the tip and substrate when performing experiments in a liquid environment, which significantly reduces the total adhesive interaction between the tip and surface.

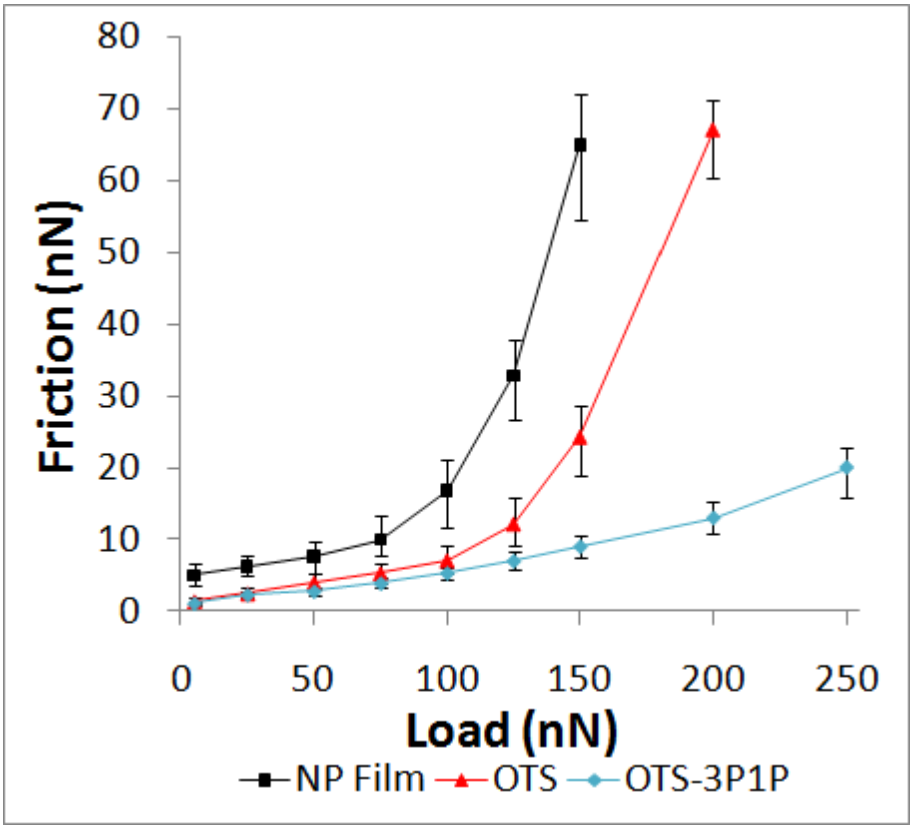

FIGURE 5.2: Friction vs. load results for unfunctionalized nanoparticle films (■), OTS functionalized nanoparticle films (▲), and OTS-3P1P multicomponent films (♦) in pH 3 water at a sliding velocity of 0.1 μm/s. Some error bars fall within the size of the marker. The lines connecting the data points are intended only to be guides to the eye and do not denote any trend.

During scanning, the OTS film enabled the tip to scan the surface without failure at higher loading values than the unfunctionalized surface, yet the film was observed to break down under loads of 150 nN, similar to results seen in previous studies of OTS SAMs on silica.[91] This inability to protect the surface at a loading value only 50 nN greater than the load that lead to tip failure on the unfunctionalized surface is yet another example of the inability of simple, single component SAMs to protect asperity-asperity

contacts under load. The multicomponent OTS-3P1P films showed the most favorable friction response under load, showing significant friction reduction compared to OTS SAMs alone at higher loading values. At lower loads, the behavior of the mixed film and the OTS SAM are noticeably similar. It was reported previously that this phenomenon can be attributed to the OTS component of the film contributing to the bulk of the film's tribological performance at low loads.[140] However, at higher loads, the observed lateral response by the mixed film was greatly reduced compared to the other two surfaces. Even under high loads that lead to the failure of the unfunctionalized and OTS functionalized nanoparticle films, the OTS-3P1P film was observed to have a reduced friction response and no signs of gross wear were seen on the surface.

In order to better understand how these films perform under conditions that were more fitting for a realistic environment in which MEMS would operate, the same three films were tested under an a nitrogen environment possessing 12% relative humidity as well as under dry nitrogen. Figure 5.3 shows the friction versus load response for the three films under nitrogen possessing 12% relative humidity. Compared to the friction versus load response for the same films in pH 3 water, it can be seen that for all three surfaces, the friction response at the lower loads is higher than those observed in the liquid environment. The higher friction is most likely a result of the loss of the lubricating ice-like water layers as well as the addition of a capillary meniscus between the tip and substrate. As mentioned previously, several monolayers of ice-like water are known to form at the interface between a surface and the surrounding water environment when a surface is submerged in water. With less than one monolayer of water present on

the surface in a 12% relative humidity environment, the lubricating ability of the multilayered ice-like water cap is lost, increasing the friction response between the tip and the surface. It is likely that the water present does act as lubricant to some degree; however the relative amount of lubrication reduction provided by its presence in this system is unknown.

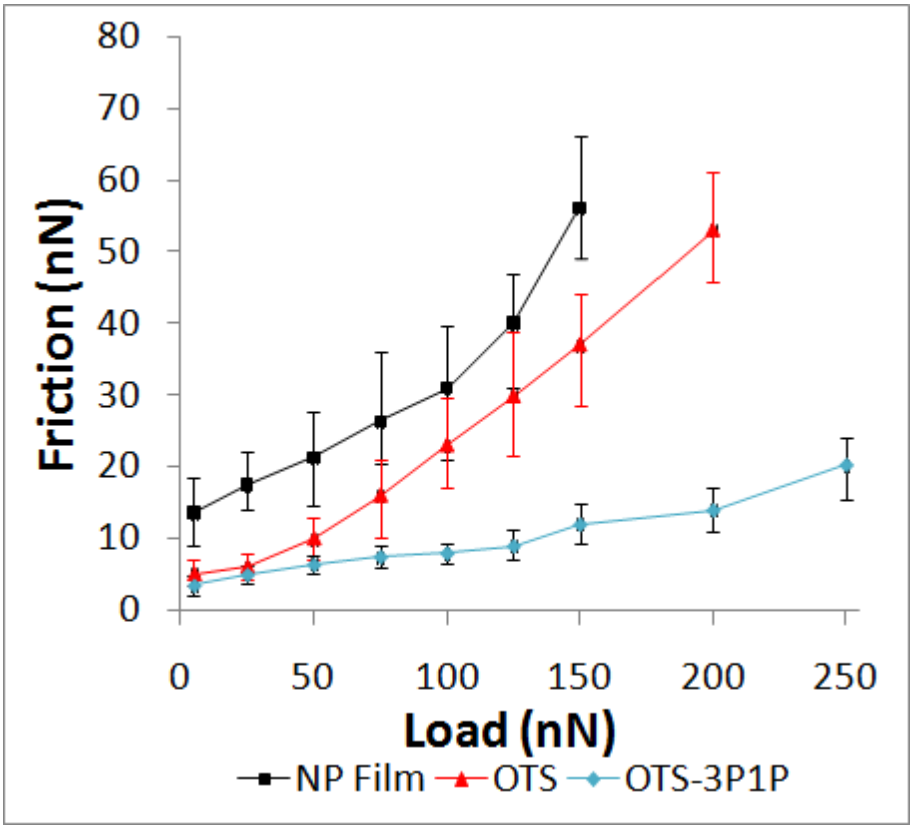

FIGURE 5.3: Friction vs. load results for unfunctionalized nanoparticle films (■), OTS functionalized nanoparticle films (▲), and OTS-3P1P multicomponent films (♦) in a 12% relative humidity environment at a sliding velocity of 0.1 μm/s. Some error bars fall within the size of the marker. The lines connecting the data points are intended only to be guides to the eye and do not denote any trend.

Similarly, the removal of bulk water from the surrounding environment enables the formation of a capillary meniscus between the AFM tip and the sample surface. Due to the fact that nanoscale friction possesses an adhesion component,[225] the increase in adhesion due to the presence of the meniscus also helps to explain at least a portion of the increase in the friction response at lower loads compared to the same films in water. At higher loads the results of the friction versus loading experiments reverse for the two systems, with the unfunctionalized and OTS functionalized films submerged in water displaying a higher friction response than the films at 12% relative humidity. This behavior is most likely the result of the relative amount of water in the two systems. Water is known to speed the breakdown of alkylsilane SAMs on silicon oxide surfaces as well as increase the rate of wear on exposed silicon oxide surfaces through catalytic Si-O bond breaking.[37, 199, 212, 215] The unfunctionalized substrates completely submerged in water display this behavior as both the tip and surface reached a state of gross wear at a load of 150 nN while the same surface under 12% relative humidity displayed an average friction response under the same load which was approximately 9 nN lower. Similarly, the OTS coated surfaces in water likely saw their protective coatings breakdown quicker than those in 12% relative humidity due to the shear amount water present in the pH 3 water system. The OTS films in the partially wet environment performed better at higher loads than their analogs under pH 3 water, it was observed that the average friction response under loads of 200 nN were approximately 14 nN lower for the OTS films under 12% relative humidity. Conversely, the multicomponent OTS-3P1P films displayed similar performance in both environments, suggesting that

the ability of the mixed film to protect the surface from wear is equal under both environmental conditions.

The films were finally probed in a dry nitrogen environment to observe what effect the absence of water had on the friction versus load performance of the different films. Figure 5.4 shows the friction versus load response for these experiments. Unlike the previous two studies, the only water present in the experimental environment during scanning was unintentionally introduced during experimental setup. The environmental chamber was constantly flushed with dry nitrogen both before and during experimentation in hopes of reducing or eliminating any of the effects which water can potentially have on the samples. It was observed that all three surfaces in the dry nitrogen environment displayed higher friction response at low loads than their analogs under pH 3 water and under 12% relative humidity. Unlike the other two wet systems, the dry nitrogen system lacks enough water to act as a lubricant in the tip surface interface, increasing the friction response under low loads. However, at higher loads, both the unfunctionalized surface and the OTS film display a lower friction response than their analogs in the other two environments, which like their responses at lower loads, is most likely due to the lack of water inside the contact. This lack of water eliminates the possibility of water catalyzed Si-O bond breaking, improving the lifetime of the OTS film as well as the unfunctionalized surface. The OTS-3P1P performed similarly under high loads as its analogs in the other two environments with all three sets of data at 200 nN falling within the experimental error of the others. This suggests that

at least for the three environments and experimental parameters explored during these experiments, OTS-3P1P film is relatively robust.

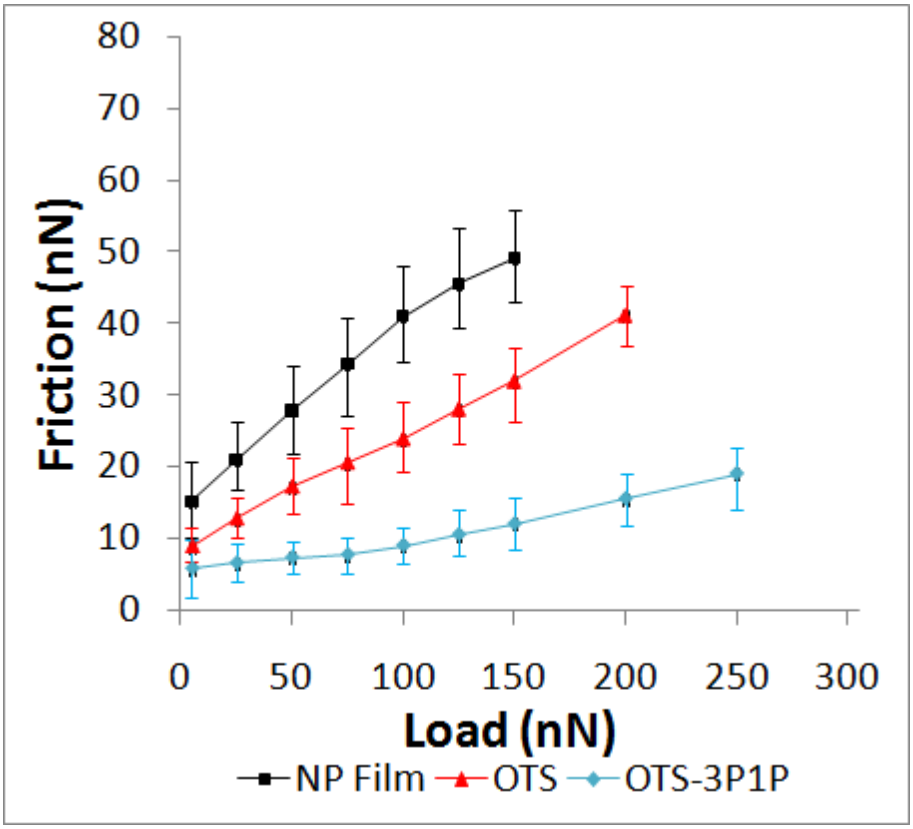

FIGURE 5.4: Friction vs. load results for unfunctionalized nanoparticle films (■), OTS functionalized nanoparticle films (▲), and OTS-3P1P multicomponent films (♦) in a nitrogen atmosphere at a sliding velocity of 0.1 μm/s. The lines connecting the data points are intended only to be guides to the eye and do not denote any trend

In order to ascertain the ability of the OTS-3P1P film to reduce wear under continual operation in the three different environments, the surfaces were subjected to friction vs. time scanning by AFM. Figure 5.5 displays the friction response versus the

number of scans for OTS-3P1P films in each environment under a load of 125 nN during the course of 5000 cycles.

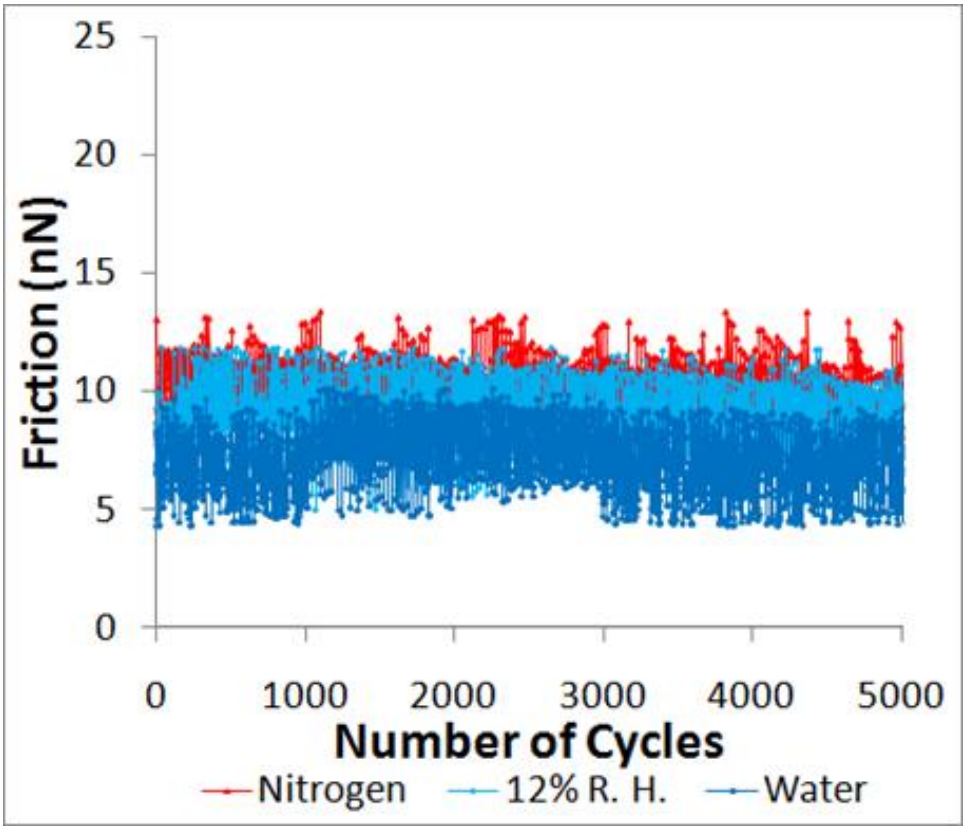

FIGURE 5.5: Friction vs. time test results for OTS-3P1P multicomponent films at a load of 125 nN and a sliding velocity of 0.1 μm/s. The lines connecting the data points are intended only to be guides to the eye and do not denote any trend.

For each experiment, the friction response is seen to remain relatively stable, even under continuous scanning with the films displaying similar friction responses throughout the experiment with the surface films protecting the surface from gross wear throughout the entirety of the experiment. These results further suggest that the mixed film performs similarly well under relatively high loads in all three environmental conditions due to the

film's ability to heal itself *in situ*. The results also indicate that ultimately, the film's performance during these studies was dictated by the environment in which it was under. The mixed film in pH 3 water was observed to display the lowest friction response, although the average value fell within the experimental error of the results for the 3P1P film in the other two environments. The low friction response is most likely due to some residual lubrication effect by water remaining in the contact, which would also explain why the film under 12% relative humidity has a slightly higher friction response than the film in pH 3 water and a slightly lower response than the film in the dry nitrogen atmosphere.

5.5 Conclusions

Here we have shown that the performance of OTS films infused with a short chain alcohol is affected by local environmental conditions under variations in load and during long term testing. Multicomponent OTS-3P1P were observed to outperform OTS SAMs alone under a variety of environmental conditions. These multicomponent systems act as self-maintaining and regenerating films as they demonstrate an ability to uptake and release molecules such as 3P1P which then likely function as mobile lubricants during contact induced stress. These studies demonstrate the means of using a disordered/reduced coverage SAM as an avenue of storing weakly bound molecules, which can then subsequently be released to lubricate the interface. Studies currently underway are exploring how shear rate dependence influences the function of these multicomponent films.

CHAPTER VI

THE INTERESTING CORRELATION BETWEEN FILM MECHANICS AND EXPERIMENTAL PROBE RATES

6.1 Overview

Octadecyltriethoxysilane (OTE) and Dodecyltrichlorosilane (DTS) self-assembled monolayers (SAMs) and their effects on friction and adhesion have been studied on both functionalized and unfunctionalized flat silicon oxide surfaces, spin coated silica nanoparticle substrates and atomic force microscopy (AFM) probes. Adhesion values were collected utilizing AFM Force-Distance spectroscopy and values were compared for the adhesive response of films assembled on the flat native oxide of Si(100) versus silica asperities possessing nanoscale curvature. It was found that the adhesion values differ for the SAMs coated on surfaces with nanoscale curvatures versus SAMs on nominally flat surfaces. The results also point toward the existence of an equilibrium process which is present during force measurements, altering the observed adhesion between similar contacts with variations of tip approach and retract rates. Additionally, multicomponent octadecyltrichlorosilane (OTS)/3-phenyl-1-propanol (3P1P) monolayers on spin coated silica nanoparticle substrates were tested for their shear response under various loads compared to single component OTS SAMs on flat Si(100) and spin coated silica nanoparticle substrates. It was found that friction versus tip speed performance for the multicomponent films was better than that of single component OTS at lower shear rates; performance for both films was similar all loading

situations at high shear speeds, which is can be attributed as an artifact of the inherent roughness of the spin coated nanoparticle substrate or possibly the inability of the multicomponent film to limit friction any better than its single component analog under high shear speeds.

6.2 Introduction

Understanding and controlling friction between components in motion is of significant importance for long-term device operation. The effects of friction acting upon the moving parts in microelectromechanical systems (MEMS) devices has intensified the need to understand friction's role at a molecular level. The earliest studies utilizing atomic force microscopy (AFM) to probe normal and friction forces between materials were conducted in 1987,[19] which lead to the development of a form of AFM that is now generally known as friction force microscopy (FFM) or lateral force microscopy (LFM). These original tribological studies on the nanoscale spawned the growth of nanotribology; the study of friction, adhesion and wear on the nanometer scale. AFM becomes advantageous as a mode for observation of nanoscale tribological properties due to inherent nature of an instrument that utilizes the motion of a nanometer sized probe over the sample's surface. During nanotribology experiments, friction forces arise when the AFM tip contacts a sample surface using a known normal load. These forces are detected by the instrument as a horizontal torsion of the cantilever, which is directly related to the affinity of the probe with the surface material. Some of the applications of AFM to nanotribology include thickness measurements on solid and liquid lubricants possessing monolayer or nanometer thickness,[226] the observation of

surface scars or wear tracks,[227] measuring nanoscale frictional forces,[6, 23, 26, 43, 228-232] characterization of surface properties such as morphology and roughness, as well as the evaluation of nanoscale mechanical properties such as hardness, elasticity, and plastic deformation.[110, 233] One of the most significant advantages of AFM as a tool for tribological studies is the ability of AFM to be used on most types of materials and environments ranging from ambient surroundings to vacuum or liquid conditions, making AFM an ideal tool for research on a wide variety of samples under a broad array of parameters.

Over the past several years, there has been a significant interest in the use of self-assembled monolayers (SAMs) as lubricants for MEMS.[4, 7, 10, 11, 13, 14] As such, the details of friction, adhesion and wear for SAMs on Si surfaces have been investigated, with these systems being described as model substrates to explore the tribological properties of these materials in MEMS like environments.[4, 92-94] Some of the many areas explored have included understanding what the effects of various modulations within the SAM matrix have an film performance, such as altering end-group functionalities,[95-99, 200] the intention formation of inter-chain lateral interactions, molecular orientation with regards to the surface and nearest neighbor molecules,[101, 102] variations in chain length,[33] the presence of chain entanglements or defects,[103-107, 203] and the effects played by variations in head group functionality;[108] all of which impact the tribological behaviors in SAM lubricant films.[100, 110-113, 234]

While experimentation on flat Si substrates has yielded invaluable information on SAM behavior, there is still a disconnect between understanding how these films

work under idealized circumstances as compared to real interfaces like those found in MEMS. Surfaces that appear smooth on the macroscopic scale, upon closer inspection are found to typically consist of nanometer scaled asperities on the order of 10-20 nanometers, whose intentional or accidental interactions ultimately control the friction, adhesion, and wear between the contacting interfaces.[117] The size of these asperities becomes particularly important when one considers that the true contact area between interfaces is localized through asperity-asperity interactions where extremely high-pressures can be produced as they contact each other. These localized high pressures have the effect of sharply increasing the local stress fields that cause materials to yield and shear as they encounter each other during sliding and intermittent contact.[12] In addition to the load distribution at nanoscale asperity-asperity contacts, asperity size will influence surface wetting and adhesion due to capillary forces localized between the contacts.[8] Because AFM tips exhibit nanoscopic curvature on the order typical of the surface asperities, the interaction of an AFM tip with a surface is thought to be a reliable model for the interaction of a single asperity with a surface (Figure 6.1). As such, there have been numerous studies of frication and adhesion at interfaces using AFM and these measurements have become a paradigm for the nanotribology community. Simply put, AFM enables researchers to establish the relationship between the structure of the SAMs and their tribological behaviors with molecular level detail[4]

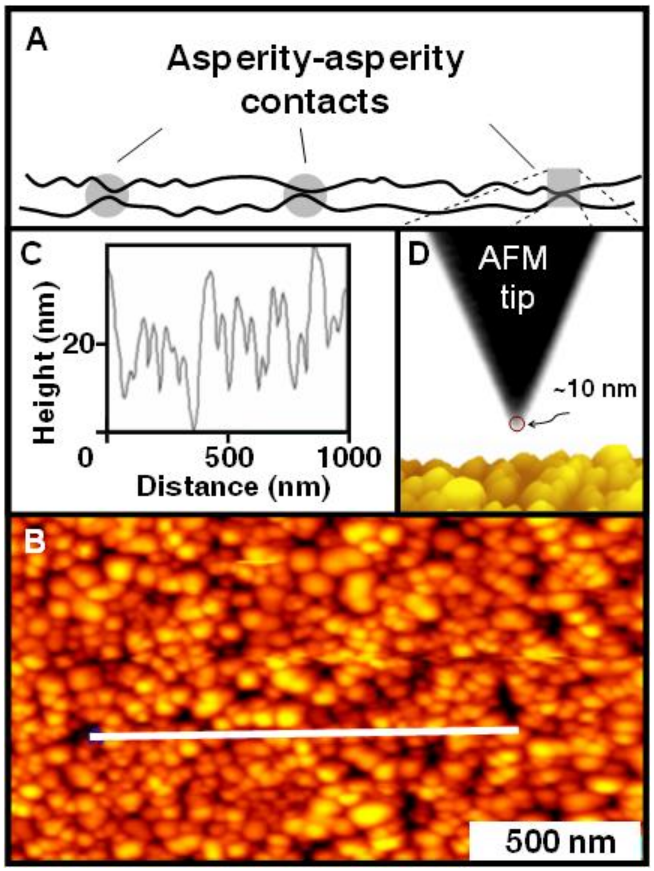

FIGURE 6.1: AFM tip-particle interactions are used to mimic asperity-asperity interactions at the nanoscale. (A) While surfaces at the nanoscale might appear to be flat, in actuality, they posses a degree of roughness. (B) Silica nanoparticle films act as simply to manufacture substrates with roughness values that correlate to real surfaces. (C) The AFM line trace from the spin coated film in section B. (D) Scanning Electron Microscope image of an AFM tip of the same manufacture as used in the these studies and a side view of spin coated silica nanoparticle film as a graphic illustration of how the AFM-nanoparticle film act to mimic a MEMS asperity-asperity junction. Reused with permission. Copyright 2008 Wiley Periodicals, Inc.[116].

The structure of applied lubricant films is highly dependent upon asperity curvature and differs from those assembled on flat surfaces.[88] Surface roughness has been known to be intentionally introduced into MEMS devices in order to reduce the stiction between device contacts.[8] However, these same asperities must later resist wear

during controlled or accidental contact during device operation. Functioning as a protective lubricant layer in such systems, self-assembled monolayers (SAMs) of alkylsilane and fluorosilane compounds with chain lengths ranging from C_{10}-C_{18} have been shown to be useful in the reduction of friction and adhesion in MEMS. Thus, it is essential to understand the tribological behavior of SAMs on such nanoscopic asperities. In most studies, SAM modified AFM tips are frequently used and it was assumed that film ordering of the SAMs on the AFM tips were comparable to SAM structures on flat surfaces.[119-126, 232, 235]

Because the molecules in self-assembled monolayers of alkylsilanes are covalently bound to substrates, they are not as prone to contact removal during multiple cycles of shear as other, physisorbed SAMs. Despite the large volume of work detailing the dependence of lubrication properties on self-assembled film order, very little fundamental knowledge exists detailing the relationship between substrate surface curvature, film ordering and SAM performance under shear. Even less is known in regards to how the various components in mixed SAMs contribute to the overall film behavior during shear. Studies of alkanethiolate SAMs on gold[236] have shown that strong intermolecular interactions in well ordered monolayers will act to keep together a large section of the SAM during shear while simultaneously inhibiting the formation of structural defects. As such, monolayers formed with longer carbon backbones, with their relatively higher packing densities and more ordered film matrix are better at withstanding the effects of shearing events.

Both experiments and simulations of SAMs composed of molecules possessing long alkyl chains under shear conditions have shown that the extent of film disorder decreases with increasing depth within the film. Close packed monolayers of eighteen carbon atom chains with methyl terminations have shown defect densities to decrease exponentially with increasing depth in the monolayer until a constant is approached in the range of 7 or 8 carbon atoms from the flat substrate surface.[237] Simulations performed in our lab have shown that self-assembled films on curved surfaces typically exhibit high defect densities at deeper depths than what has been reported for similar films on flat substrates; indicating that these more disordered SAMs may be less able to inhibit shear because of the lower amount of ordering present within the films.

In this chapter, the tribological behavior of OTE and DTS SAMs on asperities with nano-sized curvature were compared with the same films assembled on flat Si surfaces. To achieve this goal, AFM tips and silica nanoparticles were exploited to mimic nanoscale asperities. Time dependent behavior of the measured adhesion between functionalized and unfunctionalized silica surfaces was studied, which may prove to be essential information toward understanding the nature of the monolayers used in these studies. In addition, the behavior of multicomponent OTS-3P1P versus OTS alone on both flat and spin coated nanoparticle substrates films under various shear rates is detailed.

6.3 Experimental Methods

H_2O_2 (30% reagent grade) and concentrated NH_4OH, tetrahydrofuran (THF), hexanes isomers, and 3P1P were ordered from Sigma-Aldrich. Colloidal silica OX-50

was obtained from Degussa and dispersed in a sol at pH 13. Octadecyltriethoxysilane (OTE), octadecyltrichlorosilane (OTS) and dodecyltrichlorosilane (DTS), were purchased from Gelest. All chemicals were used as received. Ultra high purity water with a resistivity of no less than 18.2 MΩ·cm was sourced from a Barnstead NANOpure Diamond water filtration system.

Si(100) substrates (Virginia Semiconductor) and AFM tips (MikroMasch) were cleaned and hydroxylated using a 4:1:1(v:v:v) mixture of high purity H_2O, 35% H_2O_2 and NH_4OH at 80°C for 30 minutes. Following the cleaning procedure, the substrates were thoroughly rinsed with high purity H_2O and dried with streaming nitrogen. Nanoparticle films were made by spin coating the nanoparticle sol onto cleaned and oxidized Si(100) wafers. Following the nanoparticle spin coating, the films where annealed by heating to a temperature of 500° C for a period of 5 hrs. This step was undertaken in order to ensure the creation of a stable nanoparticle film with multiple siloxane linkages between the particles and substrate which would remain intact during future functionalization and experimentation.[37] Prior to functionalization and unfunctionalized experimentation, the annealed nanoparticle substrates were again submersed into a (4:1:1) cleaning solution for a period of 30 minutes at 80° C and were rinsed following hydroxylation for a period of 60 seconds under high purity H_2O. Any unused substrates were stored under an oxygen and water free Ar atmosphere until needed.

Self-assembled monolayers of OTE were prepared on the cleaned and hydroxylated native oxide layer of Si(100), cleaned and hydroxylated silica nanoparticle

films and cleaned and hydroxylated Si AFM tips. The OTE monolayers were made from a stock hydrolysis solution comprised of 0.25g OTE, 0.75ml of 6M HCl and 20ml THF, which had been stirred continuously for a period of at least four hours before use. Film formation was carried out in a Wheaton staining jar using 1 mL of the OTE stock solution and 20 mL of cyclohexane. Once submerged, the solution and substrates were sonicated for a period of 3 hours. After sonication, the substrates were removed to a second Wheaton staining jar containing 35 mL THF and sonicated for an additional 60 minutes. Once removed, the substrates were cleaned using high purity water and blown dry with streaming nitrogen. Unused substrates were place in vacuum at room temperature until needed.

Dodecyltrichlorosilane and octadecyltrichlorosilane monolayers were prepared submerged in a solution composed of 30 mL of hexane isomers and 15 μL of either DTS or OTS in a Wheaton staining jar.[88] The substrates and functionalization solution were then sonicated for a period of 2 hours and left to sit overnight inside of a drawer. After thirty additional minutes of sonication, the substrates were placed in a second Wheaton staining jar containing 35 mL of THF and sonicated for 30 minutes. They were then rinsed for 60 seconds in high purity water, dried under streaming nitrogen and immediately placed into a nitrogen purged FTIR for spectral analysis. Once a proper degree of functionalization had been confirmed, the substrates were used immediately or placed into a controlled Ar atmosphere until later use.

Multicomponent OTS-3P1P SAMs on spin coated nanoparticle substrates were formed by displacing trapped hexanes isomers left over from the functionalization

process with 3P1P. OTS coated spin coated nanoparticle films were submerged in neat 3P1P and sonicated for a period of 3 hours and were then placed overnight in a drawer to sit in the neat solute. The substrates were then removed from the 3P1P solution, rinsed with ethanol and dried with nitrogen. The substrates were placed into a nitrogen purged FTIR to ensure 3P1P uptake and were then stored submerged in 3P1P until further use.

All functionalized substrates were analyzed for SAM film integrity and/or 3P1P uptake with a Thermo Nicolet 6700 FTIR equipped with a liquid-nitrogen-cooled MCT A (HgCdTe) detector. Transmission FTIR measurements were collected at Brewster's angle for silicon (~74°). Each spectrum was collected with 1024 scan at a resolution of 1 cm^{-1}. The locations of the methylene symmetric (*ca*. 2850 cm^{-1}) and asymmetric (*ca*. 2918 cm^{-1}) stretching frequencies were used as a qualitative indicator of film order.[186]

AFM images and force-distance measurements on OTE and DTS were made with a Molecular Imaging PicoSPM coupled with RHK Technology SPM 1000 Electronics Revision 8. OTE and DTS adhesion measurements were performed with commercially available triangular Si AFM cantilevers form MikroMasch. All values reported for OTE were quantified using the nominal force constant and tip radii provided by the manufacturer of 0.12 N/m and 10 nm, respectively. For quantitative measurements on DTS and OTS-3P1P multicomponent films, the force constants were calibrated using the Sader method[217] instead of coupled level methods.[238] The lateral force constants for cantilevers being used during friction measurements were found utilizing the direct force balance method.[218]

To ensure a uniform measurement environment for the collected adhesion data, all adhesion experiments were performed at room temperature in high purity water at pH 3, as this is the isoelectric point for silica and this pH ensures any exposed regions of the silica surfaces remain fully hydroxylated and charge interactions between the tip and substrate are minimized.[220] The adhesion between the AFM probes and substrates were determined from the pull-off forces taken from the force-distance spectra and a minimum of 10 force-distance curves were collected and averaged for each data point reported.

SAM shear measurements were collected with an Agilent 5500 AFM using rectangular MikroMasch cantilevers calibrated for both normal[217] and lateral[218] force constants and with experimentally determined tip radii of approximately 20 nm. Prior to experimentation, the AFM tips were cleaned and hydroxylated using a (4:1:1) hydroxylation solution. The tips were submerged into the cleaning solution for a period of 60 seconds and then rinsed by submerging twice into high purity water for 60 seconds and once into ethanol for 60 seconds. The tips were then allowed to "air" dry in a dry nitrogen environment. Shear measurements were performed by loading the AFM tip to a predetermined load and scanning a 500 nm by 500 nm region at increasingly faster scan rates. The forward and reverse friction scans at each load and speed were averaged across the entire image and were used to create the reported data points.

6.4 Results and Discussion

Adhesion forces between OTE modified AFM tips and OTE modified substrates were determined using AFM based force-distance spectroscopy (Figure 6.2). In order to

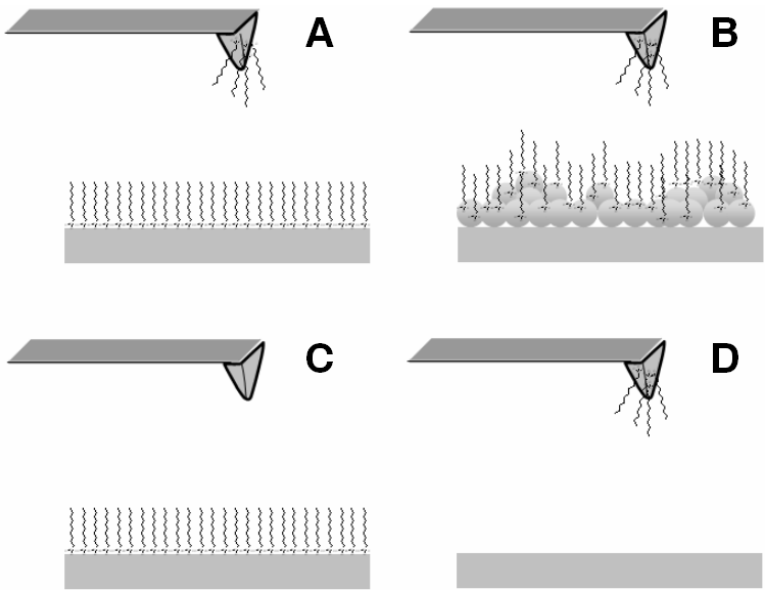

FIGURE 6.2: The four systems studied in these experiments for friction and adhesion. (A) OTE-coated silicon tip and an OTE-coated flat silicon surface; (B) OTE-coated silicon tip and an OTE-coated nanoparticle surface; (C) Bare silicon tip and an OTE-coated flat silicon surface; (D) OTE-coated silicon tip and a bare flat silicon surface. [116]

minimize the adhesive contributions from outside elements and to ensure the reported values were directly drawn from the tip-sample adhesive interactions, all adhesion measurements were carried out in pH 3 water. By performing the experiment in a liquid environment, capillary forces that are typically induced by humidity in the air are eliminated. Similarly, pH 3 was chosen because it is approximately the isoelectric point of silica, which will reduce or eliminate the effects of tip-sample charge interactions as any exposed silica surfaces should be hydroxyl terminated at the experimental pH. In the first set of studies (Figure 6.3), two different systems were evaluated. First, an OTE functionalized AFM tip was used to probe an OTE functionalized Si(100) native oxide layer. Next, an OTE functionalized AFM tip was used to probe an OTE functionalized

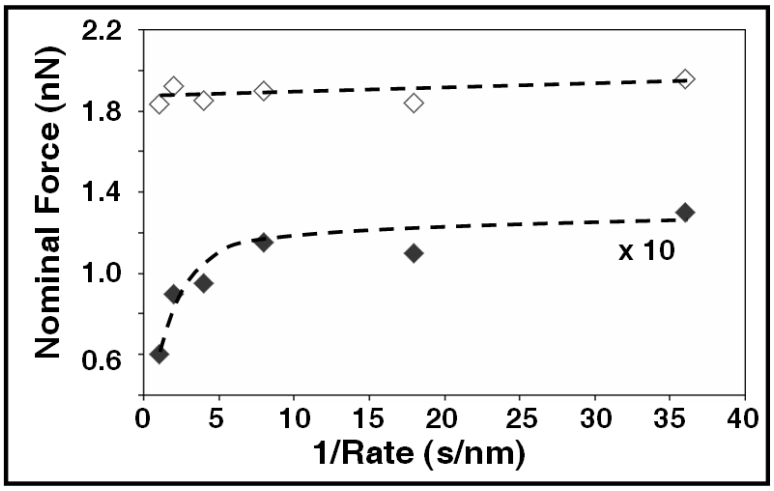

FIGURE 6.3: Adhesion forces between OTE modified AFM tips and OTE modified silicon substrates (◊) exhibited on a small dependence on attract and approach rate, while adhesion forces for OTE modified AFM tips and OTE modified 40 nm spin coated films (♦) where not only ~ 15 times lower, but demonstrated a clear dependence on approach and retract rates where adhesion values were much higher for slower approach/retract rates. The data for the OTE modified AFM tips and nanoparticle surfaces (♦) have been scaled by a factor of 10 for comparison. The lines connecting the data points are intended only to be guides to the eye and do not denote any trend. [116]

spin coated silica nanoparticle film. During force-distance curve collection on the functionalized spin coated nanoparticle film, only the highest particle asperities in the topographic images were probed in order to minimize any potential interference from nearest neighbor particles. The surface was reimaged after force-distance collection to ensure none of the nanoparticles were displaced during the experiments.

The measured adhesion between the OTE modified flat Si surfaces and the OTE modified AFM tips were approximately 15 times greater than the adhesion measured between the OTE modified spin coated surfaces and the OTE modified AFM tips. Interestingly, the adhesion forces between the OTE modified AFM tips and spin coated

surfaces clearly show a dependence on the tip approach/retract rate used during measurement with the highest adhesion values occurring along with the slowest approach/retract rates. These results are interesting due relative small difference between the contact areas for the two systems, with the nanoparticle substrate and AFM tip have approximately a 30% smaller contact area. The change in contact area alone is not enough to rectify the large difference in adhesion, which indicates that the difference must be tied to the molecular nature of the SAM coating.

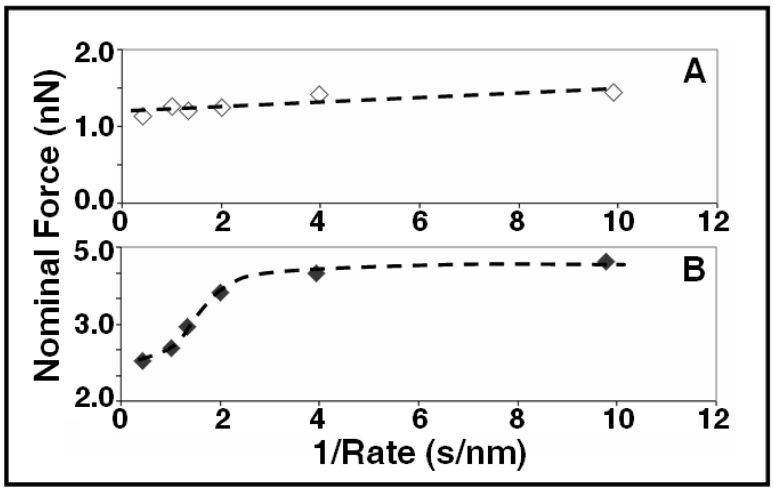

FIGURE 6.4: (A) Observed adhesion forces between an hydroxylated AFM tip and an OTE modified Si(100) surface (◊). (B) Observed adhesion forces between an OTE modified AFM tip and a hydroxylated Si(100) surface (♦). Rate-dependent behavior was again observed in these experiments as reported in Figure 6.3. The data presented in this figure were collected from two different AFM probes at different times, therefore the adhesion values were calculated using the nominal cantilever force constant. The lines connecting the data points are intended only to be guides to the eye and do not denote any trend. Copyright 2008 Wiley Periodicals, Inc.[116]

As the above results point toward some influence on SAM adhesion by surface coverage, two additional systems were tested to verify the presence of an

approach/retract rate dependence (Figure 6.4). The next two systems consisted of an unfunctionalized, cleaned and hydroxylated AFM tip probing an OTE SAM on a flat Si surface and an OTE coated AFM tip probing an unfunctionalized, cleaned and hydroxylated flat Si surface. In both systems, the chemical interactions should be equivalent in that a hydrophobic OTE SAM is interaction with a hydrophilic SiO_2 surface.

Compared with the first two systems, these two have some advantages experimentally. First, as the OTE modifies only one side of the surfaces in contact, there are no potential OTE chain entanglements that can occur during the force measurements. Second, in both cases the substrate surfaces are relatively flat and therefore allow measurement and comparison of the adhesion interactions the two systems. To make the data comparable, in each experiment the same AFM tip was used for the measurements on both systems. First, the tips were cleaned and hydroxylated and then used for investigation of functionalized surfaces. Following thorough cleaning, the same AFM tip was then dried and immersed in an OTE solution to allow for SAM formation. It was then used again for force measurements on the hydroxylated Si surface. As was seen with the first two systems, the adhesion forces measured for the OTE SAM on the flat native oxide of Si(100) showed little variation due to changes in the approach and retract rate, while the OTE functionalized AFM tip displayed a nearly 200% increase in adhesion for the slowest approach and retract rates in comparison to the fastest.

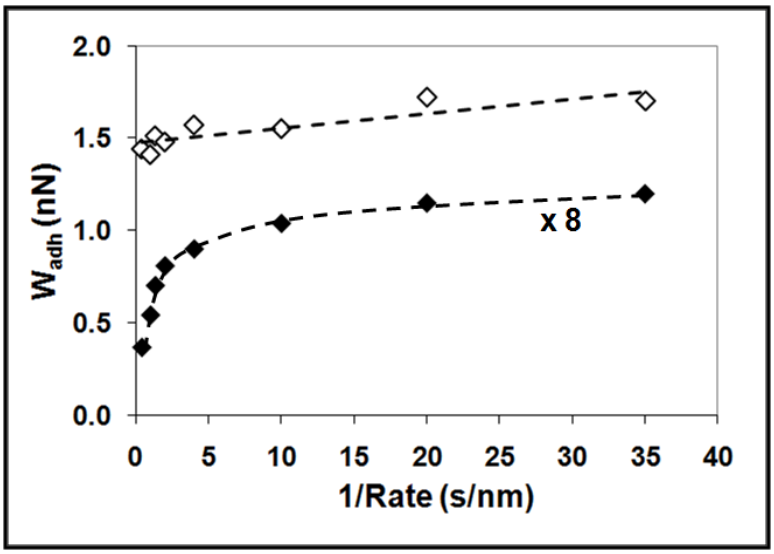

FIGURE 6.5: Adhesion forces between dodecyltrichlorosilane modified AFM tips and DTS modified silicon substrates (◊) exhibited on a small dependence on attract and approach rate, while adhesion forces for DTS modified AFM tips and DTS modified 40 nm spin coated films (♦) where not only approximately 13.6 times lower, but demonstrated a clear dependence on approach and retract rates where adhesion values were much higher for slower approach/retract rates. The data for the DTS modified AFM tips and nanoparticle surfaces (♦) have been scaled by a factor of 8 for comparison. The lines connecting the data points are intended only to be guides to the eye and do not denote any trend.

The adhesive interactions between DTS modified AFM tips and DTS modified substrates were performed in a similar fashion to the experiments completed on OTE. Again, the experiments were performed under pH 3 water to ensure the reported adhesion values are due to the actual adhesion between the tip and surface and not some contribution from charge interactions or capillary forces. In the first pair of studies reported in Figure 6.5, two different DTS functionalized systems are compared. In the first system, DTS functionalized AFM tips are used to probed adhesion against DTS functionalized Si(100) substrates and DTS functionalized spin coated nanoparticle films.

As in the previous adhesion study on functionalized nanoparticle films, force-distance curves were only collected on the highest particle asperities in the topographic images and the surface was reimaged post force-distance curve collection to ensure none of the nanoparticles had been displaced during testing.

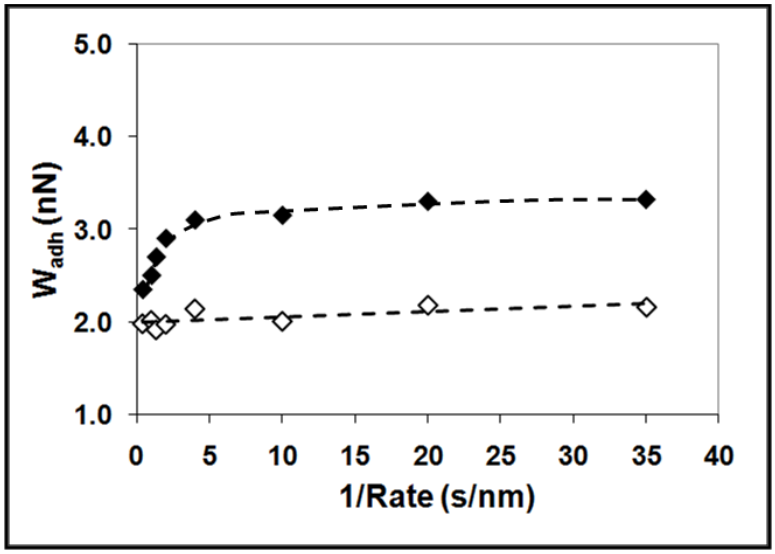

FIGURE 6.6: Observed adhesion forces between an hydroxylated AFM tip and a DTS modified Si(100) surface (◊). Observed adhesion forces between a DTS modified AFM tip and a hydroxylated Si(100) surface (♦). The lines connecting the data points are intended only to be guides to the eye and do not denote any trend.

The measured adhesion between the DTS modified flat Si(100) surfaces and the DTS modified AFM tips were approximately 13.5 times larger than the measured adhesion measured between the DTS modified spin coated substrates and the DTS modified AFM probes. In a fashion similar to the OTE functionalized surfaces, a rate dependence was observed for the collected adhesion values on the functionalized spin coated nanoparticle films, with the highest adhesion values seen for the slowest approach

and retract speeds. These results further indicate that the nature of the molecular coating plays a significant role in the measured adhesion between the surfaces and that size of the contacting interface alone is not enough to define the adhesion characteristics of a molecular contact.

Figure 6.6 further displays the existence of a rate dependent adhesion factor for molecular films. The two systems probed consisted of an unfunctionalized, cleaned and hydroxylated AFM tip probing a DTS SAM on a flat Si(100) surface and an DTS coated AFM tip probing an unfunctionalized, cleaned and hydroxylated flat Si(100) surface. Again, in both systems, the chemical interactions can be considered to be equivalent in that a hydrophobic DTS SAM is interacting with a hydrophilic SiO_2 surface, eliminating any potential chain entanglements from occurring during force-distance curve collection. The measured adhesion between the two systems show similar trends as their OTE counterparts. Adhesion between the DTS SAM on the flat Si(100) surface and the unfunctionalized AFM tip showed little variation due to changes in the approach and retract rate while the functionalized AFM probe's interactions with an unfunctionalized and hydroxylated native Si(100) oxide layer display a clear rate dependence between the slowest approach and retract rates in comparison to the fastest.

As mention previously, the difference observed in the adhesion values for the self-assembled cannot be explained solely by variations in the contact areas between the different systems, so some sort of molecular influence based on the nature of the surface the film is assembled on must be at play. A functionalized AFM tip possessing a radius of curvature of 10 nm would have a silane SAM with a packing density lower than on an

atomically flat surface, resulting in a more disordered film than a SAM on flat surface comprised of the same molecular constituents.[88, 216] The loss in order can be attributed to the lower packing density as well as the effects of curvature discussed in Chapter III. Briefly, the disorderd state of the film is due to the reduction of the number of stabilizing lateral van der Waals interactions between the molecules making up the SAM, creating a surface film with a more amorphous character and a lower elastic modulus.

When compared to SAMs on the nominally flat Si(100) substrates, the lower packing density on the functionalized AFM probes while in the presence of water results in a softer film than its well ordered counterpart. The greater degree of mobility afforded to the molecules in the AFM tip films allows for some degree of rearrangement to minimize their contact with the surrounding environment. Once the SAMs are immersed in water, the molecules have to arrange themselves to minimize their contact with the surrounding water. One possible arrangement is the formation of islands of SAMs circumvented by channels of water. This explanation is unlikely however, as work previously completed in the lab observed that OTS SAMs formed on oxidized Si3N4 AFM tips have the ability to protect the probe from wear under aggressive aqueous environments that would normally lead to oxide dissolution, in this case, pH 13 water.[239] Another likely explanation is that the SAM chains collapse into themselves and become more disordered, increasing the contact area between the probe and substrate and exposing a greater number of polar methylene units to the hydroxylated surface, which would show a greater adhesive response than the nonpolar methyl end groups. Similarly, when the SAM on the tip's surface collides with the substrate, some

amount of disorder is imparted into the system. Gauche defects caused by the contact rearrangement of the SAM molecules allow an even larger proportion of polar methylene units to be brought into contact with the surface during spectral acquisition. The inability of the AFM tip SAM to reorder over the limited contact timeframe further suggests that an equilibrium process is present.

As such, these data have a number of implications in the measurement of adhesion forces using chemical force microscopy approaches. Due to the typically disordered nature of SAMs on nanoscopic asperities such as AFM tips, adhesion measurements must report not only the details of the lever spring constant and tip radius, but they must also report the approach and retract rates of the measurements as well as the contact time. As such, we propose that chemical force measurements should report not only calibrated tip dimension and lever force constants, but also the timing and sequencing of their measurements to enable other labs to reproduce their results more accurately.

Multicomponent OTS-3P1P self assembled films on silica nanoparticle substrates, single component OTS SAMs on silica nanoparticle substrates and OTS SAMs on nominally flat Si(100) were probed for their friction response under increasing scan rates from 0.1 μm/s to 750 μm/s under four different loads: 1 nN, 50 nN, 125 nN and 200 nN. Under very low loading forces (Figure 6.7), both SAMs on nanoparticle surfaces showed similar behavior than the OTS film on Si(100). The friction forces for the films on nanoparticle surfaces at each tip velocity were higher than the OTS films on assembled on flat surfaces, which is most likely attributable to the roughness of the

nanoparticle film compared to the nominally flat OTS functionalized Si(100) substrate (approximately 25 nm RMS versus 0.2 nm RMS, respectively).

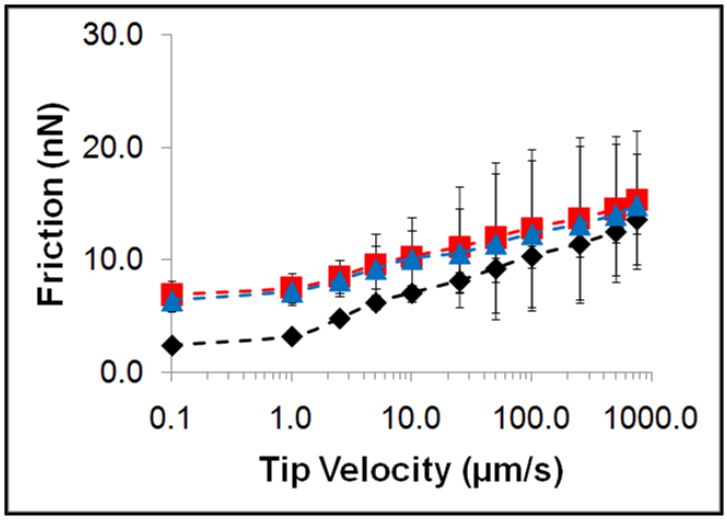

FIGURE 6.7: Shear rate analysis results for multicomponent for OTS on flat Si(100) (♦), OTS on spin coated silica nanoparticle films (■) and OTS-3P1P films self-assembled on spin coated silica nanoparticle substrates (▲) at a loading forces of 1 nN. The lines connecting the data points are intended only to be guides to the eye and do not denote any trend.

Under a higher load of 50 nN, the performance of the different films can be observed to differentiate themselves at lower tip velocities (Figure 6.8). It's immediately noticeable that the friction response of the multicomponent film is much lower than the OTS film on the nanoparticle substrate and almost as low as that of OTS on the flat Si(100) wafer. This can be attributed to the superior friction versus load performance of these films reported in Chapters IV and V. However, at higher tip velocities, the two films on the nanoparticle substrates exhibit similar friction behavior, most likely due to their formation on the roughened surface and the effects of that

roughness has in limiting the friction reduction abilities of the films at high shear rates. Interestingly, all three systems exhibit a transition in friction response highlighted by an

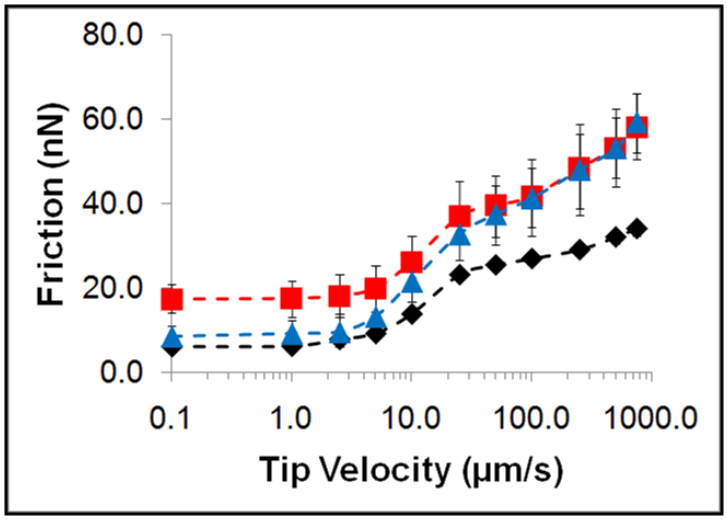

FIGURE 6.8: Shear rate analysis results for multicomponent for OTS on flat Si(100) (♦), OTS on spin coated silica nanoparticle films (■) and OTS-3P1P films self-assembled on spin coated silica nanoparticle substrates (▲) at a loading forces of 50 nN. The lines connecting the data points are intended only to be guides to the eye and do not denote any trend.

sudden increase in the rate of friction versus tip velocity rate change between 5 and 25 µm/s followed by a second transition to a friction versus rate plateau beginning at a rate of 50 µm/s. It has been proposed the roots of this friction versus velocity transition are due to localized phase transitions within the film which are induced by flow; however the precise origins of the transition is still unknown.[240]

Figure 6.9 shows the friction response versus tip velocity found for the three systems under a loading force of 125 nN. A similar trend is observed in the friction behavior at low sliding velocities with the friction response gradually increasing with

increasing tip velocities, with the two SAMs on the nanoparticle films exhibiting relatively identical friction characteristics at the higher sliding speeds, again attributable to the surface roughness of the nanoparticle film dominating the friction response at higher tip speeds.

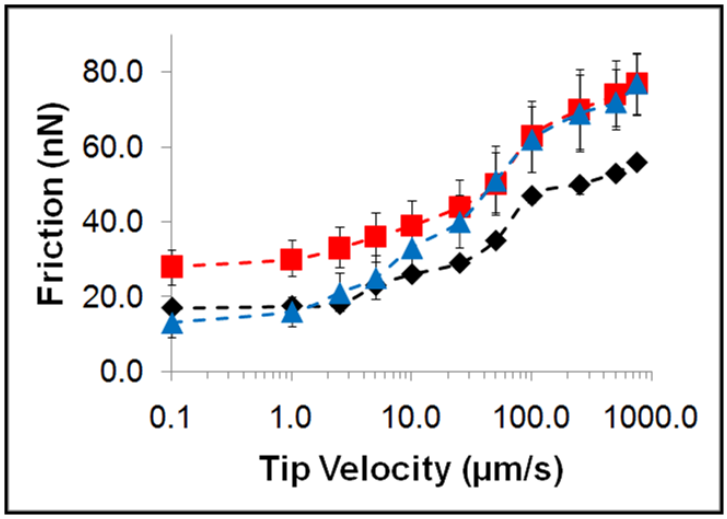

FIGURE 6.9: Shear rate analysis results for multicomponent for OTS on flat Si(100) (♦), OTS on spin coated silica nanoparticle films (■) and OTS-3P1P films self-assembled on spin coated silica nanoparticle substrates (▲) at a loading forces of 125 nN. The lines connecting the data points are intended only to be guides to the eye and do not denote any trend.

Figure 6.10 shows the friction versus tip velocity response for the three systems under a loading force of 200 nN. Similar to the performance that was observed under the other loading regimes, the two SAMs on the spin coated films showed similar friction response at high tip velocities, however the two films only show significant differences in friction response at the lowest tip velocities, indicating that the surface roughness was becoming too much for the SAMs to overcome under high loads.

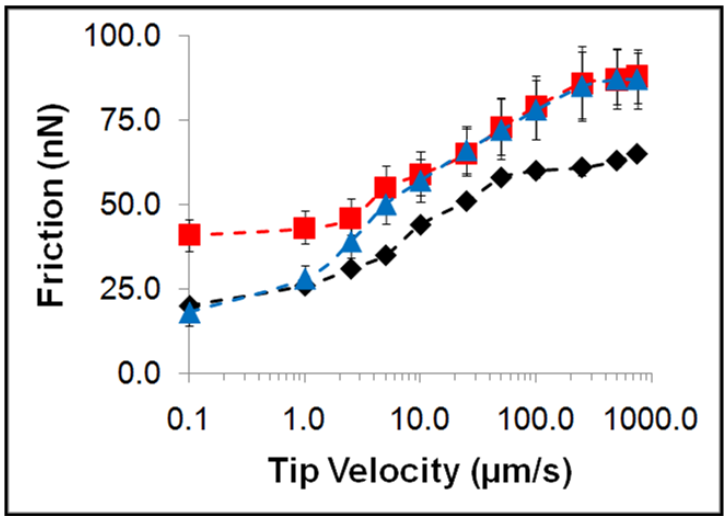

FIGURE 6.10: Shear rate analysis results for multicomponent for OTS on flat Si(100) (♦), OTS on spin coated silica nanoparticle films (■) and OTS-3P1P films self-assembled on spin coated silica nanoparticle substrates (▲) at a loading forces of 200 nN. The lines connecting the data points are intended only to be guides to the eye and do not denote any trend.

At the lowest of applied loads, both SAMs on the spin coated substrates displayed similar friction versus sliding velocity response at all speeds, indicating that both films were able to insulate the contacts similarly in these conditions. However, as the loads under evaluation progressively increased, the performance of the multicomponent film was seen to better that of the OTS film at low tip velocities. However, as the normal load being exerted on the tip progressively increased, it became apparent that the surface roughness was becoming the major contributor to the overall friction signal at higher sliding velocities, possibly indicating that the multicomponent film fairs no better in high shear environments than OTS alone.

6.5 Conclusions

Using AFM tips and nanoparticles we were able to study the tribological behavior of OTE and DTS SAMs on surfaces with nano-sized curvature in water. With functionalized AFM tips, it was found that the adhesion of SAMs on nanoparticle surfaces is much smaller than that of SAMs on flat surfaces. Moreover, adhesion of SAMs on nanoparticle surfaces is time dependent and increases with a decrease in tip approach/retract rates. To further study the tribology behavior of SAMs on asperities, we compared the adhesion forces in between both bare AFM tips and SAMs on flat Si surfaces in addition to functionalized AFM tips and flat unfunctionalized silica surfaces. The results indicate the presence of equilibrium process during the force measurement, resulting in different adhesion forces measured with different tip approach/retract rates. Additionally, multicomponent octadecyltrichlorosilane (OTS)/3-phenyl-1-propanol (3P1P) monolayers on spin coated silica nanoparticle substrates were found to possess similar shear response under load as single component OTS SAMs at high tip speeds. While it was found that friction versus tip speed performance was better for the multicomponent SAMs at lower shear rates, as the tip speed was increased, performance was found to be similar for both films under all loading situations. This high shear speed performance is likely an artifact of the inherent roughness of the spin coated nanoparticle substrate, but could possibly be explained as an inability of the multicomponent film to reduce friction any better than the single component film in these high stress environments.

CHAPTER VII

SUMMARY AND FUTURE DIRECTIONS

7.1 Summary

Understanding and controlling tribological interactions between surfaces is paramount in developing and implementing advanced technologies such as microelectromechanical systems devices. Limiting the effects that friction, wear and time have on silicon surfaces under contact is the ultimate goal of researchers in this field due to the fact that most MEMS devices are fabricated from polycrystalline Si. The surfaces of these devices often display nanoscale roughness with the surface asperities dictating the tribological properties between interfaces. This surface roughness necessitates the need for laboratory experiments on substrates that mimic true device surfaces, yet the vast majority of past research has utilized flat, single crystal silicon substrates as models for the surfaces found in actual devices.

In this dissertation, a newly discovered, two component self-assembled film is introduced along with information detailing its development and performance during mechanical testing in multiple environments. The combination of 3-phenyl-1-propanol and octadecyltrichlorosilane on spin coated nanoparticle supports have proven to produce lower friction response and longer film lifetimes under load than their single component analogs of just silanes, opening new, intriguing possibilities for self-assembled monolayer based microelectromechanical systems devices lubricants.

A systematic relationship between the affects that asperity size and chain length play on film ordering for self-assembled alkylsilane SAMs has been detailed as it has been shown that conformational disorder within films on flat and curved surfaces can be readily tracked utilizing FTIR spectroscopy. Using specific functionalization procedures, reasonably well ordered OTS films can be assembled on surfaces with high degrees of curvature. During the course of these studies, it was observed that films manufactured on nanoparticle surfaces showed an increased a propensity for uptake of foreign molecules present during functionalization.

This solvent uptake effect was then utilized by displacing the intercalated solvent molecules such as hexane still present in the film post functionalization with a more useful species. It was observed that over time, 3-phenyl-1-propanol could be used to displace those hexanes still inside of the self-assembled film from the functionalization process. These novel two component films were then applied to spin coated nanoparticle substrates, which better mimic the surface topography of a real MEMS device. The newly formed, multicomponent films were found to display lower friction response under load than OTS alone while also exhibiting the ability to survive multiple contact events under continuous scanning.

Further testing of the capabilities of the multicomponent films was performed to assess the ability of the two component SAM to reduce friction under load in multiple environments. Here we have shown how the performance of OTS films infused with a short chain alcohol is affected by local environmental conditions under variations in load

and during long term testing. Multicomponent OTS-3P1P were observed to outperform OTS SAMs alone in number of environmental conditions.

The rate dependence of adhesion between SAM functionalized surfaces with nanoscopic curvature was also detailed. Using AFM tips and nanoparticle spin coated films, tribological behavior of octadecyltriethoxysilane and dodecyltrichlorosilane SAMs on surfaces with nano-sized curvature were detailed. It was found that the adhesion of SAMs on curved surfaces is time dependent and increases with a decrease in tip approach/retract rates. The results indicate the presence of equilibrium process during the force measurement, resulting in different adhesion forces measured with different tip approach/retract rates.

Additionally, multicomponent octadecyltrichlorosilane (OTS)/3-phenyl-1-propanol (3P1P) monolayers on spin coated silica nanoparticle substrates were probed for their shear rate dependence in comparison to single component OTS SAMs. While it was discovered that the shear rate dependence was quite similar in both systems at higher shear speeds, OTS-3P1P films outperformed the single component OTS monolayers at lower shear rates.

7.2 Future Directions

The next step in this research will be to observe the performance of the multicomponent film when functionalized on a single asperity, i.e. a functionalized atomic force microscopy tip. The functionalized tips will be probed against unfunctionalized spin coated nanoparticle films to gauge the longevity of the tip under load in comparison to singly functionalized and unfunctionalized tips in the same

environments. These experiments will seek to ascertain how small regions of multicomponent films perform under wearing environments. It is important to know in what way the self-healing ability these films display is dependent upon the relative amount of surface area covered by the film. Other studies could possibly be performed to determine if two multicomponent film functionalized surfaces can act synergistically to mitigate wear.

Future research will look at the effect that variations in temperature have on the mechanical performance of the films. Another interesting angle is to use confocal AFM microscopy to perform in situ confocal florescence spectroscopy to probe the behavior of these two component films. Questions surrounding how the mobile molecules insert into the film can be answered by utilizing a florescent species as the mobile lubricant and tracking changes in the florescence during scanning. Large-scale Atomic/Molecular Massively Parallel Simulator calculations currently underway have detailed the nature of the molecular assemblies on the surface and will be extended to probe the nature of solvent intercalation into the self-assembled surface films. Additionally, calculations will focus on the behavior of the films during mechanical contact in hopes of understanding the molecular level details inside of an asperity-asperity contact.

Other work will focus on replacing the 3P1P in the multicomponent films with other, similar molecules in order to improve the performance of these films. Ideally, a range of molecules will be inserted and probed for their mechanical properties so that films could be tailored for a variety of different uses. While some potential molecules are commercially available, such as anthracene and pyrene derivatives with one or more

alcohol tails attached to the poly-aromatic group, some other molecules of interest will likely have to be custom synthesized before they can be explored. Along similar lines to changing the mobile component of the multicomponent SAM, research will look at the effects of alterations to the base film. It is known that limiting factor for silane SAMs packing density is a result of steric limitations due to the presence of the silicon atom within the silane molecules that comprise the film. The silicon atom needs to bind to a total of three different sites between the surface and its nearest neighbor molecules. However, the surface availability of hydroxyl binding sites dictates that the silicon atom cannot form three covalent bonds with the surface. A step which could be taken to eliminate this problem is to use simple alcohols as the molecular constituents for the surface bound SAM. It has been shown that by functionalizing the silica surface with chlorine terminations instead of hydroxyl groups, simple alcohols can be used to form well ordered, highly packed SAMs on the surface. Packing density is one of the major indicators of a well ordered film and is also critical in film performance under load; as such, improving the packing density of the base film will likely improve the performance of these multicomponent films immensely.

To take a broader outlook in regards to this research, the ultimate goal is to bring dynamic MEMS devices out of the laboratory and into large-scale consumer applications. As of now, further research is required in order to improve the performance of these films under high shear conditions, such as those seen in a working MEMS device. Once a component mixture has been found that limits wear in this regime, trial testing in a MEMS tribometer or other MEMS device can proceed. Also,

the development functionalization methods which eliminate the need to use environmentally dangerous materials and make the entire process more green in nature should be explored. Finding the proper combination of base film and mobile lubricant and developing a simple, environmentally friendly functionalization scheme will be major steps in mass implementation.

REFERENCES

(1) Sun, Y.; Piyabongkarn, D.; Sezen, A.; Nelson, B.J.; Rajamani, R. *Sensors and Actuators A*, **2002**, *102*, 49-60.

(2) de Boer, M.P.; Mayer, T.M. *MRS Bulletin*, **2001**, *26*, 302-304.

(3) Chandross, M.; Lorenz, C.A.; Grest, G.S.; Stevens, M.J.; Webb, E.B. *JOM*, **2005**, *57*, 55-61.

(4) Carpick, R.W.; Salmeron, M. *Chemical Reviews*, **1997**, *97*, 1163-1194.

(5) Bhushan, B. *Micro/Nanotribology of MEMS/NEMS Materials and Devices*, in *Springer Handbook of Nanotechnology*, B. Bhushan, Editor. Springer: Berlin, 2004.

(6) Salmeron, M. *Tribology Letters*, **2001**, *10*, 69-79.

(7) Jost, H.P. *Wear*, **1990**, *136*, 1-17.

(8) Komvopoulos, K. *Wear*, **1996**, *200*, 305-327.

(9) Maboudian, R.; Ashurst, W.R.; Carraro, C. *Sensors and Actuators A - Physical*, **2000**, *82*, 219-223.

(10) Flater, E.E.; Corwin, A.D.; de Boer, M.P.; Carpick, R.W. *Wear*, **2006**, *260*, 580-593.

(11) Srinivasan, U.; Houston, M.R.; Howe, R.T.; Maboudian, R. *Journal of Microelectromechanical Systems*, **1998**, *7*, 252-260.

(12) Maboudian, R.; Carraro, C. *Annual Review of Physical Chemistry*, **2004**, *55*, 35-54.

(13) Maboudian, R. *Surface Science Reports*, **1998**, *30*, 209-270.

(14) Maboudian, R.; Ashurst, W.R.; Carraro, C. *Sensors and Actuators*, **2000**, *82*, 219-223.

(15) Sambasivan, S.; Hsieh, S.; Fishcer, D.A.; Hsu, S.M. *Journal of Vacuum Science and Technology A*, **2006**, *24*, 1484-1488.

(16) Maboudian, R.; Howe, R.T. *Journal of Vacuum Science & Technology B*, **1997**, *15*, 1-20.

(17) de Boer, M.P.; Maboudian, R. *MRS Bulletin*, **2001**, *26*, 302-302.

(18) Maboudian R, A.W.R.; Carraro, C. *Tribology Letters*, **2002**, *12*, 95-100.

(19) Mate, C.M.; McClelland, G.M.; Erlandsson, R.; Chiang, S. *Physical Review Letters*, **1987**, *59*, 1942-1945.

(20) Weisenhorn, A.L.; Maivald, P.; Butt, H.J.; Hansma, P.K. *Physical Review B*, **1992**, *45*, 11226-11232.

(21) Tangyunyong, P.; Thomas, R.C.; Houston, J.E.; Michalske, T.A.; Crooks, R.M.; Howard, A.J. *Physical Review Letters*, **1993**, *71*, 3319-3322.

(22) Agrait, N.; Rubio, G.; Vieira, S. *Physical Review Letters*, **1995**, *74*, 3995-3998.

(23) Hu, J.; Xiao, X.D.; Ogletree, D.F.; Salmeron, M. *Surface Science*, **1995**, *327*, 358-370.

(24) Mate, C.M. *IBM Journal of Research and Development*, **1995**, *39*, 617-627.

(25) Arai, T.; Aoki, D.; Okabe, Y.; Fujihira, M. *Thin Solid Films*, **1996**, *273*, 322-326.

(26) Carpick, R.W.; Agrait, N.; Ogletree, D.F.; Salmeron, M. *Langmuir*, **1996**, *12*, 3334-3340.

(27) Khurshudov, A.G.; Kato, K.; Koide, H. *Tribology Letters*, **1996**, *2*, 345-354.

(28) Miller, J.D.; Veeramasuneni, S.; Drelich, J.; Yalamanchili, M.R.; Yamauchi, G. *Polymer Engineering and Science*, **1996**, *36*, 1849-1855.

(29) Park, N.S.; Kim, M.W.; Langford, S.C.; Dickinson, J.T. *Journal of Applied Physics*, **1996**, *80*, 2680-2686.

(30) Veeramasuneni, S.; Yalamanchili, M.R.; Miller, J.D. *Journal of Colloid and Interface Science*, **1996**, *184*, 594-600.

(31) Khurshudov, A.; Kato, K. *Wear*, **1997**, *205*, 1-10.

(32) Larson, I.; Drummond, C.J.; Chan, D.Y.C.; Grieser, F. *Langmuir*, **1997**, *13*, 2109-2112.

(33) Wenzler, L.A.; Moyes, G.L.; Olson, L.G.; Harris, J.M.; Beebe, T.P. *Analytical Chemistry*, **1997**, *69*, 2855-2861.

(34) Knarr, R.F.; Quon, R.A.; Vanderlick, T.K. *Langmuir*, **1998**, *14*, 6414-6418.

(35) Schiffmann, K. *Wear*, **1998**, *216*, 27-34.

(36) Sundararajan, S.; Bhushan, B. *Wear*, **1998**, *217*, 251-261.

(37) Batteas, J.D.; Quan, X.H.; Weldon, M.K. *Tribology Letters*, **1999**, *7*, 121-128.

(38) Bloo, M.L.; Haitjema, H.; Pril, W.O. *Measurement*, **1999**, *25*, 203-211.

(39) Burns, A.R.; Houston, J.E.; Carpick, R.W.; Michalske, T.A. *Langmuir*, **1999**, *15*, 2922-2930.

(40) Enachescu, M.; van den Oetelaar, R.J.A.; Carpick, R.W.; Ogletree, D.F.; Flipse, C.F.J.; Salmeron, M. *Tribology Letters*, **1999**, *7*, 73-78.

(41) Bassani, R.; D'Acunto, M. *Tribology International*, **2000**, *33*, 443-452.

(42) Katsuki, F.; Kamei, K.; Saguchi, A.; Takahashi, W.; Watanabe, J. *Journal of the Electrochemical Society*, **2000**, *147*, 2328-2331.

(43) Kopta, S.; Salmeron, M. *Journal of Chemical Physics*, **2000**, *113*, 8249-8252.

(44) Leng, Y.S.; Jiang, S.Y. *Journal of Chemical Physics*, **2000**, *113*, 8800-8806.

(45) Vakarelski, I.U.; Ishimura, K.; Higashitani, K. *Journal of Colloid and Interface Science*, **2000**, *227*, 111-118.

(46) Ashurst, W.R.; Yau, C.; Carraro, C.; Lee, C.; Kluth, G.J.; Howe, R.T.; Maboudian, R. *Sensors and Actuators A*, **2001**, *91*, 239-248.

(47) Burns, A.R.; Carpick, R.W.; Sasaki, D.Y.; Shelnutt, J.A.; Haddad, R. *Tribology Letters*, **2001**, *10*, 89-96.

(48) Du, B.Y.; Tsui, O.K.C.; Zhang, Q.L.; He, T.B. *Langmuir*, **2001**, *17*, 3286-3291.

(49) Perry, S.S.; Lee, S.; Shon, Y.S.; Colorado, R.; Lee, T.R. *Tribology Letters*, **2001**, *10*, 81-87.

(50) Senden, T.J. *Current Opinion in Colloid & Interface Science*, **2001**, *6*, 95-101.

(51) Attard, P. *Journal of Adhesion Science and Technology*, **2002**, *16*, 753-791.

(52) Li, J.C.; Horton, J.H. *Journal of Materials Chemistry*, **2002**, *12*, 1268-1273.

(53) Segeren, L.H.G.J.; Siebum, B.; Karssenberg, F.G.; Van den Berg, J.W.A.; Vancso, G.J. *Journal of Adhesion Science and Technology*, **2002**, *16*, 793-828.

(54) Nalaskowski, J.; Drelich, J.; Hupka, J.; Miller, J.D. *Langmuir*, **2003**, *19*, 5311-5317.

(55) Qian, L.M.; Tian, F.; Xiao, X.D. *Tribology Letters*, **2003**, *15*, 169-176.

(56) Helt, J.M.; Batteas, J.D. *Langmuir*, **2004**, *21*, 633-639.

(57) Sokolov, I.; Ong, Q.K.; Shodiev, H.; Chechik, N.; James, D.; Oliver, M. *Journal of Colloid and Interface Science*, **2006**, *300*, 475-481.

(58) Stevens, F.; Langford, S.C.; Dickinson, J.T. *Journal of Applied Physics*, **2006**, *99*, 023529.

(59) Ma, J.Q.; Pang, C.J.; Mo, Y.F.; Bai, M.W. *Wear*, **2007**, *263*, 1000-1007.

(60) Singh, R.A.; Yoon, E.S.; Han, H.G.; Kong, H. *Wear*, **2007**, *262*, 130-137.

(61) Bharat, B.; et al. *Journal of Physics: Condensed Matter*, **2008**, *20*, 365207.

(62) Singh, R.A.; Kim, J.; Yang, S.W.; Oh, J.E.; Yoon, E.S. *Wear*, **2008**, *265*, 42-48.

(63) Liang, Q.; Hongnian, L.; Yabo, X.; Xudong, X. *Journal of Physical Chemistry B*, **2006**, *110*, 403-409.

(64) Gao, G.T.; Cannara, R.J.; Carpick, R.W.; Harrison, J.A. *Langmuir*, **2007**, *23*, 5394-5405.

(65) Polaczyk, C.; Schneider, T.; Schofer, J.; Santner, R. *Surface Science*, **1998**, *402-404*, 454-458.

(66) Hertz, H. *Journal fur die Reine und Angewandte Mathematik*, **1881**, *92*, 156-171.

(67) Johnson, K.L.; Kendall, K.; Roberts, A.D. *Proceedings of the Royal Society of London Series A*, **1971**, *324*, 301-313.

(68) Derjaguin, B.V.; Muller, V.M.; Toporov, Y.P. *Journal of Colloid and Interface Science*, **1975**, *53*, 314-326.

(69) Tabor, D. *Journal of Colloid and Interface Science*, **1977**, *58*, 2-13.

(70) Maugis, D. *Journal of Colloid and Interface Science*, **1992**, *150*, 243-269.

(71) Schreiber, F. *Progress in Surface Science*, **2000**, *65*, 151-257.

(72) Parikh, A.N.; Allara, D.L.; Azouz, I.B.; Rodelez, F. *Journal of Physical Chemistry*, **1994**, *98*, 7577-7590.

(73) Zhang, Q.; Archer, L.A. *Langmuir*, **2005**, *21*, 5405-5413.

(74) Depalma, V.; Tillman, N. *Langmuir*, **1989**, *5*, 868-872.

(75) Netzer, L.; Iscovici, R.; Sagiv, J. *Thin Solid Films*, **1983**, *100*, 67-76.

(76) Wang, Y.; Lieberman, M. *Langmuir*, **2003**, *19*, 1159-1167.

(77) Tillman, N.; Ulman, A.; Schildkraut, J.S.; Penner, T.L. *Journal of the American Chemical Society*, **1988**, *110*, 6136-6144.

(78) Wasserman, S.R.; Tao, Y.-T.; Whitesides, G.M. *Langmuir*, **1989**, *5*, 1074-1087.

(79) Brzoska, J.B.; Benazouz, I.; Rondelez, F. *Langmuir*, **1994**, *10*, 4367-4373.

(80) Bierbaum, K.; Grunze, M.; Baski, A.A.; Chi, L.F.; Schrepp, W.; Fuchs, H. *Langmuir*, **1995**, *11*, 2143-2150.

(81) Maoz, R.; Sagiv, J. *Journal of Colloid and Interface Science*, **1984**, *100*, 465-496.

(82) Gun, J.; Iscovici, R.; Sagiv, J. *Journal of Colloid and Interface Science*, **1984**, *101*, 201-213.

(83) Gun, J.; Sagiv, J. *Journal of Colloid and Interface Science*, **1986**, *112*, 457-472.

(84) Cohen, S.R.; Naaman, R.; Sagiv, J. *Journal of Physical Chemistry*, **1986**, *90*, 3054-3056.

(85) Wasserman, S.R.; Whitesides, G.M.; Tidswell, I.M.; Ocko, B.M.; Pershan, P.S.; Axe, J.D. *Journal of the American Chemical Society*, **1989**, *111*, 5852-5861.

(86) Stevens, M.J. *Langmuir*, **1999**, *15*, 2773-2778.

(87) Kojio, K.; Ge, S.; Takahara, A.; Kajiyama, T. *Langmuir*, **1998**, *14*, 971-974.

(88) Jones, R.L.; Pearsall, N.; Batteas, J.D. *Journal of Physical Chemistry C*, **2009**, *113*, 4507-4514.

(89) Kulkarni, S.A.; Mirji, S.A.; Mandale, A.B.; Vijayamohanan, K.P. *Thin Solid Films*, **2006**, *496*, 420-425.

(90) Zou, J.; Baldwin, R.K.; Pettigrew, K.A.; Kauzlarich, S.M. *Nano Letters*, **2004**, *4*, 1181-1186.

(91) Flater, E.E.; Ashurst, W.R.; Carpick, R.W. *Langmuir*, **2007**, *23*, 9242-9252.

(92) de Boer, M.P.; Knapp, J.A.; Michalske, T.A.; Srinivasan, U.; Maboudian, R. *Acta Materialia*, **2000**, *48*, 4531-4541.

(93) de Boer, M.P.; Luck, D.L.; Ashurst, W.R.; Maboudian, R.; Corwin, A.D.; Walraven, J.A.; Redmond, J.M. *Journal of Microelectromechanical Systems*, **2004**, *13*, 63-74.

(94) Maboudian, R.; Ashurst, W.R.; Carraro, C. *Tribology Letters*, **2002**, *12*, 95-100.

(95) Christendat, D.; Abraham, T.; Xu, Z.; Masliyah, J. *Journal of Adhesion Science and Technology*, **2005**, *19*, 149-163.

(96) Green, J.B.D.; McDermott, M.T.; Porter, M.D.; Siperko, L.M. *Journal of Physical Chemistry*, **1995**, *99*, 10960-10965.

(97) Kim, H.I.; Houston, J.E. *Journal of the American Chemical Society*, **2000**, *122*, 12045-12046.

(98) Kim, H.I.; Koini, T.; Lee, T.R.; Perry, S.S. *Langmuir*, **1997**, *13*, 7192-7196.

(99) Noy, A.; Vezenov, D.V.; Lieber, C.M. *Annual Review of Materials Science*, **1997**, *27*, 381-421.

(100) Frisbie, C.D.; Rozsnyai, L.F.; Noy, A.; Wrighton, M.S.; Lieber, C.M. *Science*, **1994**, *265*, 2071-2074.

(101) Barrena, E.; Kopta, S.; Ogletree, D.F.; Charych, D.H.; Salmeron, M. *Physical Review Letters*, **1999**, *82*, 2880-2883.

(102) Benitez, J.J.; Kopta, S.; Diez-Perez, I.; Sanz, F.; Ogletree, D.F.; Salmeron, M. *Langmuir*, **2003**, *19*, 762-765.

(103) Brewer, N.J.; Foster, T.T.; Leggett, G.J.; Alexander, M.R.; McAlpine, E. *Journal of Physical Chemistry B*, **2004**, *108*, 4723-4728.

(104) Chandross, M.; Webb, E.B.; Stevens, M.J.; Grest, G.S.; Garofalini, S.H. *Physical Review Letters*, **2004**, *93*, 166103.

(105) Lee, S.; Shon, Y.S.; Colorado, R.; Guenard, R.L.; Lee, T.R.; Perry, S.S. *Langmuir*, **2000**, *16*, 2220-2224.

(106) Mikulski, P.T.; Harrison, J.A. *Journal of the American Chemical Society*, **2001**, *123*, 6873-6881.

(107) Xiao, X.; Hu, J.; Charych, D.H.; Salmeron, M. *Langmuir*, **1996**, *12*, 235-237.

(108) Ulman, A. *Chemical Reviews*, **1996**, *96*, 1533-1554.

(109) Major, R.C.; Kim, H.I.; Houston, J.E.; Zhu, X.Y. *Tribology Letters*, **2003**, *14*, 237-244.

(110) Meyer, E.; Howald, L.; Overney, R.; Brodbeck, D.; Luthi, R.; Haefke, H.; Frommer, J.; Guntherodt, H.J. *Ultramicroscopy*, **1992**, *42*, 274-280.

(111) Meyer, E.; Overney, R.; Luthi, R.; Brodbeck, D.; Howald, L.; Frommer, J.; Guntherodt, H.J.; Wolter, O.; Fujihira, M.; Takano, H.; Gotoh, Y. *Thin Solid Films*, **1992**, *220*, 132-137.

(112) Overney, R.M.; Meyer, E.; Frommer, J.; Brodbeck, D.; Luthi, R.; Howald, L.; Guntherodt, H.J.; Fujihira, M.; Takano, H.; Gotoh, Y. *Nature*, **1992**, *359*, 133-135.

(113) Overney, R.M.; Meyer, E.; Frommer, J.; Guntherodt, H.J.; Fujihira, M.; Takano, H.; Gotoh, Y. *Langmuir*, **1994**, *10*, 1281-1286.

(114) Kim, H.I.; Boiadjiev, V.; Houston, J.E.; Zhu, X.Y.; Kiely, J.D. *Tribology Letters*, **2001**, *10*, 97-101.

(115) Batteas, J.; Quan, X.; Weldon, M. *Tribology Letters*, **1999**, *7*, 121-128.

(116) Xu, C.; Jones, R.L.; Batteas, J.D. *Scanning*, **2008**, *30*, 106-117.

(117) Greenwood, J.A.; Willamson, J.B.P. *Proceedings of the Royal Society of London A*, **1966**, *295*, 300-319.

(118) Wei, Z.Q.; Wang, C.; Wang, Z.G.; Liu, D.G.; Bai, C.L. *Surface and Interface Analysis*, **2001**, *32*, 275-277.

(119) Grinevich, O.; Mejiritski, A.; Neckers, D.C. *Langmuir*, **1999**, *15*, 2077-2079.

(120) Barrat, A.; Silberzan, P.; Bourdieu, L.; Chatenay, D. *Europhysics Letters*, **1992**, *20*, 633-638.

(121) Nakagawa, T. *Japanese Journal of Applied Physics*, **1997**, *36*, L162-L165.

(122) Nakagawa, T.; Ogawa, K.; Kurumizawa, T. *Journal of Vacuum Science & Technology B*, **1994**, *12*, 2215-2218

(123) Nakagawa, T.; Ogawa, K.; Kurumizawa, T.; Ozaki, S. *Japanese Journal of Applied Physics*, **1993**, *32*, L294-L296.

(124) Tsukruk, V.V.; Bliznyuk, V.N. *Langmuir*, **1998**, *14*, 446-455.

(125) Ito, T.; Namba, M.; Buhlmann, P.; Umezawa, Y. *Langmuir*, **1997**, *13*, 4323-4332.

(126) Ton-That, C.; Campbell, P.A.; Bradley, R.H. *Langmuir*, **2000**, *16*, 5054-5058.

(127) Liu, Y.; Wolf, L.K.; Messmer, M.C. *Langmuir*, **2001**, *17*, 4329-4335.

(128) Tutein, A.B.; Stuart, S.J.; Harrison, J.A. *Journal of Physical Chemistry B*, **1999**, *103*, 11357-11365.

(129) D'Acunto, M. *Nanotechnology*, **2006**, *17*, 2954-2962.

(130) Srinivasan, G.; Pursch, M.; Sander, L.C.; Muller, K. *Langmuir*, **2004**, *20*, 1746-1752.

(131) Macphail, R.A.; Strauss, H.L.; Snyder, R.G.; Elliger, C.A. *Journal of Physical Chemistry*, **1984**, *88*, 334-341.

(132) Prathima, N.; Harini, A.; Rai, N.; Chandrashekara, R.H.; Ayappa, K.G.; Sampath, S.; Biswas, S.K. *Langmuir*, **2005**, *21*, 2364-2374.

(133) Khatri, O.P.; Biswas, S.K. *Surface Science*, **2006**, *600*, 4399-4404.

(134) Parikh, A.N.; Liedberg, B.; Atre, S.V.; Ho, M.; Allara, D.L. *Journal of Physical Chemistry*, **1995**, *99*, 9996-10008.

(135) Smith, M.B.; Efimenko, K.; Fischer, D.A.; Lappi, S.E.; Kilpatrick, P.K.; Genzer, J. *Langmuir*, **2007**, *23*, 673-683.

(136) Singh, S.; Wegmann, J.; Albert, K.; Muller, K. *Journal of Physical Chemistry B*, **2002**, *106*, 878-888.

(137) Cann, P.M.; Spikes, H.A. *Tribology Letters*, **2005**, *19*, 289-297.

(138) Ang, T.P.; Wee, T.S.A.; Chin, W.S. *Journal of Physical Chemistry B*, **2004**, *108*, 11001-11010.

(139) Ando, Y.; Inoue, Y.; Kakuta, K.; Igari, T.; Mori, S. *Tribology Letters*, **2007**, *27*, 13-20.

(140) Jones, R.L.; Harrod, B.L.; Batteas, J.D. *Langmuir*, **2010**, *26*, 16355–16361.

(141) Johnson, K.L. *Contact Mechanics*. Cambridge University Press: Cambridge, **1987**.

(142) Asay, D.B.; Dugger, M.T.; Kim, S.H. *Tribology Letters*, **2008**, *29*, 67-74.

(143) Binnig, G.; Quate, C.F.; Gerber, C. *Physical Review Letters*, **1986**, *56*, 930-933.

(144) Tambe, N.S.; Bhushan, B. *Tribology Letters*, **2005**, *20*, 83-90.

(145) Liao, Y.C.; Roberts, J.T. *Journal of the American Chemical Society*, **2006**, *128*, 9061-9065.

(146) Fiorilli, S.; Rivolo, P.; Descrovi, E.; Ricciardi, C.; Pasquardini, L.; Lunelli, L.; Vanzetti, L.; Pederzolli, C.; Onida, B.; Garrone, E. *Journal of Colloid and Interface Science*, **2008**, *321*, 235-241.

(147) Kessel, C.R.; Granick, S. *Langmuir*, **1991**, *7*, 532-538.

(148) Nagle, J.F. *Faraday Discussions*, **1986** 151-162.

(149) Casal, H.L.; Mantsch, H.H.; Hauser, H. *Biochemistry*, **1987**, *26*, 4408-4416.

(150) Poirier, G.E. *Langmuir*, **1999**, *15*, 1167-1175.

(151) Nuzzo, R.G.; Korenic, E.M.; Dubois, L.H. *Journal of Chemical Physics*, **1990**, *93*, 767-773.

(152) Wang, R.; Guo, J.; Baran, G.; Wunder, S. *Langmuir*, **2000** 568-576.

(153) Wang, R.; Wunder, S.L. *Langmuir*, **2000**, *16*, 5008-5016.

(154) Brust, M.; Walker, M.; Bethell, D.; Schiffrin, D.J.; Whyman, R. *Journal of the Chemical Society - Chemical Communications*, **1994** 801-802.

(155) Terrill, R.H.; Postlethwaite, T.A.; Chen, C.H.; Poon, C.D.; Terzis, A.; Chen, A.D.; Hutchison, J.E.; Clark, M.R.; Wignall, G.; Londono, J.D.; Superfine, R.; Falvo, M.; Johnson, C.S.; Samulski, E.T.; Murray, R.W. *Journal of the American Chemical Society*, **1995**, *117*, 12537-12548.

(156) Badia, A.; Singh, S.; Demers, L.; Cuccia, L.; Brown, G.R.; Lennox, R.B. *Chemistry - a European Journal*, **1996**, *2*, 359-363.

(157) Badia, A.; Cuccia, L.; Demers, L.; Morin, F.; Lennox, R.B. *Journal of the American Chemical Society*, **1997**, *119*, 2682-2692.

(158) Hostetler, M.J.; Stokes, J.J.; Murrary, R.W. *Langmuir*, **1996**, *12*, 3604-3612.

(159) Badia, A.; Demers, L.; Dickinson, L.; Morin, F.G.; Lennox, R.B.; Reven, L. *Journal of the American Chemical Society*, **1997**, *119*, 11104-11105.

(160) Murthy, S.; Bigioni, T.P.; Wang, Z.L.; Khoury, J.T.; Whetten, R.L. *Materials Letters*, **1997**, *30*, 321-325.

(161) Sarathy, K.V.; Raina, G.; Yadav, R.T.; Kulkarni, G.U.; Rao, C.N.R. *Journal of Physical Chemistry B*, **1997**, *101*, 9876-9880.

(162) Hostetler, M.J.; Wingate, J.E.; Zhong, C.J.; Harris, J.E.; Vachet, R.W.; Clark, M.R.; Londono, J.D.; Green, S.J.; Stokes, J.J.; Wignall, G.D.; Glish, G.L.; Porter, M.D.; Evans, N.D.; Murray, R.W. *Langmuir*, **1998**, *14*, 17-30.

(163) Hostetler, M.J.; Zhong, C.J.; Yen, B.K.H.; Anderegg, J.; Gross, S.M.; Evans, N.D.; Porter, M.; Murray, R.W. *Journal of the American Chemical Society*, **1998**, *120*, 9396-9397.

(164) Kang, S.Y.; Kim, K. *Langmuir*, **1998**, *14*, 226-230.

(165) Sandhyarani, N.; Antony, M.P.; Selvam, G.P.; Pradeep, T. *Journal of Chemical Physics*, **2000**, *113*, 9794-9803.

(166) Sandhyarani, N.; Resmi, M.R.; Unnikrishnan, R.; Vidyasagar, K.; Ma, S.G.; Antony, M.P.; Selvam, G.P.; Visalakshi, V.; Chandrakumar, N.; Pandian, K.; Tao, Y.T.; Pradeep, T. *Chemistry of Materials*, **2000**, *12*, 104-113.

(167) Wuelfing, W.P.; Green, S.J.; Pietron, J.J.; Cliffel, D.E.; Murray, R.W. *Journal of the American Chemical Society*, **2000**, *122*, 11465-11472.

(168) Chen, S.W.; Sommers, J.M. *Journal of Physical Chemistry B*, **2001**, *105*, 8816-8820.

(169) Kumar, R.V.; Mastai, Y.; Diamant, Y.; Gedanken, A. *Journal of Materials Chemistry*, **2001**, *11*, 1209-1213.

(170) Shimizu, T.; Teranishi, T.; Hasegawa, S.; Miyake, M. *Journal of Physical Chemistry B*, **2003**, *107*, 2719-2724.

(171) Hostetler, M.J.; Stokes, J.J.; Murray, R.W. *Langmuir*, **1996**, *12*, 3604-3612.

(172) Weeraman, C.; Yatawara, A.K.; Bordenyuk, A.N.; Benderskii, A.V. *Journal of the American Chemical Society*, **2006**, *128*, 14244–14245.

(173) Bordenyuk, A.N.; Weeraman, C.; Yatawara, A.; Jayathilake, H.D.; Stiopkin, I.; Liu, Y.; Benderskii, A.V. *Journal of Physical Chemistry C*, **2007**, *111*, 8925-8933.

(174) Thompson, W.R.; Pemberton, J.E. *Analytical Chemistry*, **1994**, *66*, 3362-3370.

(175) Ho, M.; Cai, M.; Pemberton, J.E. *Analytical Chemistry*, **1997**, *69*, 2613-2616.

(176) Ho, M.; Pemberton, J.E. *Analytical Chemistry*, **1998**, *70*, 4915-4920.

(177) Orendorff, C.J.; Ducey, M.W.; Pemberton, J.E.; Sander, L.C. *Analytical Chemistry*, **2003**, *75*, 3369-3375.

(178) Orendorff, C.J.; Ducey, M.W.; Pemberton, J.E.; Sander, L.C. *Analytical Chemistry*, **2003**, *75*, 3360-3368.

(179) Tutein, A.B.; Stuart, S.J.; Harrison, J.A. *Journal of Physical Chemistry B*, **1999**, *103*, 11357-11365.

(180) D'Acunto, M. *Nanotechnology*, **2006**, *17*, 2954-2962.

(181) Liu, Y.; Wolf, L.K.; Messmer, M.C. *Langmuir*, **2001**, *17*, 4329-4335.

(182) Ulman, A. *An Introduction to Ultrathin Organic Films*. Academic Press: New York, **1991**.

(183) Nuzzo, R.G.; Fusco, F.A.; Allara, D.L. *Journal of the American Chemical Society*, **1987**, *109*, 2358-2368.

(184) Porter, M.D.; Bright, T.B.; Allara, D.L.; Chidsey, C.E.D. *Journal of the American Chemical Society*, **1987**, *109*, 3559-3568.

(185) Ducey, M.W.; Orendorff, C.J.; Pemberton, J.E.; Sander, L.C. *Analytical Chemistry*, **2002**, *74*, 5585-5592.

(186) Allara, D.L.; Parikh, A.N.; Judge, E. *Journal of Chemical Physics*, **1994**, *100*, 1761-1764.

(187) Ducey, M.W.; Orendorff, C.J.; Pemberton, J.E.; Sander, L.C. *Analytical Chemistry*, **2002**, *74*, 5576-5584.

(188) Hansen, R.H.; Harris, J.M. *Analytical Chemistry*, **1996**, *68*, 2879-2884.

(189) Hansen, R.L.; Harris, J.M. *Analytical Chemistry*, **1995**, *67*, 492-498.

(190) Carr, J.W.; Harris, J.M. *Analytical Chemistry*, **1987**, *59*, 2546-2550.

(191) Lane, J.M.D.; Chandross, M.; Stevens, M.J.; Grest, G.S. *Langmuir*, **2008**, *24*, 5209-5212.

(192) Lane, J.M.D.; Chandross, M.; Lorenz, C.D.; Stevens, M.J.; Grest, G.S. *Langmuir*, **2008**, *24*, 5734-5739.

(193) Pemberton, J.E.; Ho, M.K.; Orendorff, C.J.; Ducey, M.W. *Journal of Chromatography A*, **2001**, *913*, 243-252.

(194) Nuzzo, R.G.; Dubois, L.H.; Allara, D.L. *Journal of the American Chemical Society*, **1990**, *112*, 558-569.

(195) Chau, K.H.L.; Lewis, S.R.; Zhao, Y.; Howe, R.T.; Bart, S.F.; Marcheselli, R.G. *Sensors and Actuators A*, **1996**, *54*, 472-476.

(196) Eaton, W.P.; Smith, J.H. *Smart Materials & Structures*, **1997**, *6*, 530-539.

(197) Verdonckt-Vandebroek, S. *Proceedings of SPIE-Micromachined Devices and Components III*, **1997**, *3224*, 180-184.

(198) Fan, L.S.; Tai, Y.C.; Muller, R.S. *Sensors and Actuators*, **1989**, *20*, 41-47.

(199) Maboudian, R. *MRS Bulletin*, **1998**, *23*, 47-51.

(200) Tormoen, G.W.; Drelich, J.; Beach, E.R. *Journal of Adhesion Science and Technology*, **2004**, *18*, 1-17.

(201) Lio, A.; Morant, C.; Ogletree, D.F.; Salmeron, M. *Journal of Physical Chemistry B*, **1997**, *101*, 4767-4773.

(202) Burns, A.R.; Houston, J.E.; Carpick, R.W.; Michalske, T.A. *Physical Review Letters*, **1999**, *82*, 1181-1184.

(203) Lio, A.; Charych, D.H.; Salmeron, M. *Journal of Physical Chemistry B*, **1997**, *101*, 3800-3805.

(204) Ruhe, J.; Novotny, V.J.; Kanazawa, K.K.; Clarke, T.; Street, G.B. *Langmuir*, **1993**, *9*, 2383-2388.

(205) Patton, S.T.; Cowan, W.D.; Eapen, K.C.; Zabinski, J.S. *Tribology Letters*, **2000**, *9*, 199-209.

(206) Rye, R.R.; Nelson, G.C.; Dugger, M.T. *Langmuir*, **1997**, *13*, 2965-2972.

(207) Hsu, S.M. *Tribology International*, **2004**, *37*, 537-545.

(208) Choi, J.H.; Kawaguchi, M.; Kato, T. *Tribology Letters*, **2003**, *15*, 353-358.

(209) Sung, I.H.; Yang, J.C.; Kim, D.E.; Shin, B.S. *Wear*, **2003**, *255*, 808-818.

(210) Ren, S.; Yang, S.R.; Zhao, Y.P.; Zhou, J.F.; Xu, T.; Liu, W.M. *Tribology Letters*, **2002**, *13*, 233-239.

(211) Henck, S.A. *Tribology Letters*, **1997**, *3*, 239-247.

(212) Strawhecker, K.; Asay, D.B.; McKinny, J.; Kim, S.H. *Tribology Letters*, **2005**, *19*, 17-21.

(213) Asay, D.B.; Kim, S.H. *Langmuir*, **2007**, *23*, 12174-12178.

(214) Asay, D.B.; Dugger, M.T.; Ohlhausen, J.A.; Kim, S.H. *Langmuir*, **2008**, *24*, 155-159.

(215) Barnette, A.L.; Asay, D.B.; Kim, D.; Guyer, B.D.; Lim, H.; Janik, M.J.; Kim, S.H. *Langmuir*, **2009**, *25*, 13052-13061.

(216) Tian, F.; Xiao, X.D.; Loy, M.M.T.; Wang, C.; Bai, C.L. *Langmuir*, **1999**, *15*, 244-249.

(217) Sader, J.E.; Chon, J.W.M.; Mulvaney, P. *Review of Scientific Instruments*, **1999**, *70*, 3967-3969.

(218) Asay, D.B.; Hsiao, H.; Kim, S.H. *Review of Scientific Instruments*, **2009**, *80*, 066101.

(219) Iler, R.K. *The Chemistry of Silica*. Wiley- Interscience: New York, **1979**.

(220) Jolivet, J. *Metal Oxide Chemistry and Synthesis: From Solution to Solid State*. 1st ed. Wiley: New York, **2000**.

(221) Jeffrey, G.A. *An Introduction to Hydrogen Bonding*. Oxford University Press: New York, **1997**.

(222) Lorenz, C.D.; Chandross, M.; Lane, J.M.D.; Grest, G.S. *Modelling and Simulation in Materials Science and Engineering*, **2010**, *18*, 034005.

(223) Lorenz, C.D.; Chandross, M.; Grest, G.S.; Stevens, M.J.; Webb, E.B. *Langmuir*, **2005**, *21*, 11744-11748.

(224) Yang, Y.; Ruths, M. *Langmuir*, **2009**, *25*, 12151-12159.

(225) Bowden, F.P.; Tabor, D. *The Friction and Lubrication of Solids*. Clarendon Press: Oxford, **1950**.

(226) Meyer, E.; Howald, L.; Overney, R.M.; Heinzelmann, H.; Frommer, J.; Guntherodt, H.J.; Wagner, T.; Schier, H.; Roth, S. *Nature*, **1991**, *349*, 398-400.

(227) Perry, S.S.; Ager, J.W.; Somorjai, G.A. *Journal of Materials Research*, **1993**, *8*, 2577-2586.

(228) Erlandsson, R.; Hadziioannou, G.; Mate, C.M.; McClelland, G.M.; Chiang, S. *Journal of Chemical Physics*, **1988**, *89*, 5190-5193.

(229) Carpick, R.W.; Agrait, N.; Ogletree, D.F.; Salmeron, M. *Journal of Vacuum Science & Technology B*, **1996**, *14*, 1289-1295.

(230) Demirel, A.L.; Granick, S. *Journal of Chemical Physics*, **1998**, *109*, 6889-6897.

(231) Piner, R.D.; Mirkin, C.A. *Langmuir*, **1997**, *13*, 6864-6868.

(232) Wei, Z.Q.; Wang, C.; Bai, C.L. *Langmuir*, **2001**, *17*, 3945-3951.

(233) Bhushan, B.; Koinkar, V.N. *Applied Physics Letters*, **1994**, *64*, 1653-1655.

(234) Overney, R.M.; Leta, D.P. *Tribology Letters*, **1995**, *1*, 247-252.

(235) Tsukruk, V.V.; Bliznyuk, V.N.; Wu, J.; Visser, D.W. *Polymer Preparations*, **1996**, *37*, 575.

(236) McDermott, M.T.; Green, J.-B.D.; Porter, M.D. *Langmuir*, **1997**, *13*, 2504-2510.

(237) Koike, A.; Yoneya, M. *Langmuir*, **1997**, *13*, 1718-1722.

(238) Green, C.P.; Lioe, H.; Cleveland, J.P.; Proksch, R.; Mulvaney, P.; Sader, J.E. *Review of Scientific Instruments*, **2004**, *75*, 1988-1996.

(239) Garno, J.C.; Zangmeister, C.D.; Batteas, J.D. *Langmuir*, **2007**, *23*, 7874-7879.

(240) Liu, Y.; Evans, D.F.; Song, Q.; Grainger, D.W. *Langmuir*, **1996**, *12*, 1235-1244.

APPENDIX A

SUPPORTING INFORMATION FOR CHAPTER III*

A.1 TGA analysis of C_{18} on 40 nm silica nanoparticles

Film coverage of C_{18} functionalized 40 nm silica nanoparticles was determined by Thermal Gravimetric Analysis (TGA) which was performed using a TA Instruments Q50 TGA (Figure A1.1). The basis for these measurements and the film coverage calculations were as follows.[1] Based a value of 5.0 silanols per square nanometer,[2] the mass of a theoretically ideal film on Si(100) would be 2.1 mg/m^2. Based on the mass loss during analysis, an average coverage value of 32% was calculated for 40 nanometer particles functionalized with C_{18}. Calculated coverage values using reported Aerosil silanol densities of 2.2,[3] 3.3,[1] and 3.5[4] silanols per square nanometer where determined to be 73%, 49%, and 46%, respectively.

A.2 AFM characterization of C_{18} on Si(100)

Atomic Force Microscopy (AFM) was employed to ensure uniform film formation on Si(100) substrates (Figure A1.2). C_{18} samples where scanned to verify the absence of micelles as well as multilayer formation resulting from extended functionalization times. Surface areas on the C_{18} modified Si(100) substrates are flat with an RMS roughness over an area of 1 μm^2 of approximately 0.4 nm.

The RMS roughness for the hydroxylated oxide layer of unfunctionalized Si(100) was typically found to be ~ 0.1 nm. Multiple holes were made in the SAM by nanoshaving to further verify the presence of only one self-assembled layer (Figure A 1.3).

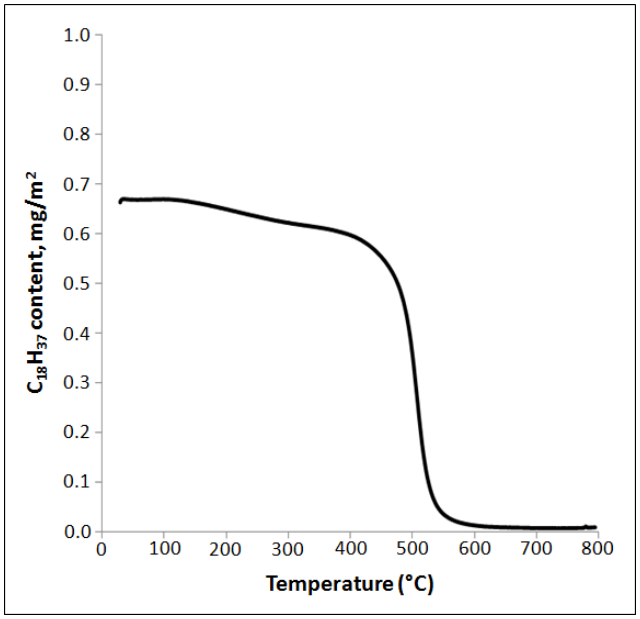

FIGURE A.1: TGA Plot of degradation C18 on 40 nm silica nanoparticles.

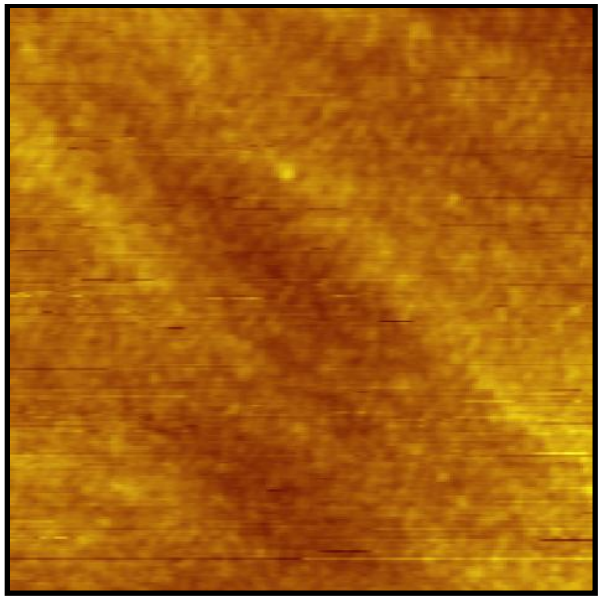

FIGURE A.2: Topographic AFM images of Si(100) functionalized with C_{18} (1 μm x 1 μm; z = 2.2 nm) The roughness is ~ 0.4 nm RMS.

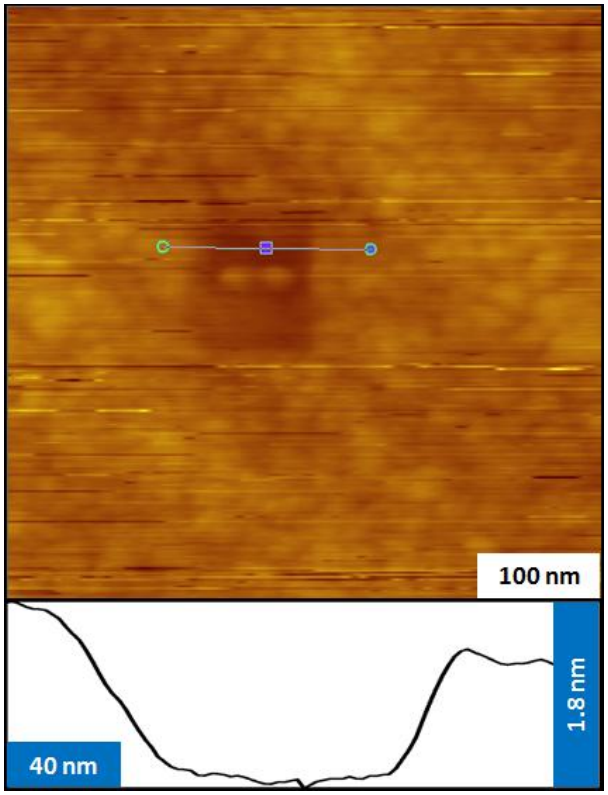

FIGURE A.3: Top - $(500\ nm)^2$ topographic image of C_{18} on Si(100) with the SAM shaved away from a centralized $(100\ nm)^2$ square. Bottom – line trace across the shaved region.

APPENDIX B

SUPPORTING INFORMATION FOR CHAPTER IV*

B.1 XPS Characterization of OTS-3P1P on Spin Coated Silica Nanoparticle Films

XPS data were acquired with a Kratos Axis ULTRA X-ray photoelectron spectrometer equipped with a 165 mm hemispherical electron energy analyzer. The incident radiation was the monochromated Al Kα X-ray line (1486.7 eV) with a source power of 120 W (12 kV, 10 mA). The analysis chamber was maintained at a typical base pressure of ~ 6×10^{-9} Torr during sample analysis. XPS survey spectra of OTS-3P1P multicomponent films were taken with a pass energy of 140 eV at a rate of 600 seconds/scan, averaging 5 scans to create each spectrum. A correction of +1.5 eV was applied during scanning to correct for the spectrometer work function. To avoid any surface charging of the silica nanoparticle film, a charge neutralizer was employed at a setting of 1.85 A and 2.8 V with a filament bias of 1 V. The high resolution scans were then collected at a pass energy of 40 eV, with 50, one minute scans averaged at each location.

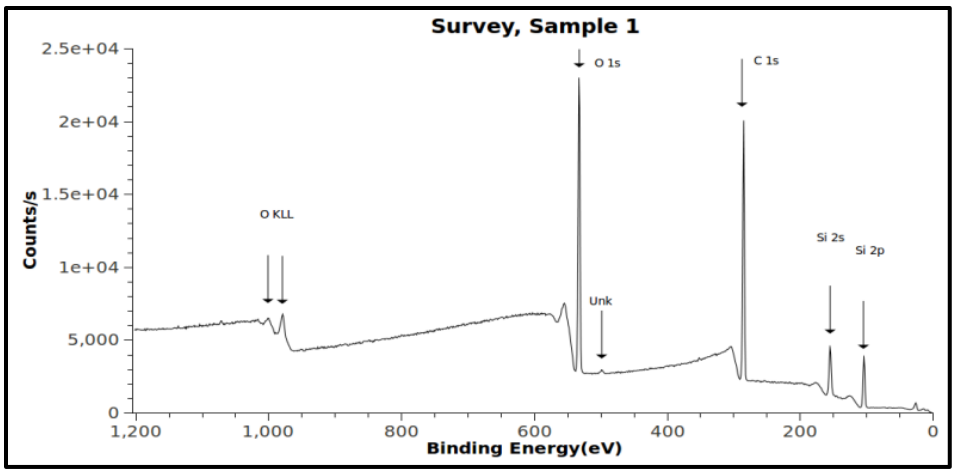

FIGURE B.1: XPS Survey Spectra of an OTS-3P1P multicomponent film.

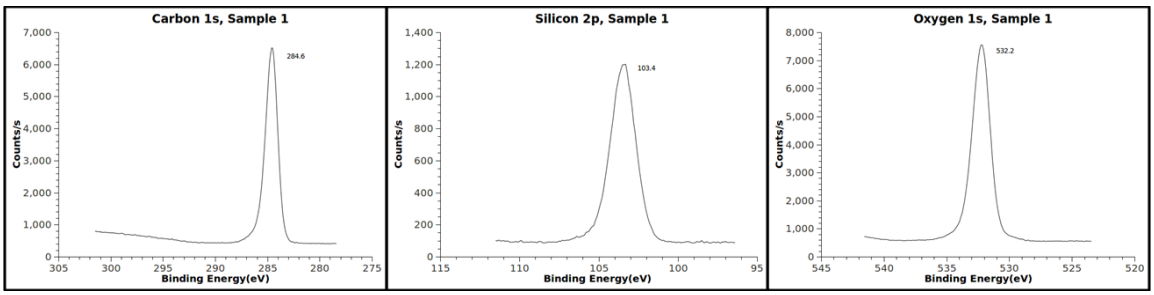

FIGURE B.2: High resolution XPS scans of the Carbon 1s, Silicon 2p and Oxygen 1s peaks for an OTS-3P1P multicomponent film. The peak locations are indicated next to each peak.

Little information was gleaned as to the physical construction of the intercalated film as a clear signature of the carbon peaks from the phenyl ring of the 3P1P, or the C-O bond were not distinguished. This suggests several possibilities. First, since the 3P1P is likely only weakly bound (physisorbed in the monolayer), that it desorbs from the surface when exposed to vacuum. Comparing the C(1s) signals for an OTS film and that of a mixed monolayer showed virtually no differences (Figure S3). We believe that the

3P1P most likely desorbs from the surface upon exposure to vacuum as IR spectra collected before and after XPS measurements show the loss of the peaks associated with the 3P1P. This same result was found when the samples were simply exposed to low vacuum (mTorr) for equivalent amounts of time (Figure B.4).

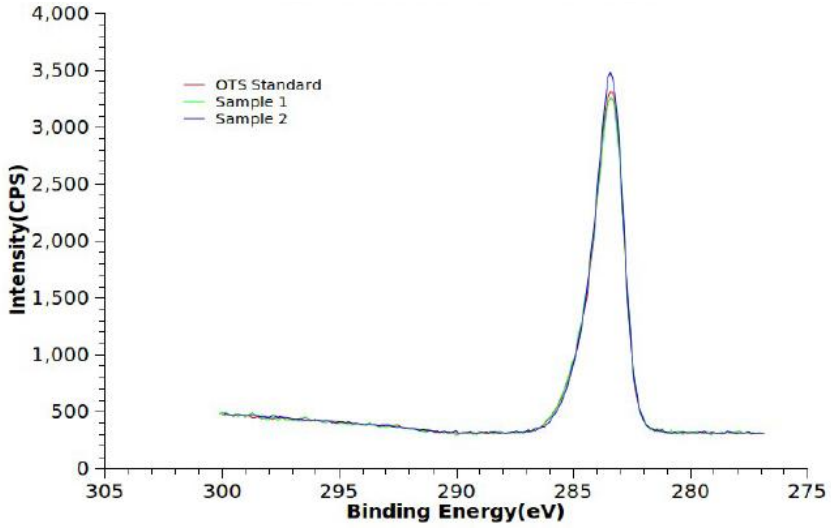

FIGURE B.3: C(1s) photoelectron spectra of an OTS SAM and two different mixed monolayer samples.

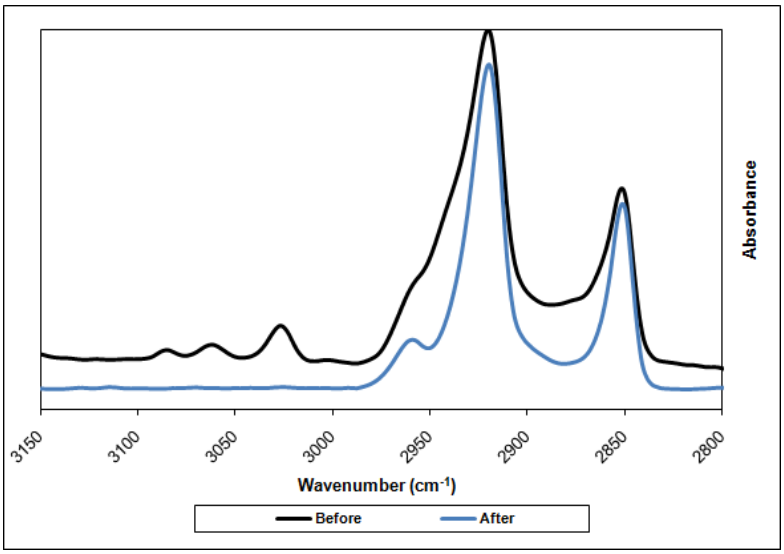

FIGURE B.4: IR spectra taken of mixed monolayers before and after exposure to vacuum.

Presuming that it does not completely desorb, the 3P1P cannot be on top of the film, or be a multilayer as it is not observed at all in the XPS. If any is retained in the film however, one additional reason that it may not be observed is that it is screened by the surrounding OTS matrix, since the molecule would then be sunken into the film by nearly 0.5 nm or more which would reduce the signal from the C(1s) electrons associated with the phenyl ring to be below the typical detection limit of *ca.* 10% of a monolayer. As such, this effect combined with its apparent desorption under vacuum would result in the apparent absence of the peak.

B.2 FTIR Analysis of the 3P1P Percentage

Aperture Size Calculation: Using calibration numbers provided by Thermo Nicolet, a plot was created to deduce the beam spot size at the focal point and the beam radius at

the focal point (r_{FP}) based on the numerical aperture iris setting (I) for each measurement.

$$r_{FP} = \frac{1.1813\, I^{0.4287}}{2}\ \text{cm}$$

The total area contained within the beam spot (A_{FP}) can be calculated in μm^2.

$$A_{FP} = 1x10^8\, \pi r_{FP}^2$$

OTS Number Calculation: The total surface area (A_S) contained within a 1 μm x 1 μm spin coated nanoparticle film was determined by averaging the surface area of ten 1 μm x 1 μm images. The total surface area (A_T) contained within the beam spot of the IR beam was calculated by extended the average surface area by the area contained within the beam spot.

$$A_T = A_S * A_{FP}$$

The average OTS surface coverage (C_{OTS}) was determined experimentally by TGA to be 1.5 molecules per square nanometer.[1] The total number of OTS molecules (N_{OTS}) within the beam path was then calculated by multiplying the total surface area by the surface coverage.

$$N_{OTS} = C_{OTS} * A_T$$

3P1P Number Calculation: The total number of 3P1P molecules (N_{3P1P}) within the beam path was determined by creating a 3P1P Beer's Law plot (Figure S5) using fifteen 3P1P solutions ranging in molarity from 0.1 M to 0.5 μM. In order to accurately correlate values taken at different aperture settings, the absorbance values used to construct the plot as well as the absorbance values from the spin coated films were normalized by the transmission intensity at the photodetector.

$$Abs_{3P1P_N} = \frac{Abs_{3P1P}}{T}$$

where Abs_{3P1PN} is the normalized absorbance value, Abs_{3P1P} is the absorbance value of the measurement and T is the transmission intensity at the detector for the measurement.

The amount of 3P1P within the film is determined by calculating the molarity of a 3P1P solution (M_{3P1P}) with the same peak intensity observed with each functionalized film fit to the Beer's Law plot.

$$M_{3P1P} = \frac{Abs_{3P1P_N} - 0.0000234}{3.3424215}$$

The number of moles of 3P1P (Mol_{3P1P}) contained within scan is determined by multiplying the resulting molarity value by the volume of the cylinder contained within the beam spot (V_{FP}) based on the radius of the focal point for the scan and the width of the liquid cell.

$$V_{FP} = \pi r_{FP}^2 * w$$

$$Mol_{3P1P} = M_{3P1P} * V_{FP}$$

The value for N_{3P1P} can now be calculated by multiplying Mol_{3P1P} by Avogadro's number (N_A).

$$N_{3P1P} = \frac{Mol_{3P1P} * N_A}{2}$$

The value is divided by two due to the substrate being functionalized on both sides.

The final percentage of 3P1P to OTS is calculated thusly.

$$\%_{3P1P} = \frac{N_{3P1P}}{N_{OTS}} * 100$$

The average amount of 3P1P found within the multicomponent films was calculated to be 15.42% +/- 1.04%.

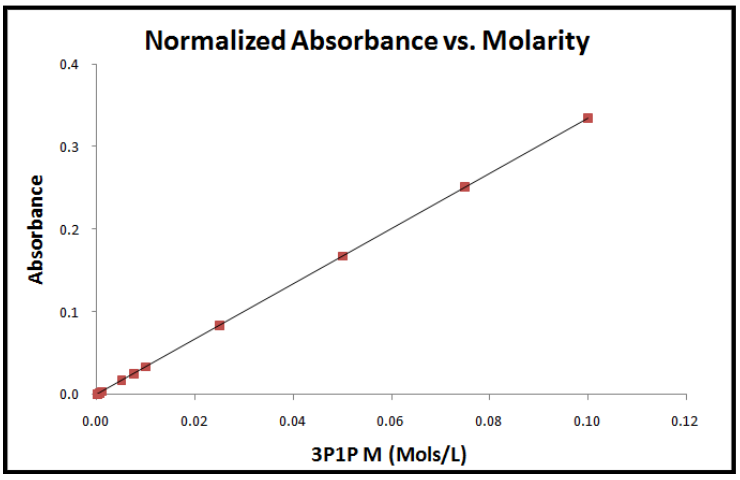

FIGURE B.5: Beer's Law plot for 3P1P. The top plot is before normalization and the bottom plot is after the values have been normalized by the transmission intensity.

Thermogravimetric Analysis (TGA) Measurements

A TA Instruments Q50 TGA was used to analyze OTS-3P1P functionalized 40 nm silica nanoparticles. TGA was performed in an N_2 atmosphere using a ramp rate of 10 °C/min. The temperature was increased from room temperature and held at 100 °C for 0.5 h, and then ramped at 10 °C/min to a temperature of 800 °C. The 3P1P was observed to outgas from the sample during the baking period at 100 °C. Analysis of the mass loss for each event in this sample reveals an OTS coverage of 1.44 molecules per nm^2 and a 3P1P intercalation value of 14.4% by mols after accounting for any residual water uptake (Figure S6).

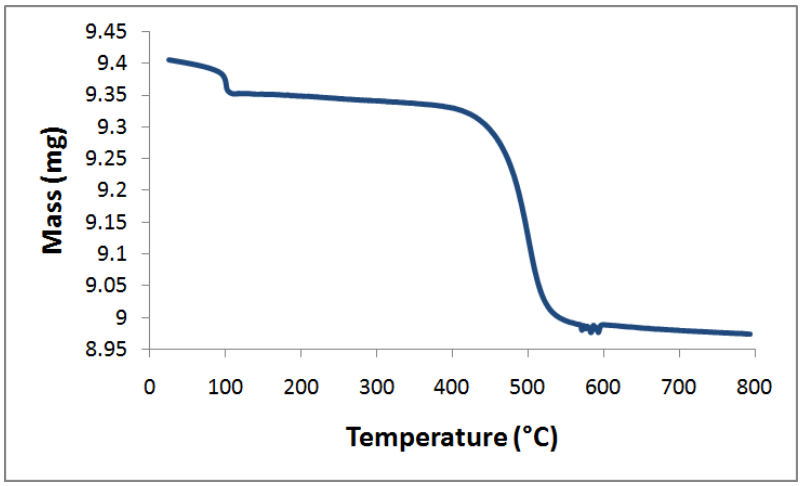

FIGURE B.6: TGA of a mixed monolayer film.

APPENDIX C

SPREADSHEETS

C.1 AFM Tip Quality Factor Calculator

$$Q = \frac{\sqrt{3}\omega_f}{\Delta\omega}$$

Quality Factor Calculation

ω_f =	Resonant Frequency of the Cantilever						
$\Delta\omega_f$ =	Peak Width of Resonance Frequency Peak at Half Height						
ω_m =	Resonant Frequency Max			=	2.465	Half Max =	1.349
ω_b =	Resonant Frequency Measurement Baseline			=	0.233		

		ω_l	ωf_e
ω_f =	30.017		
$\Delta\omega$ =	0.73	42.14	42.865
Q =	71.71168		

Quality Factor Calculation

$$Q = \frac{\sqrt{3}\omega_f}{\Delta\omega}$$

ω_f =	Resonant Frequency of the Cantilever							
$\Delta\omega_f$ =	Peak Width of Resonance Frequency Peak at Half Height							
ω_m =	Resonant Frequency Max			=	2.465	Half Max =	=(J17-J18)/2+J18	
ω_b =	Resonant Frequency Measurement Baseline			=	0.233			
ω_f =	30.017	ω_l	ωf_e					
$\Delta\omega$ =	=H21-G21	42.14	42.865					
Q =	=(SQRT(3)*E20)/E21							

C.2 Tip loading force calculator

From Force Distance Curve

Trial	Δy (V)	Δx (μm)		Δx (m)
	4.4801	0.338	=	3.38E-07

Slope (V/m) =	1.33E+07
Slope (V/nm) =	1.33E-02
Slope (nm/V) =	75.44

V_A (V) =	0.2040

From Cantilever Calibration

Spring Constant (N/m)	
k =	0.642

Applied Load

$$L_A = \left[\left(\frac{k}{m}\right) * V_A\right] \div 1E^{-9}$$

L_A =	Applied Load
k =	Cantilever Spring Constant
m =	Force Distance Curve Slope
V_A =	Approach Voltage

L_A = 9.881 nN/m

From Force Distance Curve

Trial	Δy (V)	Δx (μm)		Δx (m)
	4.4801	0.338	=	=D57/1000000

Slope (V/m) = **=C57/F57**
Slope (V/nm) = **=D59/1000000000**
Slope (nm/V) = **=1/D60**

V_A (V) = **0.2040**

From Cantilever Calibration

Spring Constant (N/m)

k = **0.642**

Applied Load

$$L_A = \left[\left(\frac{k}{m}\right) * V_A\right] \div 1E^{-9}$$

L_A = **Applied Load**
k = **Cantilever Spring Constant**
m = **Force Distance Curve Slope**
V_A = **Approach Voltage**

L_A = =((I57/D59)*D63)/0.000000001 nN/m

C.3 Contact pressure calculation

Variables			
E^*_{Sample} =	Young's Modulus for Silica =	73.00	GPa
E^*_{Tip} =	Young's Modulus for Silicon =	128.00	GPa
ν_{Sample} =	Poisson's Ratio for Silica =	0.165	
ν_{Tip} =	Poisson's Ratio for Silicon =	0.280	
F_L =	Loading Force =	350.00	nN
R_{Sample} =	Sample Radius of Curvature =	10000.00	nm
R_{Tip} =	Tip Radius of Curvature =	25.00	nm
F_{adh} =	Force of Adhesion =	6.20	nN

Formulas			
ε =	Reduced Elastic Modulus =	64.96	GPa
a =	Contact Radius =	5.60	nm
A =	Contact Area	98.367	nm^2
W_{adh} =	Work of Adhesion =	0.053	nN/nm
R =	Effective Radius =	24.94	nm
π =	pi =	3.142	
P =	**Contact Pressure =**	**3.56**	**GPa**

$$W_{adh} = \frac{F_{adh}}{1.5\pi R}$$

$$\varepsilon = \frac{4}{3}\left[\frac{1-\nu_{Tip}^2}{E_{Tip}} + \frac{1-\nu_{Sample}^2}{E_{Sample}}\right]^{-1}$$

$$P = \frac{F_L}{A}$$

$$A = \pi \frac{R^{2/3}}{\varepsilon^{2/3}}\left(F_L + 3\pi W_{adh} R + \sqrt{6\pi W_{adh} R F_L + \left(3\pi W_{adh} R\right)^2}\right)^{2/3} = \pi a^2$$

$$r = \left(\frac{3\pi W_{adh} R^2}{2\varepsilon}\right)^{2/3}$$

$$R = \left[\frac{1}{R_{Tip}} + \frac{1}{R_{Sample}}\right]^{-1}$$

Variables			
E^*_{Sample} =	Young's Modulus for Silica =	73.00	GPa
E^*_{Tip} =	Young's Modulus for Silicon =	128.00	GPa
ν_{Sample} =	Poisson's Ratio for Silica =	0.165	
ν_{Tip} =	Poisson's Ratio for Silicon =	0.280	
F_L =	Loading Force =	350.00	nN
R_{Sample} =	Sample Radius of Curvature =	10000.00	nm
R_{Tip} =	Tip Radius of Curvature =	25.00	nm
F_{adh} =	Force of Adhesion =	6.20	nN
Formulas			
ε =	Reduced Elastic Modulus =	=(4/3)*(((1-D26^2)/D24+(1-D25^2)/D23))^-1	GPa
a =	Contact Radius =	=(D35/D38)^(1/2)	nm
A =	Contact Area	=D38*((D37^(2/3))/(D33^(2/3)))*(D27+3*D38*D36*D37+(6*D38*D36*D37*D27+(3*D38*D36*D37)^2)^(1/2))^(2/3)	nm^2
W_{adh} =	Work of Adhesion =	=D30/(1.5*D38*D37)	nN/nm
R =	Effective Radius =	=((1/D29)+(1/D28))^(-1)	nm
π =	pi =	=PI()	
P =	**Contact Pressure =**	**=D27/D35**	**GPa**

C.4 Tip radius calculation (replaced by blind tip reconstruction)

AFM Tip Radius of Curvature: $r_T = \dfrac{(w/2)^2 + h^2}{2h}$

Where w = Width of Feature

h = Height of Feature

r_T = Average of Ten r_T values from Ten Separate Features

r_T = 25.0620 nm

w_1 =	19.3519	r_{T1} =	20.9124	w_{11} =	30.0000	r_{T11} =	25.1615
h_1 =	2.3731			h_{11} =	4.9600		
w_2 =	36.8032	r_{T2} =	25.9530	w_{12} =	11.6111	r_{T12} =	20.0703
h_2 =	7.6517			h_{12} =	0.8580		
w_3 =	34.7452	r_{T3} =	27.4736	w_{13} =	12.5043	r_{T13} =	18.9363
h_3 =	6.1900			h_{13} =	1.0619		
w_4 =	29.1576	r_{T4} =	21.8038	w_{14} =	14.4395	r_{T14} =	17.1923
h_4 =	5.5907			h_{14} =	1.5894		
w_5 =	29.1576	r_{T5} =	30.4092	w_{15} =	35.7321	r_{T15} =	32.2477
h_5 =	3.7225			h_{15} =	5.4015		
w_6 =	30.8142	r_{T6} =	27.4483	w_{16} =	37.0424	r_{T16} =	35.9884
h_6 =	4.7320			h_{16} =	5.1318		
w_7 =	13.5463	r_{T7} =	23.2003	w_{17} =	24.0451	r_{T17} =	24.8821
h_7 =	1.0107			h_{17} =	3.0973		
w_8 =	22.1803	r_{T8} =	23.1989	w_{18} =	29.2440	r_{T18} =	20.7607
h_8 =	2.8225			h_{18} =	6.0229		
w_9 =	28.8790	r_{T9} =	26.8708	w_{19} =	27.2914	r_{T19} =	28.6154
h_9 =	4.2094			h_{19} =	3.4632		
w_{10} =	22.2223	r_{T10} =	23.9135	w_{20} =	21.2387	r_{T20} =	26.2022
h_{10} =	2.7381			h_{20} =	2.2484		

AFM Tip Radius of Curvature: $r_T = \dfrac{(w/2)^2 + h^2}{2h}$

Where w = Width of Feature

h = Height of Feature

r_T = Average of Ten r_T values from Ten Separate Features

r_T = =AVERAGE(G45,G47,G49,G51,G53,G55,G57,G59,G61,G63,L45,L47,L49,L51,L53,L55,L57,L59,L61,L63)

w_1 =	19.3519	r_{T1} =	=((E45/2)^2+E46^2)/(2*E46)	w_{11} =	30.0000	r_{T11} =	=((J45/2)^2+J46^2)/(2*J46)
h_1 =	2.3731			h_{11} =	4.9600		
w_2 =	36.8032	r_{T2} =	=((E47/2)^2+E48^2)/(2*E48)	w_{12} =	11.6111	r_{T12} =	=((J47/2)^2+J48^2)/(2*J48)
h_2 =	7.6517			h_{12} =	0.8580		
w_3 =	34.7452	r_{T3} =	=((E49/2)^2+E50^2)/(2*E50)	w_{13} =	12.5043	r_{T13} =	=((J49/2)^2+J50^2)/(2*J50)
h_3 =	6.1900			h_{13} =	1.0619		
w_4 =	29.1576	r_{T4} =	=((E51/2)^2+E52^2)/(2*E52)	w_{14} =	14.4395	r_{T14} =	=((J51/2)^2+J52^2)/(2*J52)
h_4 =	5.5907			h_{14} =	1.5894		
w_5 =	29.1576	r_{T5} =	=((E53/2)^2+E54^2)/(2*E54)	w_{15} =	35.7321	r_{T15} =	=((J53/2)^2+J54^2)/(2*J54)
h_5 =	3.7225			h_{15} =	5.4015		
w_6 =	30.8142	r_{T6} =	=((E55/2)^2+E56^2)/(2*E56)	w_{16} =	37.0424	r_{T16} =	=((J55/2)^2+J56^2)/(2*J56)
h_6 =	4.7320			h_{16} =	5.1318		
w_7 =	13.5463	r_{T7} =	=((E57/2)^2+E58^2)/(2*E58)	w_{17} =	24.0451	r_{T17} =	=((J57/2)^2+J58^2)/(2*J58)
h_7 =	1.0107			h_{17} =	3.0973		
w_8 =	22.1803	r_{T8} =	=((E59/2)^2+E60^2)/(2*E60)	w_{18} =	29.2440	r_{T18} =	=((J59/2)^2+J60^2)/(2*J60)
h_8 =	2.8225			h_{18} =	6.0229		
w_9 =	28.8790	r_{T9} =	=((E61/2)^2+E62^2)/(2*E62)	w_{19} =	27.2914	r_{T19} =	=((J61/2)^2+J62^2)/(2*J62)
h_9 =	4.2094			h_{19} =	3.4632		
w_{10} =	22.2223	r_{T10} =	=((E63/2)^2+E64^2)/(2*E64)	w_{20} =	21.2387	r_{T20} =	=((J63/2)^2+J64^2)/(2*J64)
h_{10} =	2.7381			h_{20} =	2.2484		

C.5 Nanoparticle Surface Coverage Calculator

Average Particle Diameter =			7	nm	Particle Surface Area =		153.94	nm^2	=	1.54E-16	m^2
Sample Mass Before TGA =			7.51	mg	Particle Volume =		179.59	nm^3	=	1.80E-19	cm^3
Sample Mass After TGA =			6.01	mg	Density of Fused Silica =		2.201	g/cm^3			
	Change in Mass =		1.50	mg		Particle Mass =	3.95E-19	g	=	3.95E-16	mg
	Mass of SA Film =		1.50	mg	Number of Particles in Sample =		1.52E+16	particles			
Ideal Coverage Initial Mass =			9.94	mg	Total Surface Area =		2.34	m^2			
50% Ideal Coverage Initial Mass =			7.97	mg	Ideal (100%) Suface Coverage =		1.68	mg/m^2	=	4.0	$molecules/nm^2$
	Silanol Density =		4.0	(per nm^2)	Actual Surface Coverage =		0.64	mg/m^2	=	1.53	$molecules/nm^2$
Film Molecule Molecular Weight =			99.00	g/mol	Percent Actual Suface Coverage =		30.520%				
			Sample 1 Coverage -	31.40%							
			Sample 2 Coverage -	34.55%							
			Sample 3 Coverage -	30.52%							
			Average Coverage -	32.1567%							
			Standard Deviation -	2.12%							

Average Particle Diameter =	7	nm	Particle Surface Area =	=4*PI()*(0.5*D20)^2	nm^2	=	=I20*1E-18	m^2			
Sample Mass Before TGA =	7.51	mg	Particle Volume =	=(4/3)*PI()*(0.5*D20)^3	nm^3	=	=I21*1E-21	cm^3			
Sample Mass After TGA =	6.01	mg	Density of Fused Silica =	2.201	g/cm^3						
Change in Mass =	=D21-D22	mg	Particle Mass =	=I22*L21	g	=	=I23/0.001	mg			
Mass of SA Film =	=D21-D22	mg	Number of Particles in Sample =	=D22/L23	particles						
Ideal Coverage Initial Mass =	=(I26*I25)+D22	mg	Total Surface Area =	=I24*L20	m^2						
50% Ideal Coverage Initial Mass =	=(I26*(I25*0.5))+D22	mg	Ideal (100%) Suface Coverage =	=D27*(1/6.022E+23)*253.24*1E18*1000	mg/m^2	=	4.0	$molecules/nm^2$			
Silanol Density =	4.0	(per nm^2)	Actual Surface Coverage =	=D24/I25	mg/m^2	=	=(L26/I26)*I27	$molecules/nm^2$			
Film Molecule Molecular Weight =	99.00	g/mol	Percent Actual Suface Coverage =	=I27/I26							
Sample 1 Coverage -	31.40%										
Sample 2 Coverage -	34.55%										
Sample 3 Coverage -	30.52%										
Average Coverage -	=AVERAGE(F31:F33)										
Standard Deviation -	=STDEV(F31:F33)										

APPENDIX D

DETAILED EXPERIMENTAL PROCEEDURES

D.1 Spin-coated nanoparticle film preparation

1. Prepare substrates by cutting silicon wafers to desired size. Clean substrates by submerging in a cleaning/hydroxylating solution consisting of a 4:1:1 mixture of high purity water (4), 35% hydrogen peroxide (1), and ammonium hydroxide (1) for 30 minutes at 85 °C. After 30 minutes, remove the substrates from the solution and rinse for 60 seconds under streaming high purity water. Dry thoroughly with nitrogen and place individually in wafer holders until use.

2. In a small, screw top vial, add 500 mg of the desired silica nanoparticle followed by 5 mL of pH 13 water. Close vial and shake to combine.

3. Sonicate solution for at least 30 minutes, but longer is acceptable.

4. Prepare spin-coating station by having everything on hand and ready before removing the nanoparticle solution from the sonicator, this is important because the nanoparticles will begin aggregating soon after being removed, resulting in overly rough films.

5. Spin-coat each substrate at a revolution rate of 7000 RPM for sixty seconds. Allow substrate to come up to speed (approximately 5 seconds) before slowly adding 10 drops of the nanoparticle solution to the substrate. Allow for a two second pause between drops and let the substrate continue to spin until the 60 second period is up. Once the substrate has come to a stop, remove and place individually in a wafer holder.

6. Repeat step 5 for each substrate until all substrates are completed.

7. Place substrates into kiln, they should be laid flat directly on the foam insert on the bottom of the inside chamber. Program a temperature sequence as follows:

1. Ramp temperature at a rate of 100 °C per hour to a temperature of 500 °C.
2. Hold at 500 °C for five hours.
3. Ramp temperature at a rate of 25 °C per hour to room temperature.

8. Once the temperature program is completed, remove substrates to individual wafer holders and store in a dry environment until needed.

E.2 Silane Functionalization Procedures

Si Substrate Preparation

1. Cut Si substrate to size depending on experimental needs.

2. Rinse substrate with ethanol and water to remove any dust from the scribing process.

3. In a 100 mL orange top Pyrex glass bottle, place enough 4:1:1 (water:hydrogen peroxide:ammonium hydroxide) solution to cover the substrates while leaning against the inside walls of the bottle.

4. Place bottle inside an 85 degree C oven for 35 to 40 minutes, be sure to stand up any substrates that have fallen during transport and seal the bottle tightly.

5. After the prescribed time has passed, remove the bottle from the oven to the hood (or place under the vent on top of the UV-Ozone cleaner if not being used), crack open the lid and allow to sit for another 10 minutes.

6. Rinse the substrate with water for 60 seconds and dry thoroughly with streaming nitrogen.

7. Store the substrates in the glove box or under ethanol until used.

Nanoparticle Film Spin Coating Procedure

1. Skip these steps if a spin coated film is not desired.

2. Clean and dry a screw top vial.

3. Measure 500 milligrams of OX50 and place inside the screw top vial

4. Add 5 milliliters of pH13 water to the vial

5. Sonicate sol for 60 minutes

6. Spin coat cleaned and dried substrate with nanoparticle sol at 5000 rpm for 60 seconds, dropping 15 drops from a glass pipette at a rate of 1 drop per second.

7. Place spin coated substrates into the kiln and bake by programming a ramp setting that heats by 100 degrees per hour to a final temperature of 500 degrees C and then ramps down at 25 degrees per hour to a final temperature of 25 degrees C.

8. Store the substrates in the glove box or under ethanol until used.

Si Substrate Functionalization

1. Place substrates into a 100 mL orange top Pyrex glass bottle and add 50 mL of hexanes (more if there are a number of large substrates).

2. Top the bottle with nitrogen (at a low flow rate) and seal tightly.

3. Place the bottle inside the glove box.

4. Add the desired silane at a rate of 1 μL of silane per 1 mL of hexanes. Seal the silane bottle with Parafilm and return to the glass desiccator inside of the glove box, never remove the silanes from the inert atmosphere of the glove box.

5. Tightly close the Pyrex bottle and remove from the glove box.

6. Sonicate for 90 minutes or longer if time allows.

7. Allow substrates and solution to sit overnight inside a drawer or somewhere else away from direct contact with light.

8. In the morning, sonicate the substrates for 30 minutes.

9. Rinse the substrates with water for 60 seconds and dry thoroughly with streaming nitrogen.

10. Place the substrates to another 100 mL orange top Pyrex glass bottle containing 60 mL of THF, close the bottle tightly and sonicate for 60 minutes.

11. Again, rinse the substrates with water for 60 seconds and dry thoroughly with streaming nitrogen.

12. Characterize films with FTIR to ensure proper film formation.

13. Store functionalized substrates in the glove box or under hexane until use, away from light.

Solvent Intercalation

1. Place functionalized nanoparticle substrate into a neat solution of the desired molecule.

2. Sonicate for at least 90 minutes or more if time allows. Allow substrate to sit in the bath overnight.

3. Remove substrate from solution, rinse with water for 30 seconds and dry thoroughly with streaming nitrogen.

4. Characterize films with FTIR to ensure proper solvent intercalation.

5. Repeat steps as necessary until desired degree of solvent intercalation is achieved.

VITA

Ryan Lane Jones received his Bachelor of Science degree in chemistry from Texas A&M University Corpus Christi in 2005, where he studied under Eugene and Fereshteh Billiot looking at the occurrence of endocrine disrupting chemicals in the soil and waterways of South Texas. Additionally, he worked synthesizing a variety of amino acid based surfactants which were used for performing chiral separations with Capillary Electrophoresis. He entered the Chemistry program at Texas A&M University to work under James D. Batteas in June 2005 where his work has centered around understanding how self-assembled monolayers order on surfaces with nanoscopic curvature and how they act to protect surfaces from damage during contact. He was awarded a Ph.D. in Chemistry on February 17th 2011.

Dr. Jones may be reached at:

Department of Chemistry
Texas A&M University
P.O. Box 30012
College Station, TX 77842-3012

Dr. Jones may also be reached by email at rjones@mail.chem.tamu.edu.